CHALMERS

Quality assessment of LMD/w Ti-6Al-4V alloy components using conventional NDT techniques

Diploma work in the Master programme Production Engineering

AGNIESZKA KISIELEWICZ

Quality assessment of LMD/w Ti-6Al-4V alloy components using conventional NDT techniques

by

Agnieszka Kisielewicz

Diploma work No. 155/2015

at Department of Materials and Manufacturing Technology

CHALMERS UNIVERSITY OF TECHNOLOGY

Gothenburg, Sweden

Diploma work in the Master programme Production Engineering

Performed at: Department of Process Engineering, 9634, Research and Technology Center, GKN Aerospace Engine Systems, Trollhättan

Supervisor: Per Henrikson, Dept. 9634, R&T, GKN Aerospace, Trollhättan

Examiner: Håkan Wirdelius ass. Professor, Director
Department of Materials and Manufacturing Technology
Chalmers University of Technology, SE - 412 96 Gothenburg

Quality assessment of LMD/w Ti-6Al-4V alloy components using conventional NDT techniques
AGNIESZKA KISIELEWICZ ©

Quality assessment of LMD/w Ti-6Al-4V alloy components using conventional NDT techniques

Agnieszka Kisielewicz
Department of Materials and Manufacturing Technology
Chalmers University of Technology

SUMMARY

In order to reduce costs of production and increase economic sustainability it is necessary to perform non-destructive tests at an early stage in the manufacturing process. Laser metal deposition (LMD) of titanium alloys using wire feed technology is a fairly young technology and is still in a developing stage. Thus the necessity of introducing non-destructive examination adapted to LMD/wire parts is even higher. The main purpose of the project was to evaluate usability of ultrasonic immersion testing for detecting lack of fusion defects in specific LMD test samples. Additionally, eddy current technique was examined as probable complementary inspection.

Initially, theoretical study was performed on applying ultrasonic tests to LMD parts as well as on the characteristics of lack of fusion and its detectability. The experimental part of ultrasonic tests consisted of evaluation of available probes for the application, creating and optimizing amplification curves according to the reference as well as performing planar scans on available samples. Different incidence surfaces and their conditions were evaluated in terms of usability for inspection. As the result, several inspection limitations were identified. Subsequently, complimentary theoretical study was performed focusing on eddy current inspection. Eddy current experiments were performed on reference plate, using both plane surface as well as surface containing notches. Additionally, scans were performed on LMD/w samples with two different surface conditions. Comparison of the results was provided.

Applying ultrasonic immersion testing for LMD/w test pieces showed satisfying results in terms of usability of the method. The results of the ultrasonic testing revealed a number of limitations when it came to inspection capabilities. To start with, raw surface conditions reduced the reliability of the inspection. Certain volumes close to the incidence surface as well as close to the edges of component were restricted from inspection. Using optimized settings it was possible to detect flaws producing signals comparable to the target (i.e. 0.4 mm flat bottom hole).

Eddy current inspection showed capabilities of being used as a complementary method for inspection of limited volumes of close to the edge area. Yet, the conclusion was based mainly on reference defects. Additionally, depending on the size of reference defects, the detectability of flaws varied regarding to the depth. The milled surface condition of LMD parts provides similar inspection conditions to the ones of reference plate.

Keywords: NDT, Ultrasonic Testing, Eddy Current Testing, LMD, titanium alloy

Abbreviations

ALM	Additive Layer Manufacturing
DAC	Distance Amplitude Correction
ECT	Eddy Current Testing
EDM	Electro Discharge Machining
EMATs	Electromagnetic Acoustic Transducers
FBH	Flat Bottom Holes
FSH	Full Screen H
ISI	In-Service Inspection
IqNDE	Integrity and quality assessment by NDE
LMD	Laser Metal Deposition
LMD/w	wire feed Laser Metal Deposition
LoF	Lack of Fusion
NDT	Non-Destructive Testing
NDE	Non-Destructive Evaluation
QNDE	Quantitative Non-Destructive Evaluation
SDH	Side Drilled Hole
UT	Ultrasonic Testing
TCG	Time Corrected Gain

Acknowledgements

Gothenburg, June, 2015
Agnieszka Kisielewicz,

Table of Contents

1 Introduction

This master thesis is the graduation project of my Master of Science degree in Production Engineering program at Chalmers University of Technology. The experiments described in this paper were performed at the GKN NDT laboratory in the Production Technology Center (PTC) in Trollhättan, Sweden between January and June 2015.

1.1 Background of the project

In order to assure more sustainable and robust production, it is necessary to include non-destructive testing as a method for product's quality control. Non-destructive inspections enable identification of components with defects without any destructive examination. The relevant advantages of these inspections are lowering the scrap rate, diversity of properties that can be inspected as well as increasing sustainability of production. If applied at an early stage of the manufacturing process, they can prevent costly and time consuming processing of faulty parts.

Laser Metal Deposition is a recently developed manufacturing technique that gained high interest in e.g. the aerospace industry. It enables to create 3D objects of complex shapes with much lower material losses and reduced requirement of additional machining in comparison to traditional manufacturing techniques. Yet, in order to be introduced as a production tool, more research needs to be performed to obtain robust manufacturing process with accurate quality inspection standards.

1.2 Objectives of the project

The objectives of this project were to perform the preliminary study of usability of two different NDT methods: ultrasonic immersion testing (UT) and eddy current testing for inspection of Ti-6Al-4V wall-shaped LMD parts. The main focus was placed on evaluating UT for detecting lack of fusion defects. The target reference defect was set to be a 0.4 mm flat-bottom hole. The project intended also to give general information about limitations of inspection. The objective for eddy current tests was to investigate whether it can be used as a complimentary method to UT for this specific application.

1.3 Limitations and risks of the project

There were several limiting factors that influenced the project. To start with, the project was held as Master's thesis work. Due to this, the time span of the project was set to a period between January and May 2015. What is more, the experimental part was limited to the resources available at GKN Aerospace. Additionally, the progress of the work was dependent on accessibility of test pieces provided by the company. Moreover, regarding experimental characteristic of this project, it had to be considered that some unexpected circumstances, concerning e.g. usability of methods, quality of components, could also have impact on the progress of the work. Last but not least, the level of experience of the researcher could also be an influential factor.

Regarding the limitations stated above, a few risks can be pointed out. Since the project intended to cover wide range of experiments, depending on previously mentioned factors, not all of the problems may be addressed in an extensive way. What is more, one major risk is that the quality of produced results is highly dependent on circumstances as availability of resources as well as its quality. Regarding the fact that the project was carried out by one researcher, all proceedings and decisions were limited by one judging perspective. Even though the work up-dates were consulted with the examiner and the supervisor, the risk of limited judgment was still considerable.

2 Introduction to NDT

There is an increasing focus toward accurate and sustainable manufacturing methods, producing lowest possible amounts of scrap and waste. It has thus become essential to be able to characterize defects and assess their impact on the final product at early stages of manufacturing. Due to this, non-destructive tests (NDT), that enable evaluation of components without causing any damage to the object, are gaining of attention both in industry and academia.

NDT is the general name used to describe wide group of analyzing techniques that can provide information on material's mechanical and physical properties as well as assess its quality, giving indication of presence of defects, their characteristic features and quantity. The result of a test and information obtained from the examination varies depending on chosen technique and its capabilities in connection to the specific application.

Inspections involving NDT can be divided into three groups: in-service inspection (ISI), quality assessment and properties characterization. The first one, is performed on parts that are exposed to heavy work conditions and it focuses on identification and assessment of in-service damage (e.g. fatigue or stress-corrosion cracks). Depending on the requirements, the tests are performed in pre-set intervals. The second type of inspection is performed on newly produced components and aims on assessing the quality of the piece. It is performed just once as the results determine whether the part fulfills the quality requirements. The last mentioned type of inspection aims on assessing specific property of the material, e.g. density, elastic properties, texture or grain size.

As the term NDT relates only to the inspections themselves all the activities involving interpretation of results and quality evaluation is called non-destructive evaluation (NDE). If the analysis includes more detailed characterization of a defect like positioning and sizing it is described by the term of Quantitative NDE (QNDE). Recently, the attempts are being done to use NDT not only for quality but also for integrity assessment. This new type of evaluation is described as IqNDE and aims on assessing more complex characteristics of the test piece like, i.e. residual life and fracture toughness. It requires developing mathematical models of the inspection and dedicated simulation software.

The most common NDT techniques include visual, ultrasonic, liquid penetrant, radiographic, eddy current and magnetic-particle testing. Undoubtedly, it is essential to select a proper testing method for the application. When choosing specific NDT method several issues need to be considered. To start with, at the very beginning it is necessary to state clear reason of using NDT. Subsequently, to make a good choice the knowledge about the expected flaw is required. Due to this, more detailed information about the flaw type, e.g. presumed size, orientation and location, should be acquired. Finally, to select most proper testing technique several information about tested piece should be considered. Features like geometry, surface conditions and material characteristics should be investigated and specified. [1]

3 Titanium alloys for aerospace applications

Aerospace industry is a very specific production sector where reduction of one kilogram of weight can save about 1000 Euro in an aircraft and even up to 10 000 Euro in case of a space application [2]. In order to compare it with land-based transportation, for automotive industry it is only 10 Euro per one kilogram of weight reduction [2]. What is more, decrease of weight of an aircraft is correlated with lower fuel consumption as well as limitation of harmful environmental impact. Due to this evident cost reduction opportunity and increase of sustainability, lots of effort is being done to develop new materials and solutions that could decrease weight of aircrafts. Considering this, materials used for aerospace applications, e.g. titanium and nickel alloys, are accepted to have prices a few orders of magnitude higher than the ones applied in any other transportation system [2].

Titanium alloys tends to replace materials like aluminum alloys, high strength steels and nickel-based superalloys in applications where the specific combination of properties like weight, strength, corrosion resistance and metallurgical stability at elevated temperatures is required. Being lighter than steel and Ni-based alloys, it can be used in applications of elevated but not extremely high temperatures. [2]

In recent years, a lot of effort has been put to increase the usage of titanium alloys in aerospace products. It is used for several different parts of modern airplanes, in e.g. fuselages or thin, narrow rings mounted around the aluminum to prevent fatigue crack growth. Due to the corrosive properties, the hydraulic tubing as well as piping system for de-icing equipment is manufactured using pure titanium or titanium alloys. What is more, it is a standard material for parts of gas turbine engine like compressor blades and disks. It is also of interest that 50-70% of weight of modern fighter aircrafts accounts of titanium [2]. Considering space application, fuel and satellite tanks are common applications for titanium alloys. Due to high specific strength and corrosion resistance, titanium alloys are proper materials for demanding aerospace applications. Even though their cost is high and they are hard to machine materials, their metallurgical stability as well as high strength at elevated temperatures are the factors determining their usability [2].

3.1 Properties of Ti-6Al-4V

Ti-6Al-4V is the most commonly used titanium alloy in aerospace industry [3], [4]. Due to alloying elements, it is much stronger than pure titanium. As the entire family of titanium alloys, it is characterized by having a good combination of strength, corrosion resistance and weld ability. It is commonly used in application where the temperature reaches up to 400 ℃ [2]. The alloy's density is about 4420 $\frac{kg}{m^3}$, Young's modulus equals to 110 GPa and the tensile strength of 1000 MPa [5]. The electrical properties of this alloy are resistivity of 178 $\mu\Omega * cm$ and conductivity of $1.26 \times 10^{-5} \frac{H}{m}$ [6].

Yet, the major disadvantage of Ti-6Al-4V is the fact that it is difficult to machine using traditional methods. While machining, it is prone to heat hardening and interaction with cutting tool materials at elevated temperatures [3]. It has thus become essential to develop unconventional technique for efficient manufacturing of Ti-6Al-4V alloy.

4 Laser Metal Deposition of titanium alloys

Laser Metal Deposition (LMD) is one of a few additive layer manufacturing (ALM) techniques, where the components are built layer-by-layer based on a CAD model file [3]. The technique can be used for both producing new components as well as to repair high value components. It uses a high power laser beam to create melt pool on the surface. The build-up of next layer is possible by feeding powder metal or wire into the weld pool [3]. This type of manufacturing process enables production of flexible, complex components generating less scrap than traditional manufacturing techniques. Moreover, it has a potential of saving time and limiting additional manufacturing of the product. All of these factors result in reduced cost of manufacturing. Usually, LMD is used for manufacturing of small and medium-size parts based on Ti-6Al-4V as additive material.

4.1 Wire-feed LMD

Even though the powder feed is most commonly used method, the wire-feed deposition is growing of an interest as it creates parts with less contamination as well as is more robust solution [4]. The basic concept of this technique is presented in Figure 1. The filler material in form of wire is fed into the melt pool where it fuses with base material or previous bead. The energy needed to melt both materials is provided by laser beam. In order to ensure good quality, the process is performed in an atmosphere of shielding gas.
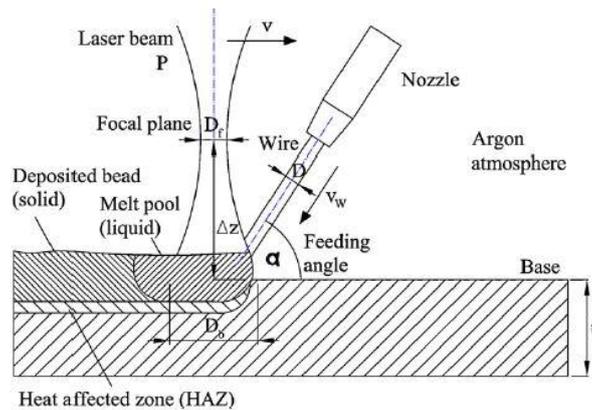
Figure 1: Schematic drawing of wire-feed LMD [7].

4.2 Microstructure of LMD Ti-6Al-4V

Sample titanium alloy blocks produced by LMD tend to be characterized by complex microstructure of α and β grains. Depending on different manufacturing conditions and heat treatment, the hexagonal close-packed (hcp) α-grains and body-centered cubic (bcc) β-grains can develop various forms. Analyzing multi-layer LMD samples, depending on heat treatment, several characteristics can be observed. Considering as-built samples, one of the characteristics is that the prior β-grains have columnar shape that grew epitaxially across several layers in direction of temperature gradient. The long and narrow columnar grains can reach length up to a few millimeters. Heat treatment in the α+β region influences only grain size and distribution of α-grains. The layer bands are clearly visible, yet they are correlated to α/α+β transus lines rather than to the deposited layers. There are differences between the microstructure of higher and lower layers. General observation is that grains in higher layers are coarser and the grain number is decreasing. Figure 2 shows sample microstructure of as-built blocks. [7]
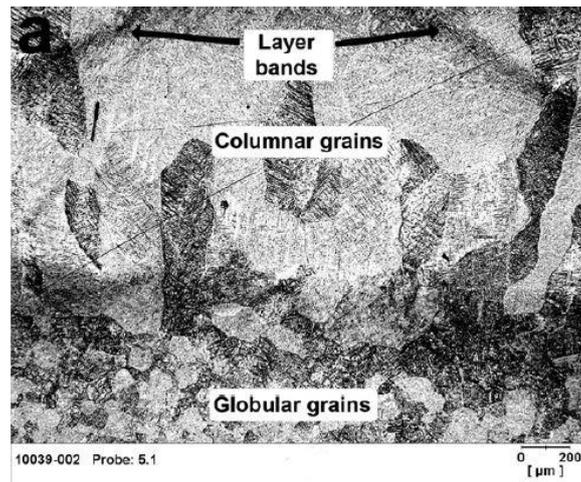
Figure 2: Microstructure of multi-layer LMD sample [7].

The blocks that were heat treated at 1200°C for 2h and then subsequently furnace cooled appear to have a different microstructure (see Figure 3). It is not possible to distinguish between the base and deposited material. There is more homogenous size and distribution of grains. Additionally, no layer bands can be observed as well as columnar β-grains.
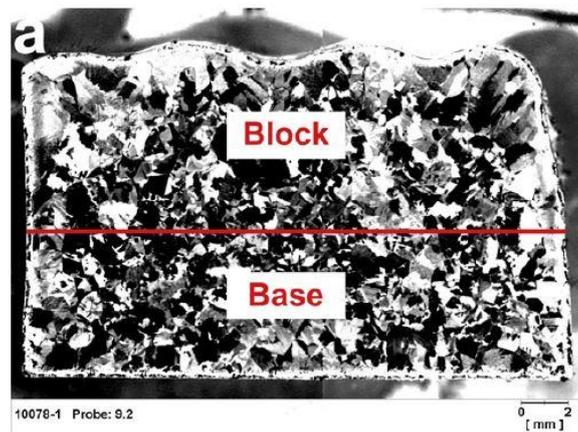
Figure 3: Microstructure of LMD multi-layer block in 1200C/2h/FC condition [7].

It is worth to mention that LMD is not being fully repeatable and stable process in regard to material's properties and therefore not yet suitable for mass production [7]. Regarding this, in order to gain more knowledge about LMD technique, it is necessary to investigate sample products more using both destructive and non-destructive techniques.

Depending on type of defect and its properties, i.e. size or shape, suitable NDT method should be chosen. Due to this, it is of highest importance to gain understanding of possible defects that may be present in the material.

Considering limitation of sources providing information about defects in LMD titanium alloys the decision was made to perform a literature survey with broader perspective including also information about flaws occurring in laser welding as well as specifically laser welding of titanium alloys. This approach is justified by the fact that both wire-feed LMD and laser welding base on similar principles and use the same technique of material deposition. Yet, due to the difference in shapes and positioning between welds and free-form parts the defects can occur in utterly different locations.

In case of the laser welding, most commonly named defects are pores, cracks as well as HAZ embrittlement [8]. To some extend lack of fusion is also mentioned as defect present by laser welding [9].

4.2.1 Porosity

Porosity often appears as one of the most frequent defects in laser welding. There is a variety of different types of pores and their distribution. Small pores are usually associated with gas entrapment and they appear more towards the surface of the weld. As for big bubbles, it is claimed that they originate from partial solidification of material before the keyhole was filled completely. They tend to be formed at the bottom of a weld. [8]

Pores observed in layers of laser-deposited Ti-6Al-4V had nearly spherical shape. Yet, no specific location of frequent occurrence was observed [10].

4.2.2 Cracks

Considering welding, cracking is the most serious defect that appears during cooling of the joint. It is caused by the restrictions to free contractions. There are two different types of hot cracking mechanism: solidification cracking and liquation cracking. Shrinkage of the material in the solidification sequence causes the first type of cracks [8]. They have intergranular form and are present in fusion zone revealing dendritic morphology [8]. Liquation cracking is typical for the partially melted zone and is caused by the grain boundaries liquation and contractions in fusion zone [11].

4.2.3 Lack of fusion (LoF)

Lack of fusion is one of the most serious defects that can occur in welded joints. It appears as incompletely fused spots both between base metal and added material as well as between weld beads. Lack of fusion is defined as planar defect caused by insufficient melting of base metal or previous layers. Additionally, the defect can have from of adhesive bonding, when incomplete penetration has been achieved – weaker bonding similar to brazing or metallization. Even though, consequences of lack of fusion are comparably severe to those caused by cracks, little information about this defect can be found in literature. [12]

Despite the fact that multi-layer LMD components are prone to this type of defect, information about characteristics of LoF in LMD samples is very limited. The available document [10] describes lack of fusion as an elongated irregularly shaped pore type of defect. It occurs parallel to the deposition's direction, along the layer boundaries. In the conducted experiment [10], the amount of LoF was much higher than gas porosity. It was also observed that the defect occurs more often in thin-substrate deposits. Figure 4 shows an example of LoF defect in powder-feed LMD block.
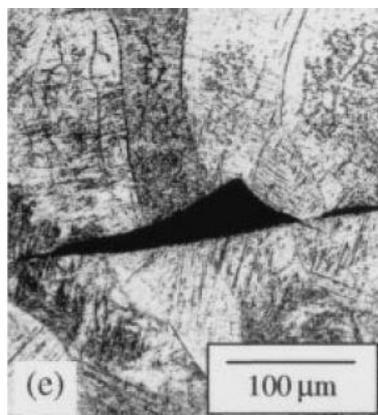
Figure 4: Lack of fusion defect in LMD sample [10].

Regarding lack of fusion in welds, there are three types of positioning of the defect: lack of side-wall fusion, lack of inter-run fusion, lack of fusion at the root of the weld. The first two cases are presentment in Figure 5 below. Additionally, data obtained in experiments [13] show that despite constant welding parameters and fully automated process there is no repeatability of LoF shape. According to the results of the experiments, the most probable positions for occurrence of LoF are corners of the runs, being the furthest points from the heat source.
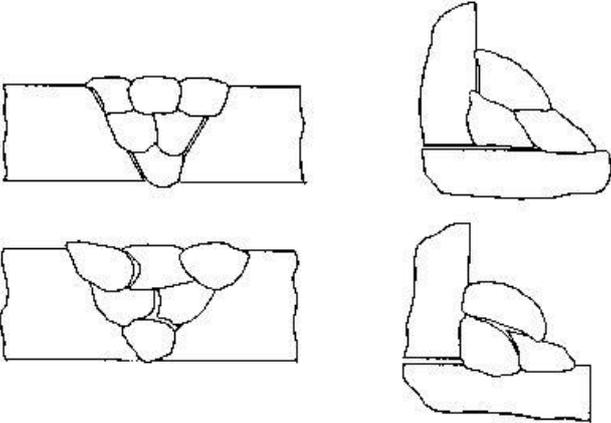
Figure 5: Simplified presentation of two types of LoF: lack of side-wall and inter-run fusion. [12]

Considering the severity of this type of defects and limited knowledge about it, the project will mostly focus on detectability of LoF in LMD titanium alloy products.

5   NDT technologies

Regarding type of material and characteristics of flaws that can possibly occur in titanium parts manufactured using wire-feed LMD, two different NDT methods were chosen. In order to investigate volumetric and planar internal defects ultrasonic technique was selected. Regarding limitations of UT to identify surface and close to the surface flaws, eddy current technique was chosen as the complementary inspection method. In the sections below both of the testing methods are described.

5.1   Ultrasonic testing

Ultrasonic testing is a very effective technique for detecting internal flaws. This is due to its high penetration power and wide range of frequencies that enables to inspect very thick materials as well as detect flaws of minute sizes. This technique has capabilities of providing information not only about the presence of the flaw but also about its size, shape and position. [14]

5.1.1   Basic principle of ultrasonic tests

The basic principle of ultrasonic NDT is simple. The ultrasonic sound wave can easily propagate through solid materials. However, if there is a defect on the way of propagation, part of the wave gets reflected and/or scattered. The consequence is a loss of energy of the wave and generation of an echo that indicates a flaw.

Ultrasonic waves can be described as mechanical vibrations of frequencies higher than the range of frequencies audible for a human, that is above 20 kHz. In conventional ultrasonic technique the waves are generated by electromechanical transducers that transform electrical signals into mechanical vibrations and vice versa. Using this principle, the piezoelectric crystal mounted in testing probe can be both generator and receiver of high frequency vibrations, depending on the chosen method and application.

As the result of the UT inspection, acquired wave signals can be presented in form of A-scan, B-scan or C-scan. The first one is the most basic presentation of ultrasonic signal. It provides information about the depth of detected defects as well as the amplitude of the signal reflected from it. It uses the horizontal line of the display screen as depth scale and vertical line as signal amplitude. B-scan is a composition of several A-scan signals presenting the vertical cross-section of test piece. It provides information on distribution of defects and their sizes. C-scan presentation provides a planar view of the test piece showing size and distribution of defects but no information on the depth. The main purpose of C-scan is to show area in focus disregarding front and back-wall signals. It is achieved by using system of time-window gates, acquiring data only from a certain depth. [14]

5.1.2   Frequency of ultrasonic wave

The frequency of ultrasonic wave is a very important parameter influencing defect's detectability. Generally, frequency of a sound wave can be described as relationship between velocity v and wavelength λ that is presented below (Eq. 1).

$$f = \frac{v}{\lambda}$$

Eq. 1

To be able to detect a defect by using an ultrasonic method the wavelength should be of the same order as the defect's size. Additionally, smaller flaws than half of the wavelength are considered undetectable [14]. While adjusting the frequency of ultrasonic wave, one should consider that its relation to the detectable flaw size is inversely proportional. Frequencies commonly used for commercial applications are of range between 1MHz and 25MHz [14].

5.1.3 Wave propagation and types of waves

Principally, the ultrasonic wave travels by displacing material's particles from their equilibrium position. Wave propagation mode is strictly correlated to the type of wave. Generally, ultrasonic waves can be divided in three different groups: longitudinal, transverse and surface waves. This division is based on the direction of vibrating particles that are moved by the propagating wave. Since the intended application is to identify defects in the volume, the focus of this section is towards the first two wave types.

Longitudinal waves force the particles to vibrate in the same direction as front of the wave, causing localized compression. Since their propagation is correlated to elastic properties of the material, the velocity of longitudinal waves depends on the value of Young's modulus of tested material [15].

On the contrary, transverse waves cause vibration of particles perpendicular to the direction of wave propagation. Considering, shearing characteristics of the vibration, the velocity of transverse waves is correlated to shear modulus of material. In case of non-viscous liquids, it is assumed that propagation of this type of waves is impossible due to low values of shear modulus [15].

Surface waves, traveling on the surface of the solid materials, can be divided into Rayleigh, Lamb and Love waves.

5.1.4 Reflection, refraction and scattering

When encountering interface between two different materials, the ultrasonic wave undergoes reflection, refraction or scattering, as well as combinations of these [14]. This phenomenon enables to detect discontinuities in material as they interact similarly to interface and produce echoes.

Analogues to light waves, when passing through an interface, ultrasonic waves follow the Snell's law describing the refraction of the beam. It states that the direction of propagation in the refractive media is dependent on the angle of incidence φ_1 and the difference in velocities in both media, v_1 and v_2. The relationship is presented in equation Eq. 2. It is worth to mention that there exists critical value of incident angle beyond which no transmission or reflection is possible. [14]

$$\frac{\sin \varphi_1}{v_1} = \frac{\sin \varphi_2}{v_2}$$

<div align="right">Eq. 2</div>
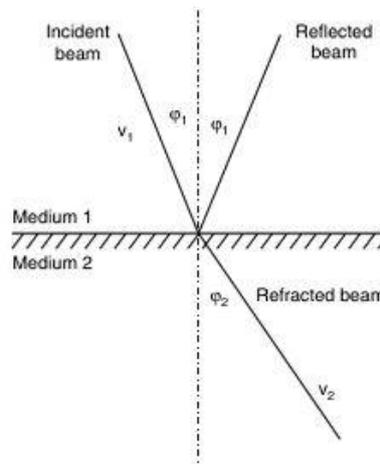
Figure 6: Incident, reflected and refracted beam according to Snell's law [14].

In case of normal incidence, both transmitted and reflected waves do not refract and they propagate in the same direction as the incident one. Additionally, they will not be split, so only one wave of each kind will propagate. The amount of the wave energy that is being transmitted and reflected depends on the properties of the both materials. If the acoustic properties of the two materials differ much, like e.g.

<div align="center">9</div>

water and titanium alloy, there will be a strong reflected wave. This is due to difference in pressure value needed to move material's particles.

5.1.5 Attenuation

In practical use the ultrasonic wave diminishes as it propagates. Regarding the fact that in order to obtain reliable results the ratio between the signal and noise needs to be high, the aspect of attenuation needs to be considered while planning UT inspection. The decrease of wave's energy can be caused by four different mechanisms.

To start with, the absorption mechanism occurs when the kinetic energy of propagating wave is partly changed into the heat energy. This mechanism gradually leads to hindering wave propagation. To some extend it can be managed by proper setting of the signal amplification. [15]

Other type of attenuation is scattering that may occur due to inhomogeneties, e.g. phase changes, grain structure as well as porosities in scale less than the size of the defect. When the ultrasonic wave front encounters this type of obstacle, it becomes randomly reflected, refracted and divided. Parts of the energy are thus scattered and new waves are produced in random directions. The amount of lost energy is dependent on the obstacles size and used frequency. This type of attenuation increases random noise of the signal, occurring as "grass" on the screen of the oscilloscope. Moreover, it is a highly unwanted phenomenon as it not only creates noise but at the same time impedes indication of a flaw and back wall. Because of that, small flaws may remain undetected. The possible countermeasure is to lower inspection frequency [15], however in this way small defects may remain undetected.

The third attenuation mechanism is beam spreading. It is connected with the fact that the wave generated by the transducer is not a plane wave. Due to this, as the distance from the source increases the divergence of the wave increases also. The consequence of this is that same amount of energy is spread on a larger area so the amplitude of vibrations decrease. [15]

Last but not least, the losses related to dispersion of the ultrasonic wave should be considered. This phenomenon is present when more than one wave type is generated. The total wave energy is spread among waves propagating with different velocities. It results in diminished value of the signal of the wave type in focus. [15]

The attenuation caused by the two first mechanisms mentioned above can be quantified and measured in decibels (dB) using equation Eq. 3. The formula compares the value of initially measured acoustic amplitude P_0 and amplitude P after traveling a certain distance. [15]

$$dB = 10 \log \frac{P^2}{P_0^2} = 20 \, \log \frac{P}{P_0} \qquad\qquad \textit{Eq. 3}$$

The attenuation is often described by the coefficient $\alpha_{dB/m}$. It combines both scattering and absorption as well as relates it to the depth of penetration Δx , see Eq. 4.

$$\alpha_{dB/m} = \left(20 \, \log \frac{P}{P_0} \right) / \Delta x \qquad\qquad \textit{Eq. 4}$$

5.1.5.1 Scattering in duplex microstructures

The issue of attenuation in single-phase materials is well examined and described by various models. However, despite strong necessity of understanding scattering in two-phase cases little attempts has been made to develop an accurate scattering model [16].

The attenuation in duplex microstructure is a complex phenomenon dependent on ultrasonic wave length, the size of colonies and parent grains as well as elongation of the grains. The combination of

these factors can enforce noise generated by the scattering that can lead to more effective masking of small-size defects. [16]

5.1.6 TCG curves

As stated above, attenuation, absorption and scattering of the signal have direct influence on the strength of the indications produced by discontinuities. To be more precise, flaws of similar dimensions being positioned at different depths in material generate indications of different intensity. In order to properly assess the size of flaw, the energy loss needs to be compensated by adjusting gain values.

TCG curve is the Time-Corrected Gain curve. It enables automatic adjustment of gain for the flaws of the equal size and various sound paths in metal. The TCG curve is only valid for the material and transducer used during calibration and it needs to be re-evaluated if one of these changes. Similarly Distance Amplitude Correction (DAC) curves are used to graphically present the decrease of the signal caused by increase of material depth. The DAC curve is normally used to provide with attenuation information and is used while interpreting A-scan results. The difference between the TCG and DAC curve in this definition is presented by the Figure 7 below.

It is a common practice to use reference blocks with Flat Bottom Holes (FBH) to create TCG curves. During the calibration, the gain is set so that the indication of each FBH would be 80% of the display screen. This way the inspector can easily assess the dimensions of detected flaw in regard to reference defects. Figure 7 presents the principle of using TCG curve to strengthen the signals of FBH at lower depths.
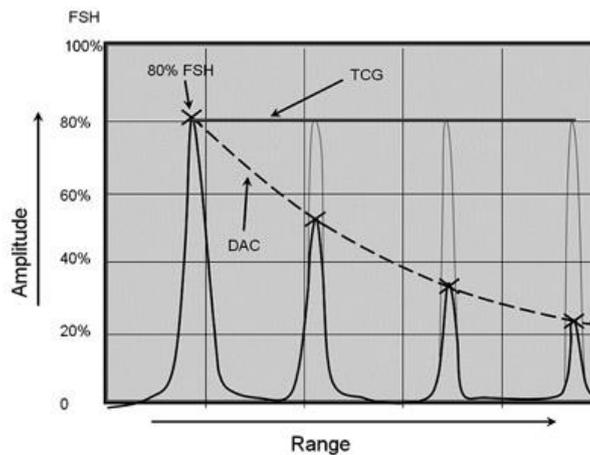

Figure 7: Presentation of a function of TCG curve and DAC curve [17].

5.1.7 Sound beam

The characteristics of the sound beam play an important role in selection of the transducer for a specific application. Parameters like near field distance Y_0^+, effective beam diameter and focal zone need to be known before the beginning of the experiments.

In the sound field of the transducer two different zones can be distinguished. The first zone between the face of transducer and first maximum $Y_0^+(N)$ is called the near field. The distance Y_0^+ represents natural focus of the transducer. In the zone between this point and the transducer, the sound beam has unstable form and should not be used for measurements. The first maximum is the transition point to the far field where the beam is stable but its amplitude gradually decreases. The schematic representation of sound field in presented in Figure 8. [18]

11
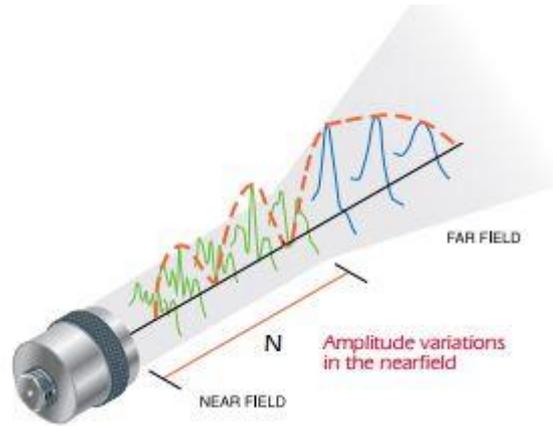
Figure 8: Schematic representation of the sound field [18].

There are two important characteristics of the sound field that describe a focused transducer: beam diameter and focal zone.
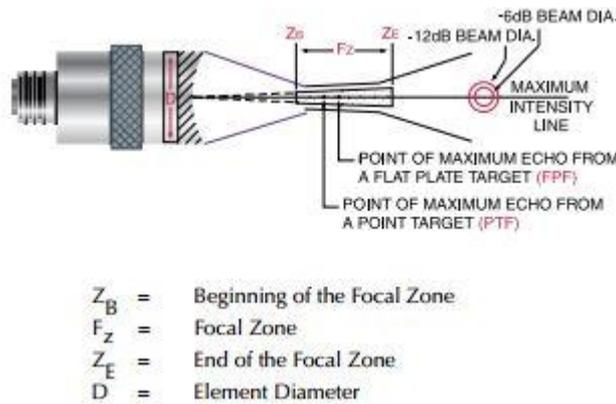

Figure 9: Graphical representation of beam diameter and focal zone [18].

Beam diameter (beam width) has influence on the sensitivity of the transducer. The more focused is the sound wave the bigger is the amount of energy reflected from the flaw. It is possible to calculate the theoretical beam diameter BD if parameters like focal length F, material sound velocity v, frequency f and element diameter D are known (Eq. 5). [18]

$$BD(-6dB) = \frac{1.02Fv}{fD}$$

Eq. 5

The focal zone is the part of the beam around the natural focus point. It is set by the points where the signal axially drops by -6 dB of amplitude at the natural focus point. The theoretical length of the focal zone can be calculated using Eq. 6, where S_F is normalized focal length. [18]

$$F_Z = N * S_F^2 \left[\frac{2}{1 + 0.5S_F} \right]$$

Eq. 6

5.1.8 Types of ultrasonic testing

There are different methods of ultrasonic testing. The section below describes principles of some of the most commonly used testing techniques.

5.1.8.1   Contact testing

Contact testing is the most commonly used type of UT inspection. During the inspection, ultrasonic probe is staying in close contact with tested material. In order to enable transfer of wave to the tested material, a special type of gel is used as coupling medium. Contact probes work in pulse-echo mode in which first piezoelectric crystal generates signal and the reflected echo of this signal is then being analyzed as a result of the test. There are three commonly used setups. The first one is using a single probe with one piezoelectric crystal being both transmitter and receiver. Similarly, the second one is also based on one probe but it contains two crystals – one being transmitter and one receiver. The third setup consists of two separate probes. The principle of pulse-echo contact probe is showed in Figure 10 below.
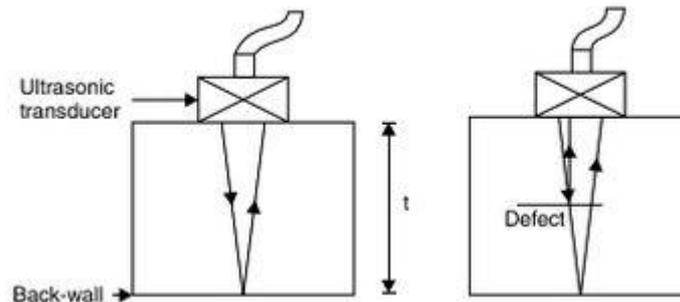

Figure 10: Single probe contact pulse-echo technique [14].

5.1.8.2   Immersion testing

This is another type of pulse-echo technique, where both test material and probe are immersed in water, and where the water is used as couplant medium to transfer ultrasonic energy into the test piece. In immersion testing, there is no physical contact between the probe and the inspected component. The process is often fully automated and all the parameters of testing unit's movement are controlled by control unit i.e. PC. This makes immersion testing advantageous to other UT techniques as the inspection is much faster, the sensitivity is increased as well as its variations are reduced due to uniform coupling [14].

For immerse application, the probe is mounted in fixture that usually can move in two perpendicular directions. The movement occurs along the top plane of the tank. In order to obtain valid results the velocity of movement needs to be adjusted to sound wave velocity and the speed of data acquisition. Figure 11 below shows general principle of immersion testing.
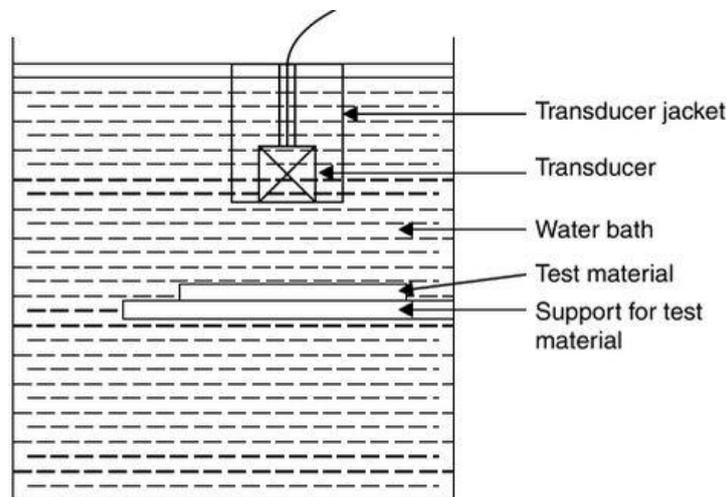

Figure 11: Schematic drawing of immersion testing [14].

5.1.8.3   Water flow testing

Similarly to immersion testing, ultrasonic tests using water flow probes apply water as a coupling medium. However, due to special nozzle that creates a continuous water flow that transmits the ultrasonic waves, the full immersion is eliminated. This solution provides higher flexibility of measurement as well as it enables to inspect components of different sizes.

5.1.8.4   Electromagnetic Acoustic Testing

In this method the ultrasonic wave is generated by an altering Lorentz force influencing the lattice structure of the material. Electromagnetic Acoustic Transducers (EMATs) uses magnetic induction to generate eddy currents ($\vec{J}$) in the test piece. As the piece is simultaneously subjected to the influence of permanent magnet ($\vec{H}$), the Lorenz force ($\vec{F}$) is created. Figure 12 shows the principles of this method. The characteristic of this type of measurement enables high-speed, contactless testing. However, it limits testing to conductive materials. [15]
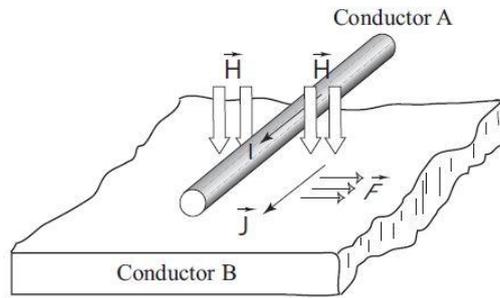

Figure 12: Schematic representation of principles of Electromagnetic Acoustic Testing [15].

5.1.9   References defects

To perform proper detection and assessment of natural defects it is necessary to base the inspection on reference standards. It is common to use metal sections similar to the parts being inspected containing artificial flaws such as flat bottom holes, side drilled holes or notches. The reference blocks are used to establish inspection parameters so that the natural defects of the certain size would be identified. Due to this, the type of reference defect and the size of it depend on the characteristics of natural flaw in focus.

Flat bottom holes and side drilled holes are very common standard reflectors. The former ones are described as ideal reflector due to its circular shape and plane surface perpendicular to the incidence beam. They are usually applied when longitudinal wave inspection is considered. Yet, it is also possible to apply FBHs as a reference for shear waves inspection, if drilled with the angle other than normal to the surface. SDHs defects are often used for investigation of surface sensitivity of the probe as well as the reference for the inspection using shear waves. The established relation between the diameter of FBH and SDH giving the same signal response is given in Eq. 7. The equation is valid if $z > 0.7N$ and $d_{SDH} > 1.5\lambda$. [19]

$$d_{FBH} = 0.67\sqrt{\lambda\sqrt{d_{SDH}}z}$$

Eq. 7

Where:

d_{FBH} – diameter of flat bottom hole

λ – wave length of ultrasonic wave

d_{SDH} – diameter of the side drilled hole

z – sound path

The reference standards are used to set a common, consistent way of signal interpretation. However, one can argue whether they are adequate representation of natural flaws. This is due to several reasons. To be more precise, factors like flaws type, shape, positioning and surface conditions have high impact on the amount of signal reflected from it. Considering this, the interpretation of ultrasonic signal based on the magnitude of the indication compared to the reference might result in faulty interpretation and sizing of the defect. Since no better approach has been established, this underlines the claim that adjusting the testing procedure to probable defects characteristics, size and positioning is essential.

Another important issue is the manufacturing of the reference defects. In order to obtain reliable reference signals, it is necessary to perform the calibration on artificial defects that are manufactured with high precision, having accurate sizes and positions in the material. Considering manufacturing of flat bottom holes, special type of drill bits have to be used to avoid the conical shape at the bottom of the hole. It is of high importance, since only plane top surface provides close to ideal reflectivity. If the manufactured defects vary from the specification, simulation can be used as a tool to assess the impact of the changes.

5.1.10 Detectability of natural defects

Considering the fact that lack of fusion has been pointed out as one of the two most critical types of defects in this work, as well as, the influence of geometric characteristics on its detectability, the research has been focused on collecting information about detectability of LoF using UT.

5.1.10.1 Lack of fusion

No information has been found in the literature on the detectability of LoF in parts manufactured using LMD technique. Since welding inter-run lack of fusion is of similar characteristic to the one occurring in LMD, this section will focus on detectability of LoF in multi-pass welding joints using ultrasonic tests.

Lack of fusion defects can be divided into two groups depending on their detectability. The first group includes voids or non-metallic inclusions that can be detected using UT. The other group are free from discontinuities, e.g. weaker bonding, that is no obstacle for ultrasonic wave and does not produce any indication. What is more, sometimes indications of the defect are so small that they will produce too weak signal to be detected. Considering the fact that even small LoF defect can be critical to fatigue behavior, UT cannot be a fully reliable method of detection. This is highly problematic in case of number of small discontinuities that can easily form a crack, if being subjected to tensile load. Nevertheless, among nondestructive tests, ultrasonic testing seems to be most effective in detecting LoF. [20]

Since inter-run lack of fusion is hard to detect by any nondestructive technique, still the most effective way of disclose it is by using destructive techniques, i.e. bend test and micrographic examination [13]. Yet, if UT used for inspection, the good practice is to use normal ultrasonic probe for detection of inter-run LoF.

While performing ultrasonic testing, it is important not to mistake the indication of pore with LoF indication since pores are to some extent, depending on the levels of acceptance, acceptable defects.

5.1.11 Simulation of ultrasonic inspection

Nowadays, the application of simulations being used in initial phase of product and process design grows of interest as it decrease the project and production lead time as well as aids to deliver solution of higher quality.

There are several simulation softwares available on the market, i.e. simSUNDT, CIVA, Image3 and many more. Though having different options available, they all are complex tools that enable optimization of inspection parameters, analysis of the design of inspection as well as provide a guiding tool for inexperienced user. [21]

5.2   Eddy Current testing (ECT)

Among many possible applications, nondestructive inspection using eddy current enables to detect material defects that are positioned at surface and in close to surface areas. In principle the eddy current technique measures materials response to electromagnetic field at a certain alternating current frequency, from a few kHz to MHz [15]. This method is very sensitive to small size defects and has the advantage of producing immediate results. However, there are two major limitations of this technique. Firstly, only conductive parts can be subjected to the inspection. Secondly, the depth of penetration is limited. There are also several other limiting factors influencing usability of ECT such as surface roughness, lift-off of the probe etc.

Even though only the impedance change is being measured during the test, there are various ways in which the response signals of eddy currents can be displayed. Often the amplitude changes are measured and simply displayed on the screen. Yet it is also common to compute the values of measurement and display them in the desired form, e.g. conductivity or coating thickness etc. If both amplitude and phase are measured then they are plotted on impedance plane.

5.2.1   Basic principle of eddy currents

The phenomenon that enables to use ECT as an inspection technique is the electromagnetic induction. To be more precise, when the altering current flows through a coil it generates a magnetic field circulating around the wire of the coil. If the conductive material is influenced by the generated magnetic field, it will produce circle shaped currents in the conductor. Induced eddy currents produce a secondary magnetic field that is opposing to the magnetic field of the coil. If there is change of conductivity of tested material caused by defects or inhomogeneities in material and physical properties of specimen, the magnitude of the secondary magnetic field will change. One of the ways to measure the changes of both secondary and primary magnetic field is to use second coil connected to measuring device. This principle is presented in the Figure 13 below. [15]
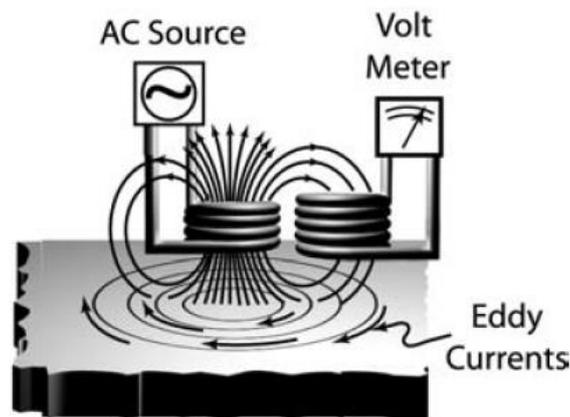

Figure 13: Basic principle of Eddy Current testing [15].

5.2.2 Self and Mutual Magnetic Induction

As mentioned before, alternating current flowing through a wire is producing a magnetic field of concentric rings that are perpendicular to the current flow. If the wire is in form of a coil then the magnetic field loops generated by the changing current will cross with loops of wire inducing a voltage in the same circuit. This voltage will oppose to the primary voltage of the circuit. The described phenomenon is called self-induction and is described by Faraday's Law, see Eq. 8. [22]

$$V_L = N \frac{d\emptyset}{dt}$$

<div align="right">Eq. 8</div>

Where:

V_L – induced voltage in volts

N – number of turns in the coil

$\frac{d\emptyset}{dt}$ – rate of change of magnetic flux in webers/second

This relation can be also presented using inductance L and the frequency of current $\frac{di}{dt}$, see Eq. 9.

$$V_L = L \frac{di}{dt}$$

<div align="right">Eq. 9</div>

According to Lenz's Law the indicated current will flow in such direction, that the magnetic field produced by it would oppose the change in primary magnetic field.

If a conductive material is positioned close to the AC circuit the mutual inductance occurs. It is based on the same principles as the self-induction. In this case the induced current in conductive material creates magnetic field opposing to changes of the primary field. The use of mutual inductance is presented in the Figure 14. [22]
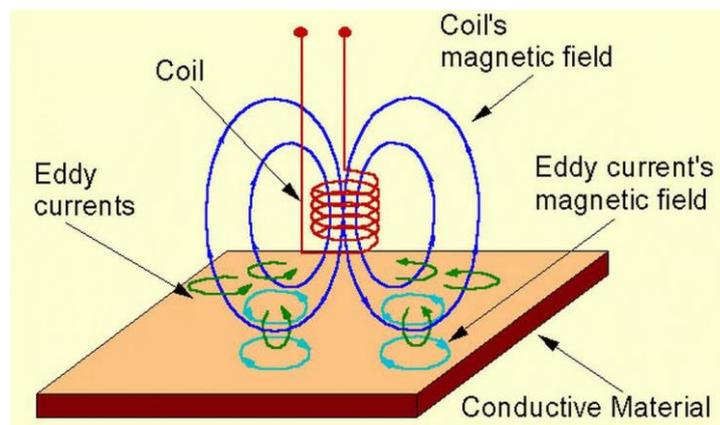

Figure 14: The use of mutual induction in the ECT inspection [22].

5.2.3 Impedance plane

Electrical impedance Z is described as the entire opposition to the current flow created by the circuit. As the ECT probe consists of a wire coil, one should consider influence of both resistance R and inductive reactance X_L to be able to assess the opposition to the current flow. Considering the fact that resistance and inductive reactance are 90° out of phase the impedance is calculated as the vector sum of both.

The vector representation of the resistance and inductive reactance is used to display the results of eddy current test on impedance plane. The schematic vector representation of the parameters is shown in Figure 15.
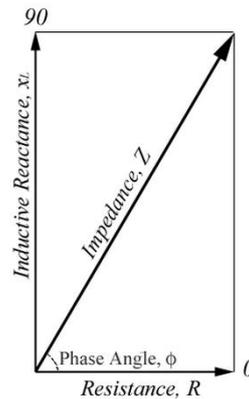

Figure 15: Basic concept of impedance plane created by resistance and inductive reactance [22].

There are several causes for change in impedance of the coil, e.g. varying conductivity, magnetic permeability, liftoff, sample thickness or layer thickness, influence of the edge of the sample. Additionally, one important factor is the presence of flaws in the material. Figure 16 below presents sample responses of the impedance depending on a change of one of the parameters. As can be noticed in the figure, the positioning of the indication on impedance plane depends also on the material type and its properties.
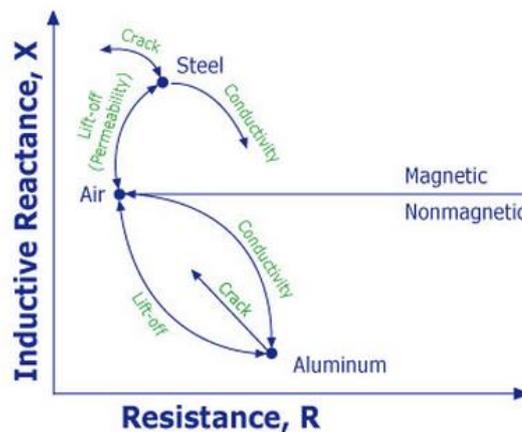

Figure 16: Response of the signal on impedance plane regarding to change of one of parameters: liftoff, crack appearance, conductivity [22].

5.2.4 Depth of penetration

The eddy current technique is suitable for near surface and shallow sub-surface measurements. The magnitude of eddy current decreases exponentially as the depth below the surface increases. This phenomena is called skin effect. The depth of penetration d in the material depends on several factors like: frequency of alternating current f, magnetic permeability μ as well as electrical conductivity σ. The relation can be described by the equation Eq. 10 below. [14]

$$d = (\pi f \mu \sigma)^{-0.5}$$ *Eq. 10*

Simplified relation between probe frequency, conductivity, permeability is shown in the Figure 17 below.
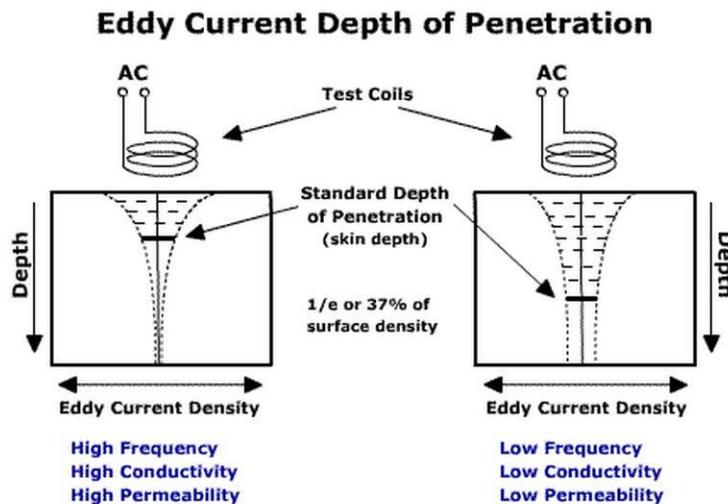

Figure 17: General influence of frequency of measurement, materials conductivity and permeability on the depth of penetration. [22].

5.2.5 Eddy Current probes

Eddy current probes work based on the same principle as electromagnetic transformers. One coil, being excitation circuit, produces a magnetic field of known properties whereas the secondary coil measures the output being the response to the created magnetic field. Both of these elements must be very accurate in order to detect very small changes. Depending whether the excitation coil is separate of the secondary coil there can be two configuration labels: single and double. [15]

Depending on the configuration of the secondary coil two types of eddy current probes can be distinguished: absolute and differential. The first type measures changes in the test piece in relation to itself. It is applicable for both detection of sudden changes, i.e. cracks, and slow change of geometry. On the other hand, differential probes base detection of a flaw on comparing responses of two coils. They are commonly used for detection flaws like pores, cracks and voids as they are able to detect sudden, minute changes in magnetic field at the same time being insensitive to slow variations caused by change of materials properties and geometry. Figure 18 shows the difference in response of the probe depending on configuration.
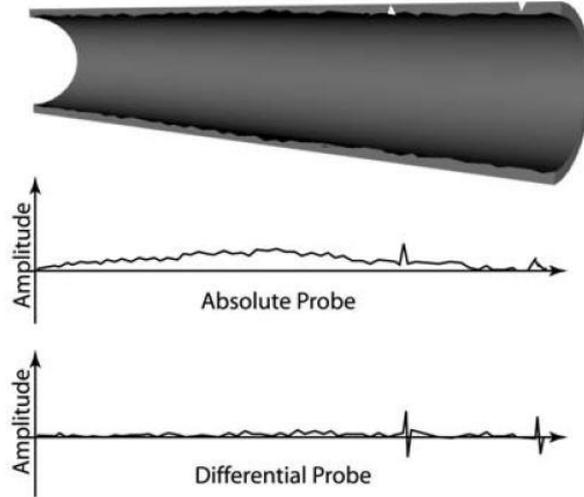
Figure 18: Difference in response of absolute and differential probe for material thinning, void and crack [22].

5.2.6   Frequency of the probe

Frequency of the eddy current probe influences both depth of penetration as well as the probe impedance response. If the value of the frequency is high then the depth of penetration will be small. At the same time if the frequency tends approaches infinity, the resistive losses of the material will also decrease. Due to low resistance, the secondary magnetic field will have similar magnitude as the primary one. As a consequence the differential value between both fields will be low. Decreasing the frequency, deeper penetration is possible however at the same time resistive part of the impedance will increase as well. The influence on the impedance plane is presented in the Figure 19 below. The graphs present the normalized impedance in order to reduce the effects of internal resistance of the probe as well as frequency. In this way, the value of impedance depends only on the properties of the target.
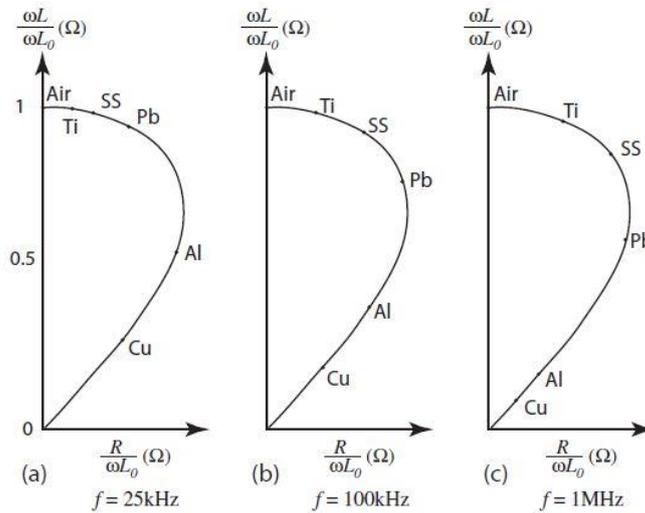

Figure 19: Influence of the measurement frequency on the normalized impedance for different kinds of material [15].

5.2.7   Liftoff

The distance between the test piece and the testing probe is called liftoff. The value of this parameter has direct impact on the inductive coupling between the probe and sample. As the distance increases the influence of magnetic field decreases. The impact of the liftoff depends also on the diameter of probe in use. Small diameter probes are much more sensitive to the liftoff changes. Additionally, the impedance changes are more significant when the probe is positioned close to the surface of the test piece.

20

6 Methods and experiments

The experiments included the two NDT techniques described before. The majority of the research was focused on the ultrasonic application for detecting internal LoF defects. Eddy current method was used as a complementary inspection technique to be used in areas where UT has limited capabilities.

6.1 Ultrasonic testing

Initially, conventional ultrasonic testing technique was used for quality evaluation of LMD/w titanium pieces. The activities included in this part of the project were focused on establishing reference for the measurements, defect detection in wall-shaped components as well as recognizing limitations of the inspection for this particular application.

6.1.1 Equipment

During ultrasonic experiments immersion testing was used. This method is commonly used as an inspection technique in quality assessment at GKN Aerospace production facility in Trollhättan. It enables automatic scans and acquisition of A-scan data for further processing.

6.1.1.1 Immersion testing

The immersion tests were performed using LS-200 inspection system produced by IRT ScanMaster. The device consists of a scanning machine with positioning system using 3 linear and 3 angular axes. Automatic scanning can be performed using transverse movement in two axis. The traversing system enables to perform planar scans as well as scans of cylindrical shapes. The machine has built-in accurate motion control system and ultrasonic hardware in combination with a signal processing software. Due to this, it allows not only to obtain real time, good quality B-scans and C-scans, but also advanced post processing of measurements and analysis of signal to noise ratio. The Figure 20 below shows the immersion equipment used for the measurements at GKN NDT laboratory at the Production Technology Centre (PTC) in Trollhättan.

Figure 20: Ultrasonic immersion equipment ScanMaster LS-200.

6.1.1.2 Ultrasonic probes

The initial immersion tests were performed using two different transducers, TLC IS1010GA and I7-0512-RG. Both of them are spherical probes generating longitudinal waves, with the nominal frequency of 10 MHz and 5 MHz, respectively. These two frequency values were chosen in order to address the issues connected with different sizes of the flaws as well as possible attenuation of the material. In the

further stage of experiments two additional probes were used to improve detectability of defects corresponding to 0.4 FBH. Due to the limited time span of the project the selection of probes was based on available probes used in production lines at GKN Aerospace. More detailed information about transducers is presented in Table 1 below.

Table 1: Parameters of ultrasonic probes used in experiments.

Probe	I7-0512-RG	IS1010GA	V317	I3-2504-R
Producer	Harisonic	LTC Ultrasound	Panametrics	Harisonic
Element size	0.75"	0.375"	0.25"	0.25"
Nominal Freq.	5 MHz	10 MHz	20 MHz	25 MHz
Focal Length	6"	3"	3"	1,5"
Wave length (Ti)	1.22 mm	0.61 mm	0.35 mm	0.24 mm

6.1.2   Test pieces

In order to perform reliable assessment of usability of UT for titanium alloys, LMD components that included both reference defects and natural defects were inspected.

6.1.2.1   Reference blocks

Initially, as the reference for the inspection, a conventional step block was used. It was manufactured from Ti-6Al-4V alloy using LMD of powder metal. The block consists of 5 steps with the lowest being 5 mm high and incrementing by 10 mm. Each of the segments consists of 3 flat bottom holes (FBHs) of different diameters; 1.2, 0.8 and 0.4 mm. The depth of all holes is identical and equals to 3 mm. In this way the reference block was used both as area-amplitude and distance-amplitude reference. The designation 'step 1, step 2, (…), step 5' used later in the text refers to step of 5 mm height, step of 15 mm height and step of 45 mm height respectively. The photos of the reference block are presented in Figure 21. The reference block was used to create TCG curves necessary to inspect pieces with natural defects.
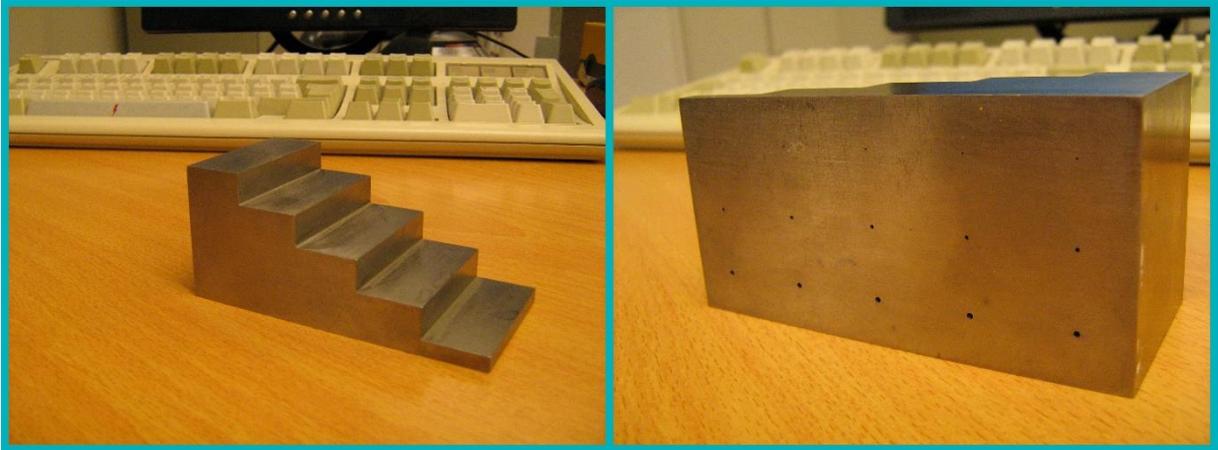
Figure 21: The reference block with flat-bottom holes.

As the project progressed, based on observed issues in LMD blocks, new reference piece was designed containing side drilled holes (SDH), see Figure 22. The aim of the new reference was to examine surface sensitivity, detectability of defects close to the edges of the walls as well as assess influence of the surface conditions on the signals produced by internal defects. More detailed drawings of the reference are presented in Appendix 1.
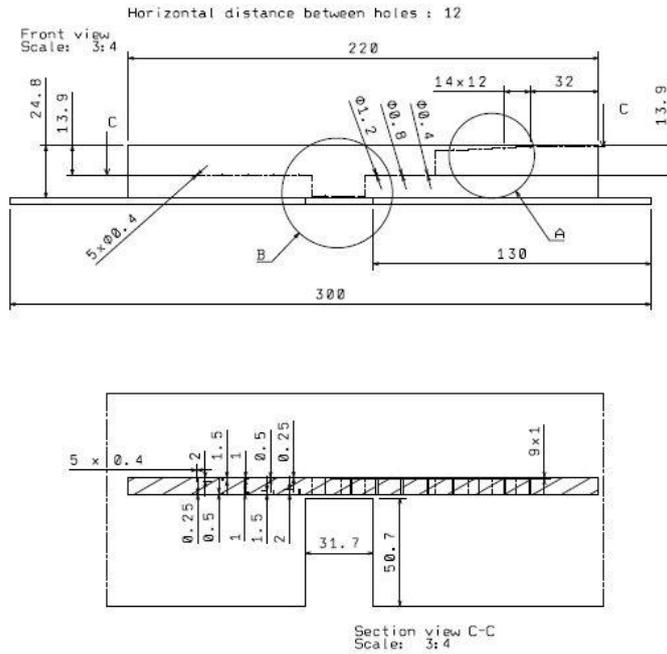
Figure 22: New reference block designed to address issues occurring while inspecting LMD pieces.

For simulation purposes an additional reference block was used. The block was made from stainless steel. Two sets of side drilled holes were used as references. The holes had two different sizes of diameter: 2.4 and 3.2 mm. More detailed information about positioning of holes included in Table 2. The Figure 23 presents the photo of the reference block.

Table 2: Depth of side drilled holes - values regarding center of the SDHs.

Diameter [mm]	2.4	3.2
Depth 1 [mm]	5	5
Depth 2 [mm]	20	20
Depth 3 [mm]	35	35
Depth 4 [mm]	50	50
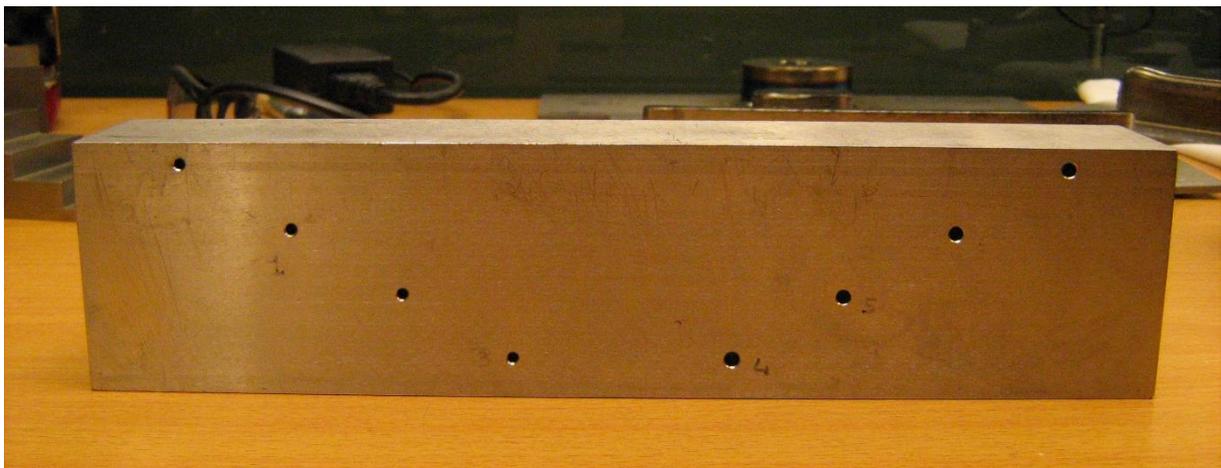
Figure 23: Reference block used to gain signal response from SHDs.

23

6.1.2.2 Test blocks containing natural flaws

A number of LMD blocks of different types were manufactured using LMD/w and tested. The initial strategy to produce relevant LMD blocks with natural flaws was to manufacture pieces with 2 beads in width and several layers in height. The thickness was determined by the internal requirements regarding LMD pieces used in a specific application. However, due to complications concerning producing natural defects that would be representative for the investigation, the group of test pieces was extended to bulky samples of various cross-sections as well as walls with more than 2 beads in thickness. Sample pieces are shown in the Figure 24.

Figure 24: Samples of pieces investigated during experiments.

In as-build state, LMD walls were characterized with smooth but rounded top surfaces as well as uneven plate surfaces distorted by the deposition of beads. In order to enable inspection, initially rounded top surface was milled to obtain surface conditions proper for UT. More detailed information about the dimensions of the pieces is included in the Table 3 below. The first block, S1ND, was manufactured with the intention of creating a reference block without defects. Parameters used for manufacturing the rest of the samples were adjusted in order to introduce LoF defects.

Table 3: Dimensions of all the tested LMD blocks.

Name	Type	Height [mm]	Width [mm]	Length [mm]
S1ND	wall	30	9.9	220
S2D	wall	30	8.8	235
S3D	wall	28.76	8.5	218
S4D	wall	29.7	8.44	220
S5D	bulky/bosses	23.1	30.9	52.56
S6D	bulky/bosses	29.1	65.3/22.1	65/21.68
S7D	wall	26.38	12.1	220
S8D	wall	26.88	12.16	219
S9D	wall	40	11.7	217
S10D	wall	30	11.5	217
S11D	wall	30	11.9	220

Figure 25 shows the as-build, raw LMD walls. In this state the walls are characterized with rounded top surface, distorted bottom surface of the plate as well as corrugated side surfaces with parallel ridges, indicating each layer of wire deposition.
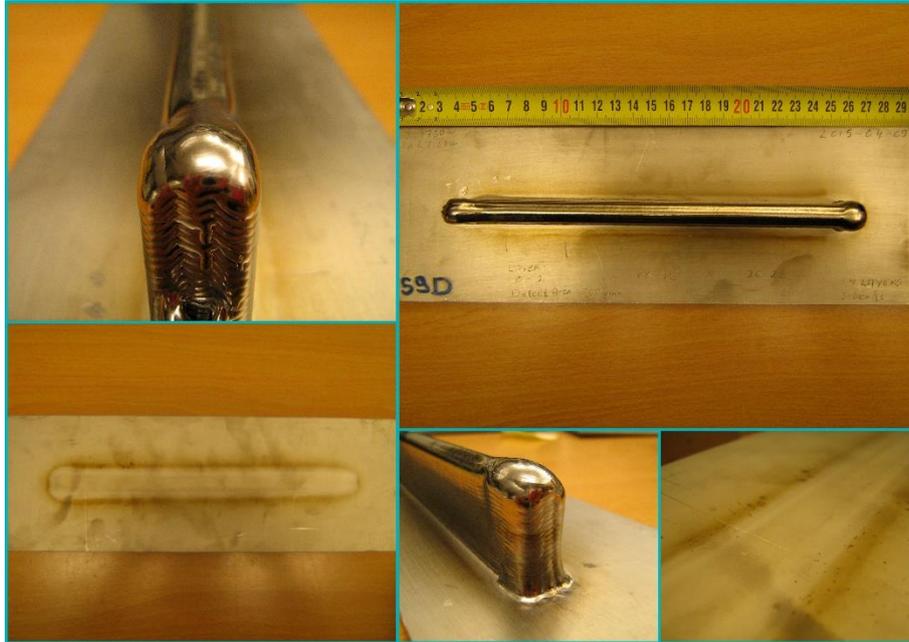
Figure 25:LMD walls in the raw state – rounded top surface (top left), distorted bottom of the piece (bottom left and right).

6.1.3 Probe evaluation

Probe evaluation was performed in several stages to obtain general knowledge about the transducers available for inspection. For each of the four transducers, theoretical values of crucial parameters were calculated. The calculations were made basing on equations Eq. 5 and Eq. 6. Damping was measured as well as attempts were made to create TCG curves according to the reference. As the proper transducer for inspection was selected, more detailed evaluation was performed.

6.1.3.1 Damping

In regard to the fact that the reference block with FBH is made from powder metal (PM) titanium alloy the suspicion was that there might be difference in damping of the signal between the blocks and the LMD pieces with natural flaws. To investigate this, the experiment was conducted for all transducers.

The procedure was based on comparing damping of signal for block step 3 and wire feed pieces of height 25 mm. The focus was set on the surface of the reference block and the gain was adjusted so that the echo of back surface was 80% of FSH. Subsequently, signal of the same amplification was induced into wire feed piece. Corresponding amplitude value of the signal from the back surface was documented.

In order to establish the attenuation coefficient $\alpha_{dB/m}$, a new experiment was performed. For both components, PM and wire feed, a comparison of damping within the material was performed. To record magnitude of second and third echo the A-scan was acquired. Similarly to previous examination, the test was performed on blocks 25 mm high. Based on equation Eq. 4 the value of attenuation coefficient was established. This method enables to include only damping of the material and the distance of penetration. For both experiments the amplification was set so that the first echo of the back wall was 80% of FSH.

6.1.4 Detailed evaluation of selected probe

In order to identify the real values of near field length as well as effective beam width, a steel ball of 3 mm diameter was used. The ball was place on conical fixture and was used as a point reflector.

To establish near field length, the amplitude of signal was maximized to 80% FSH for the nominal value of focal length. Subsequently, the probe was moved in vertical direction, so that the signal would decrease to 75%. Average of obtained values was calculated. Effective beam width was established by locating points in -/+ X and Y direction, in which the magnitude of signal would decrease to 75% using the water path established before.

6.1.5 Testing procedures

In order to present performed experiments, this section contains detailed description of testing procedure as well as the approach to interpret the results.

6.1.5.1 TCG curves

For each transducer, three TCG curves were created that correspond to 3 different sizes of flat-bottom holes manufactured in the reference block. The procedure of establishing each curve was analogous. Firstly, the probe was positioned over FBH of a certain size in the lowest step. The water path and X/Y position was adjusted to maximize the indication of FBH. The gain values were set to achieve indication of 80% FSH. After establishing starting point, the probe was moved over the FBH of the same size in the next step. Analogically, the signal from next FBH was maximized. In order to suppress the signal of the incidence surface, the amplification of acquired signal was set to 0 (Gain(T)). The initial amplification was adjusted only by the preamplifier's (Gain(P)) value.

6.1.5.2 Evaluation of scans based on TCG curves

If TCG settings are applied to the amplification settings for a scan then depending on the position on the time line, each part of the ultrasonic signal is amplified by a specific value of gain. This enables to obtain comparable signals of the flaws of the same size positioned at different depths.

When scanning components with natural flaws while using TCG settings, the interpretation of the results is based on comparison between the magnitude of the reflected signal from the defect and the level of 80% of FSH. If the indication is approximately equal to 80% of FSH it means that the defect produces similar indication as the FBH used for creating TCG curve. If the signal exceeds the 80% of FSH then it might be inferred that its size is bigger than the reference hole. However, if the indication of natural defect is reasonably weaker, it cannot be stated that the defect is smaller than the reference. One has to consider that the positioning and also surface conditions of the defect can influence its capacity as reflector of ultrasonic energy.

6.1.5.3   Ultrasonic inspection of blocks with natural flaws

In order to establish an optimal method and settings for ultrasonic inspection, several series of tests were performed. All the tests were made using IS1010GA probe with the focal point of the probe positions on the incidence surface and water path equal to 79.2 mm. This was due to the results of preliminary evaluation of probes. Table 4 provides short information on all the series of tests performed within the project. More detailed description of the measurements and results will be provided only for the ones that turned out to be relevant considering objectives of the project.

Table 4: List of performed tests including details of the setup.

Series no.	Probe	TCG	Tested blocks	Comments
series 1	IS1010GA	TCG1004	S1ND, S2-8D	---
series 2	IS1010GA	TCG1004	S5D, S6D, S7D	tested from the side of base plate, acquired A-scans of defected areas from both sides
series 3	IS1010GA	TCG1004F	S7D	tested with new TCG – suppressed front wall signal
series 4	IS1010GA	TCG1004F	reference block with FBH	scans of all steps
series 5	IS1010GA	TCG1004F	S4D, S7D, S8D	pieces after additional milling, sharp edges
series 6	IS1010GA	TCG1004F	S7D, S8D	after milling plate side, top and bottom surface
series 7	IS1010GA	TCG1004F	S4D	investigation of signals appearing close to the edge, top surface
series 8	IS1010GA	---	SDH reference block	line scan of the steel reference block for simulation purposes
series 9	IS1010GA	TCG1004F	S9D, S10D, S11D	pieces in as-build condition, scan to position LoF
series 10	IS1010GA	TCG1004F	S9D	scan after milling 5 mm of top surface
series 11	IS1010GA	----	S1ND	scan from the bottom plate surface, 3 zones, probe tilted 3 deg
series 12	IS1010GA	----	S10D	side of the wall as incidence

Three setups with different incidence surfaces were used during experiments, see Figure 26. It enabled to assess influence of various surface conditions on the ultrasonic measurements.
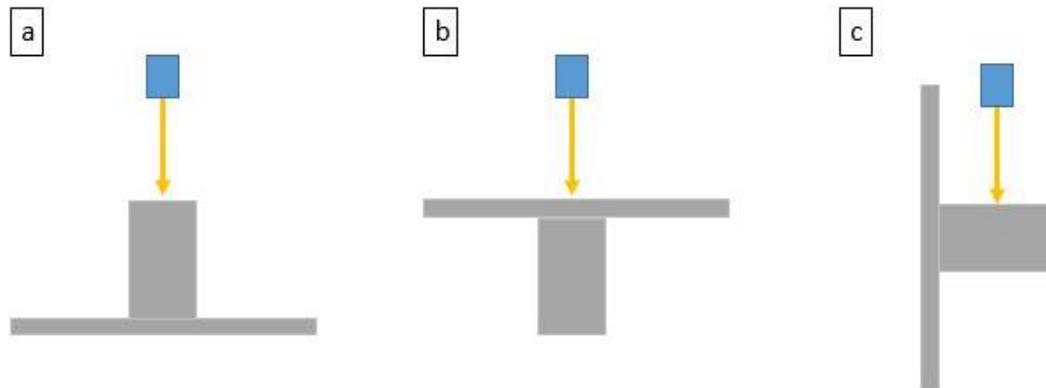
Figure 26: Three different setups: a) top surface as incidence surface; b) bottom surface as incidence surface; c) side of a wall as incidence surface.

First series of tests was performed using IS1010GA probe with center frequency of 10 MHz and amplification settings: TCG1004. There were several reasons for using this setup initially. First of all, the first series of tests was aimed to gain general information whether any defects can be detected in the blocks. Due to this, the approach was to use the most universal probe that could penetrate entire depth of various pieces. As a result of the probe evaluation, the IS1010GA probe was assessed to be the most suitable for detection defects at required depths. Top surfaces of pieces were used for incidence of the ultrasonic wave, see Figure 26 a. Since the study is focused on detecting flaws corresponding to 0.4 FBH, the TCG1004 curve was chosen. In the first series of tests all the pieces were inspected. The time gate was set to capture approximately 22 mm of the material. Due to the front wall signal, the first 3 mm of the material were not included in the measurement. Similarly, last 2 mm of the material were excluded from the measurement due to back wall signal.

The second series of measurements was performed using similar settings to series 1 however the scans were performed from two different incidence sides; firstly one more time from the top milled surface (Figure 26 a) subsequently from the base plate side (Figure 26 b). The aim of this test was to establish whether it is possible to inspect from the plate side as well as to compare the indications of defects depending on incidence side. Separate scans were performed over the defected area in order to acquire full A-scans that allowed more complex data processing and generation of B-scans.

The third series of scans was performed using new TCG curve with suppressed front wall echo; TCG1004F. This was performed in order to limit the dead zone by the top surface. The focus of the experiments was placed on the wall pieces so only test piece S7D was examined. The scan was performed using two different incidence surfaces (Figure 26 a, b).

Measurements of series 5 were performed on the pieces after additional milling of the top layers. The milling was performed to obtain better edge conditions.

In series 6 of measurements the test pieces S7D and S8D were scanned from both sides (Figure 26 a, b), top and plate side after the last one was milled to achieve fine surface. Afterwards, the results were compared with previous measurements.

Measurements included in series 11 were performed to address question of influence of plate's surface condition on the measurement when used as incidence surface. The plate was divided into three different zones: raw (as-build), polished and milled. In order to observe possible reflections in directions other than normal to plate surface the scan was performed with probe tilted 3°, see Figure 27.
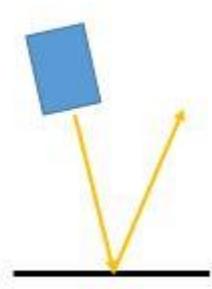
Figure 27: The setup used to check reflections of the ultrasonic beam.

Series 12 focused on investigating the possibility of using side surfaces of the LMD walls for ultrasonic inspection, see Figure 26 c. Both raw and milled surface conditions were evaluated.

6.1.5.4   Simulation

As producing reference and natural flaws corresponding to small size LoF turned out to be a complex task the decision was made to include simulation software simSUNDT to create model of probe IS1010GA. The simulation model of the probe could be later used in the simulation of inspection including detecting LoF defects.

SimSUNDT is the software developed by SCeNDT (Scientific Centre of Non-Destructive Testing) at Chalmers University of Technology. It enables to simulate the whole testing procedure including different types of UT methods, various defects and many more parameters. The software consists of windows based pre-processor and the post-processor as well as mathematical kernel enabling mathematical modelling. [23]

The results of simulations were compared with the real scans of the reference piece.

To establish similar values of signal loss between the real test and simulation parameters like elements diameter, damping and accuracy of the simulation were changed. In some cases simulation in time was preformed including probes characteristics like center frequency and band width.

In the simulations of immersion testing the SDH on depth 1 was used as the reference hole. Due to this, the losses of signal are evaluated regarding to the signal response from this reference. The water path was set to be 76.2 mm that equals to the nominal values provided by the manufacturer.

The damping in the material is not an option in the software when immersion testing is chosen. Therefore the contact probe was used to include the influence of damping. The simulated contact probe was of frequency 10 MHz and diameter 6 mm. To avoid numerical problems in simulation the SDH positioned on the depth 20 mm was used as the reference.

6.2 X-ray inspection

In order to perform comparison of the results obtained from ultrasonic inspection, x-ray inspection was performed on the samples S1ND, S2D – S8D. The x-ray images were generated using top, milled surface and side surface as an incidence.

6.3 Eddy current testing

The ECT technique was introduced with the aim of verifying possibility of inspecting areas close to the surface where the ultrasonic inspection capabilities are limited.

6.3.1 Equipment

Eddy current inspection was performed using a traverse system with two movable axis that enabled to create planar scans of the test piece. The dedicated software developed in LabView environment gave possibility to set parameters of the scan like e.g. motor rotation speed and scanning path. For the eddy current signal generation ELOTEST® B1 testing equipment was used. It enabled conditioning of signal by changing various parameters, e.g. frequency of the current, amplification of the entire impedance as well as separate amplification of resistance and inductive reactance. The impedance change was displayed on the impedance plane as well as in form of line scan and C-scan.

6.3.1.1 Eddy currents probes

Three different types of probes were available for measurements. One of the three probes was a double probe with transmitter and receiver coil, which was custom made for GKN Aerospace. The other two available probes were absolute probes that use higher inspection frequencies than the former one.

6.3.2 Test pieces

Eddy current tests were performed on two different types of test pieces. The experiments started with establishing inspection parameters using a reference plate. Subsequently, tests were performed on previously prepared LMD S10D wall.

6.3.2.1 Reference plate

Within the project work, a reference plate was designed with artificial EDM notch type defects of length 0.4 mm, 0.8 mm and 30 mm. The specific size was chosen to address the defect detectability requirements. The defects were machined in a Ti-6Al-4V plate of thickness 2 mm. The notches were designed to have various depths in order to verify the depth of inspection of each probe. For equipment adjustment purposes three 30 mm long notches were machined of the depth 1.2, 0.8 and 0.4 mm. The reference plate is presented in the Figure 28.

No	1	2	3	4	5	6	7	8	9	10
Depth	1.2	0.8	0.4	1.6	1.4	1.2	1	0.8	0.6	0.4
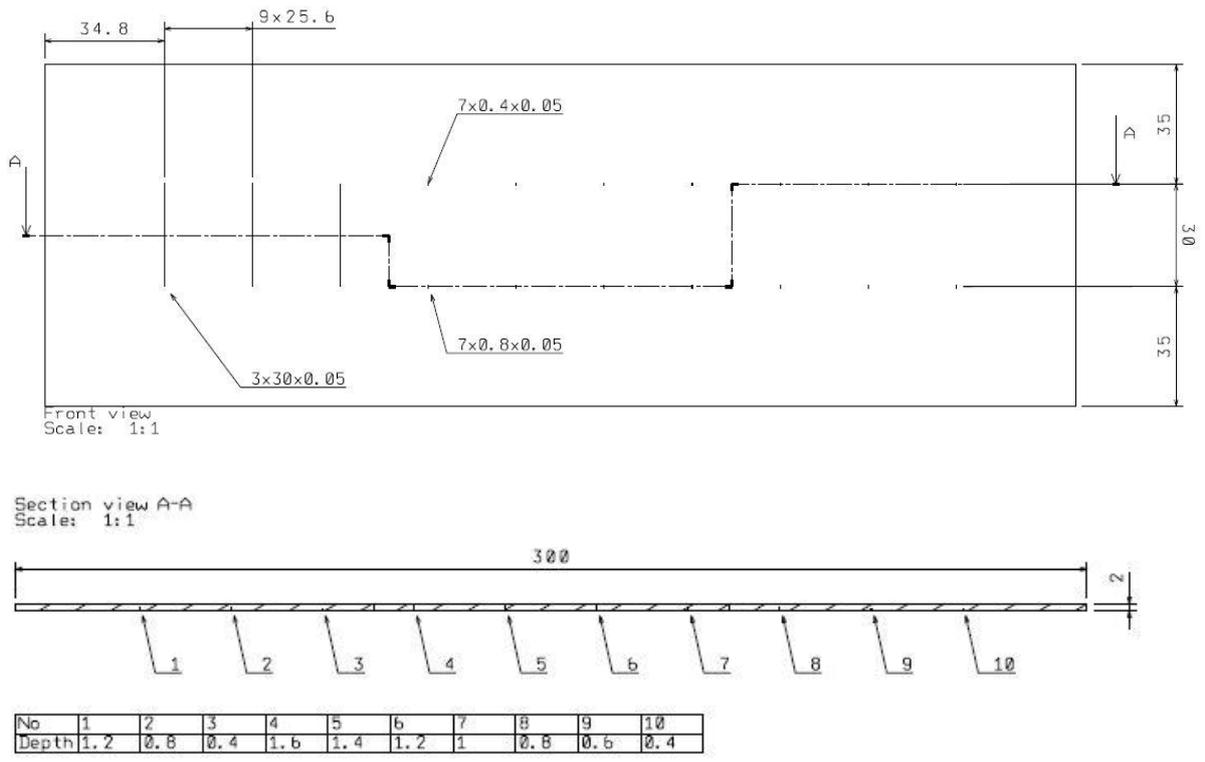
Figure 28: Reference plate for eddy current testing.

6.3.2.2 Test blocks containing natural flaws

One of the LMD wall components (S10D) was prepared for eddy current tests. The aim of these inspections was to examine influence of surface conditions on the impedance changes. Due to this one of the sides of the wall was milled in order to obtain comparison between raw and machined surface conditions Figure 29.
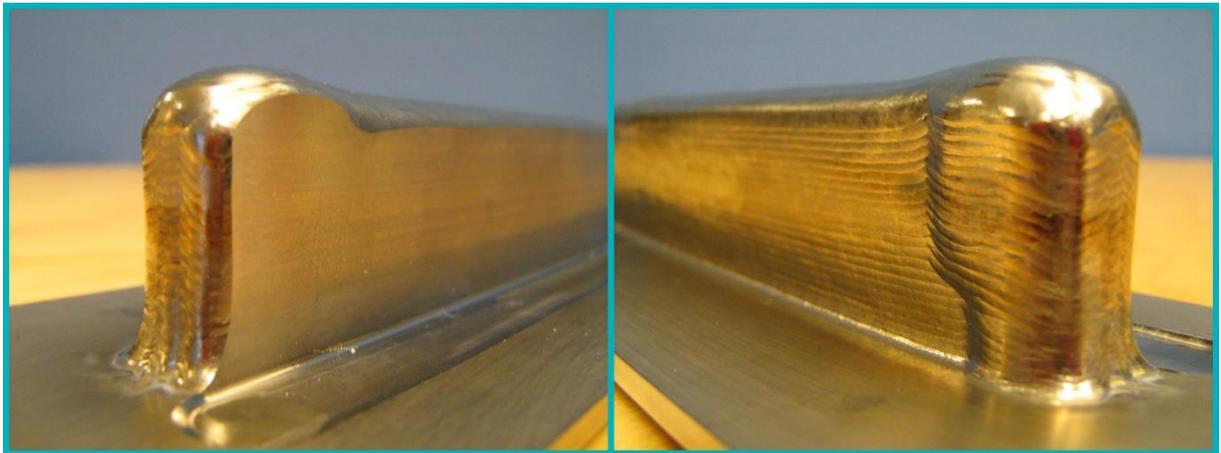
Figure 29: LMD piece prepared for eddy current inspection.

6.3.3 Testing procedures

Considering the fact that among all the available probes, the transmitter-receiver one is the most suitable for deeper penetration, the focus was placed on establishing the limits of detectability of artificial defects using this probe. Current frequency was set to $100\ kHz$ according to calculations of most optimal penetration depth.

6.3.3.1 EC inspection of the reference plate

In order to perform reliable measurement, inspection parameters like: frequency, amplification and phase had to be adjusted.

Initially, two different probe's positions, perpendicular and parallel to the length of the notches, were investigated. The tests were performed with the probe being in contact with the defect-free surface. Figure 30 shows schematic representation of described positioning, the dimensions on the drawing do not correspond to the real sizes of probe and defects.

Figure 30: Schematic drawing of probe's positioning: parallel to the length of the notch (left), perpendicular to the length of the notch (right).

Subsequently, subsurface inspection was performed using the defect-free surface. The long notches were used to establish approximate values of all necessary parameters. Applying the values, a trial scans were performed giving the information about necessary readjustments to obtain best possible detectability of 0.8 mm size notches. After each readjustment of some of the parameters and setup, the value of phase was altered so that the indication of the flaw would be aligned with vertical axis of the impedance plane. The low pass filter was applied to avoid the influence of signal noise caused related to cable vibrations. As the final result of multiple trials, parameters of inspection were established that would enable detecting all seven notches. The same settings were used to examine the 0.4 mm long notches.

Similar examination was performed to establish conditions for surface inspection. Analogous procedure of establishing settings was used. The surface with notches was used for the inspection.

6.3.3.2 EC inspection of LMD piece

Using settings established for 0.8 mm reference notches, scans were performed on two sides of the wall, one in raw condition the other in milled condition. The area of inspection included defect area with LoF positioned in the middle of the width of the wall. The positioning of the probe was adjusted so that the longer side of the probe would be aligned parallel to the top surface of the wall.

6.3.3.3 Verification of dimensions of the EDM notches

The accuracy of manufactured artificial defects is of high importance and every deviation influences magnitude of impedance change. Due to this, the size and depth of EDM notches was verified using optical microscope equipped with special devices providing accurate position of objective lenses and focal point.

The measurements of length and width of artificial defects were performed with the focus of microscope placed on the surface of the plate. Dedicated software equipped with measuring tool enabled sizing of defect. The depth of notches was established by moving focus from the surface to the bottom of the notch.

7 Results of experiments

This section provides the description of results of both ultrasonic and eddy current inspections. It starts with the description of ultrasonic inspection and continues providing results on eddy current tests.

7.1 Ultrasonic testing

In order to assess the capability of using UT for inspection of LMD wall-shaped parts, several different experiments were performed. The aim was to gather as much information as possible about available probes, damping of the signal caused by LMD Ti-6Al-4V as well as to identify limitations of inspection due to characteristics of ultrasonic testing in combination with the specific design of these components. The results of these experiments are presented in sections below.

7.1.1 Probe evaluation

Table 5 presents theoretical values of characteristic parameters of four evaluated probes.

Table 5: Calculated theoretical values.

Probe	I7-0512-RG	IS1010GA	V317	I3-2504-R
NFL Y_0^+ [mm]	306.51	168.92	136.22	170.28
Focal zone [mm]	121.38	56.10	66.62	15.33
Beam width [mm]	2.42	1.15	0.91	0.36
Wave length in Ti-6-4 [mm]	1.22	0.61	0.31	0.24

7.1.1.1 Damping

The results of initial tests comparing magnitude of background echo of reference block and LMD/w test piece are stated in the Table 6 below.

Table 6: Results of first investigation of differences in damping between the PM block and LMD/w.

Probe	I7-0512-RG	IS1010GA	V317	I3-2504-R
Reference PM [% FSH]	80	80	80	80
LMD/w [% FSH]	72	65	75	65

The second experiment, performed for the transducer IS1010GA revealed that the attenuation coefficient $\alpha_{dB/mm}$, attenuation related to distance in millimeters, was of similar value for both materials. Table 7 below presents the results of experiment.

Table 7: Results of damping coefficient values for probe IS1010GA.

Piece	Reference PM	LMD/w
2nd echo	80	80
3rd echo	34	34
$\alpha_{dB/mm}$	-0.15	-0.15

7.1.2 TCG curves

Using reference block, the TCG curves were created for all the immersion probes. However regarding specific characteristics of probes, it was impossible to create curves including FBH on each depth for the three of the four probes. Only the probe IS1010GA, nominal frequency of 10 MHz, enabled establishing of full TCG for all the steps of reference block. In Table 8 below the results for all four

probes are summarized. The section below explains limitations that were observed for each of these individual transducers.

Table 8: Summary of results for TCG curves. Symbols: + full curve, +/- possible to use in majority of the inspection depth, +/-- possible to use only for the shallow depth.

Probe	I7-0512-RG	IS1010GA	V317	I3-2504-R
0.4 FBH	+/-	+	+/-	+/--
0.8 FBH	+/-	+	+/-	+/--
1.2 FBH	+/-	+	+/-	+/--

Regarding probe I7-0512-RG, the indication of front wall echo created the dead zone of 5mm disabling detection of the FBH in the step 1 of the reference block, see Figure 31. Despite the attempts to suppress the front surface echo, the dead zone would still remain large enough to prevent the detection of the reference flaw from step 1.
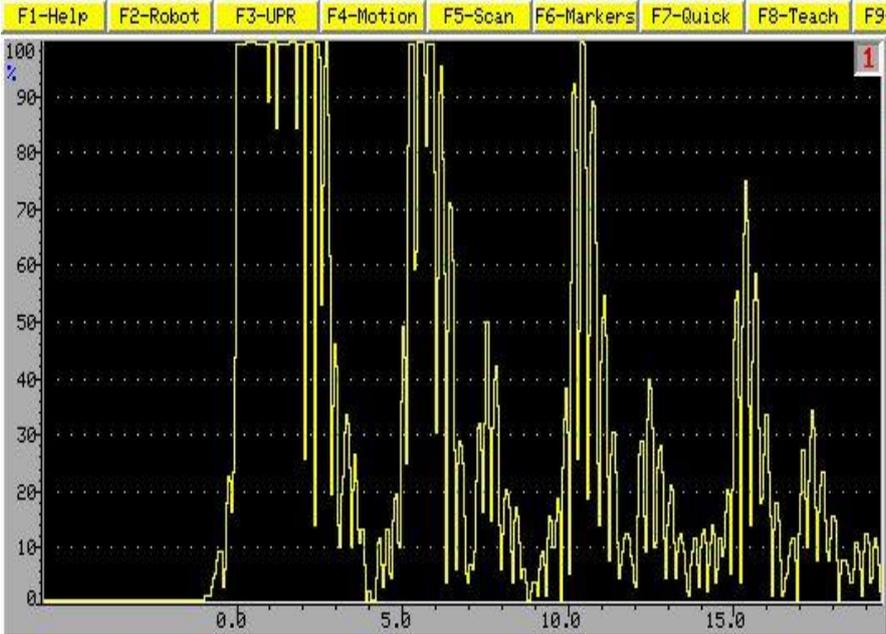
Figure 31: A-scan of the signal generated by probe I7-0512-RG placed over step 1 – the dead zone on about 4 mm.

When probe IS1010GA was used, it was possible to create TCG curves including FBHs positioned on 5 different depths for all three diameters of holes. The signal was stable even for high values of amplification. Lowering receiver amplification of front echo signal to 0 dB, it was possible to reduce the dead zone down to about 1.2 mm. However, TCG curves would show noticeable grow of background noise, see Figure 32 a. The signal to noise ratio's value would remain above 3. Adjusting of preamplifier value as well as amplitude of the voltage sent to the crystal it was possible to improve signals quality, see Figure 32 b. Still at the points on time line where the new amplification point was introduced, e.g. 32th sec and 42th sec on the A-scan, a higher value of the noise can be observed.
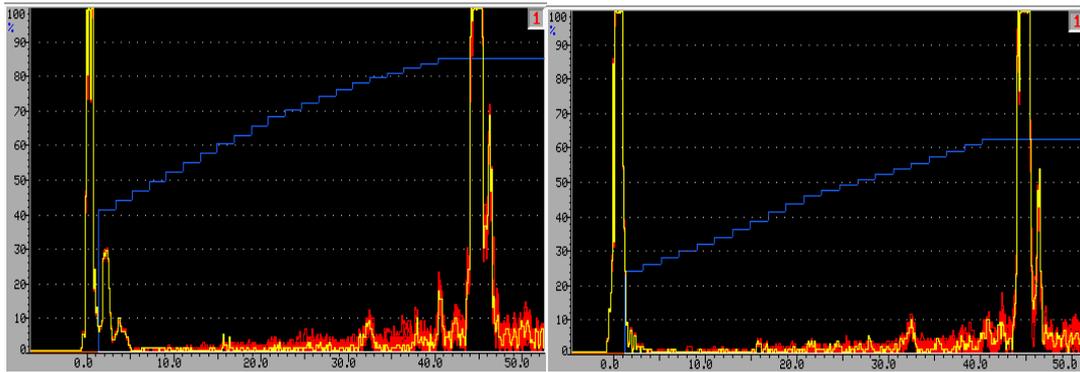
Figure 32: Probe IS1010GA - entire TCG curve: a) TCG1004F - high value of amplitude of voltage, low value of preamplifier; b) TCG1004M - low value of voltage amplitude, high value of preamplifier. Red signal shows the signal within last 3 sec of measurement.

For the probe V317, depending on the hole size, different limitations can be pointed out. To start with, for 0.4 FBH, it was possible to create amplification curve only until step 3 (25 mm). It was impossible to obtain amplification high enough to acquire signal of 80% of full screen height (FSH) for FBH in the step 4, see Figure 33. For the FBH with larger diameter, it was possible to create entire amplification curve, however for the depth larger than 35 mm the signal was unstable. Due to this, the curve could be used for defect's identification but not for quantification. Additionally, it could be observed that the noise became stronger than in case of the previous probes.
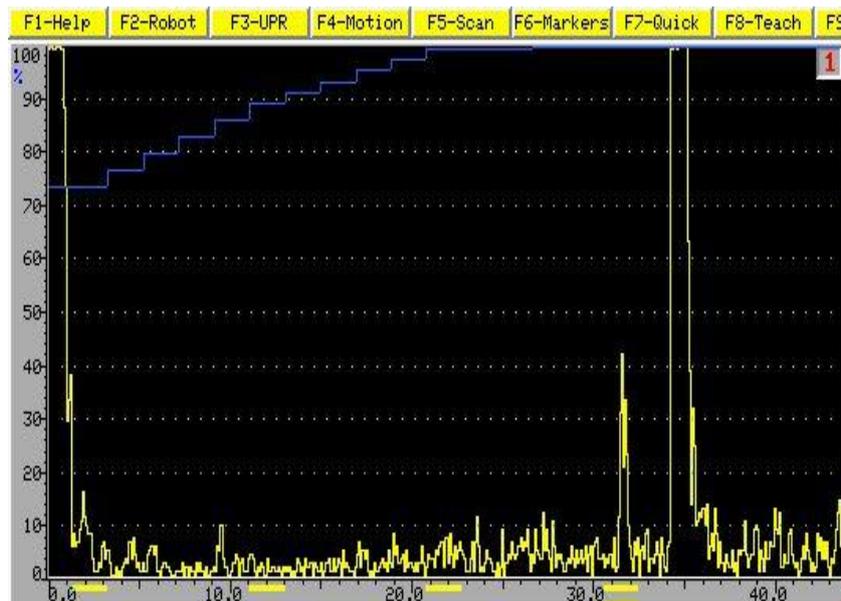
Figure 33: Probe V317 - limit of amplification for 0.4 FBH.

As expected, the examination of the probe I3-2504-R revealed that it is suitable for inspection of limited depths. Considering 0.4 FBH, the TCG curve could be created only for step 1 of the reference block. For higher penetration depth, strong random noise would appear, see Figure 34. Using lower amplification for detection 0.8 and 1.2, it was possible to create TCG curves that include defects manufactured in step 2 and 3 respectively.
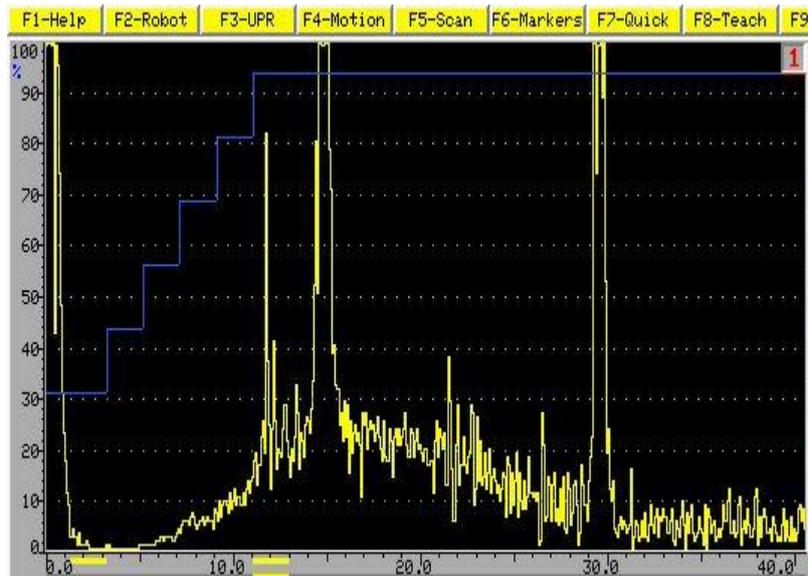
Figure 34: Probe I3-2504-R - high random noise when creating the TCG curve for 0.4 FBH, step 2.

7.1.3 Ultrasonic inspection of blocks with natural flaws

The section below describes results of significant inspection series considering the objectives of the project.

7.1.3.1 Series 1

The first series of tests resulted in identifying blocks in which defects could be detected. Only three LMD pieces, S5D, S6D and S7D showed strong indications comparable to signals reflected from 0.4 FBH. Some small changes of signal magnitudes were observed for components S2D and S3D. Figure 35, Figure 36, Figure 37 present respectively C-scan of the pieces S5D, S6D, S7D. At this stage of the study, signals of indications by the edges of blocks were disregarded. Visible pixels of red color indicate signal between 70-100% of magnitude; signals comparable to the one produced by 0.4 FBH reference. White pixels indicate signals of magnitude over the scale.
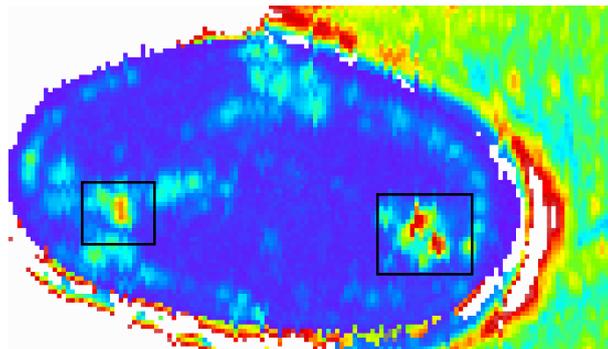
Figure 35: C-scan of part S5D – defects marked by squares. Yellow and red color indicates signal values between 70-100%. White pixels indicate signals over scale.
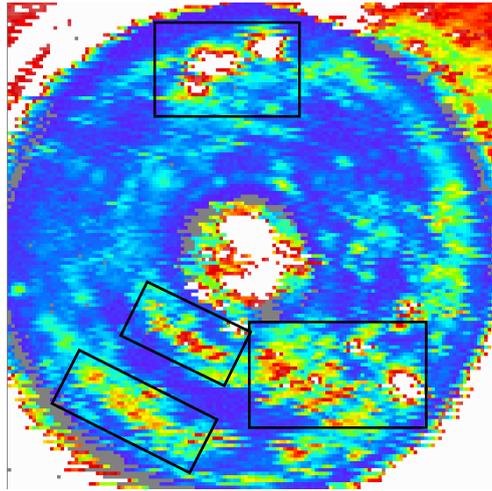
Figure 36: C-scan of part S6D – defects marked by squares. Yellow and red color indicates signal values between 70-100%. White pixels indicate signals over scale.
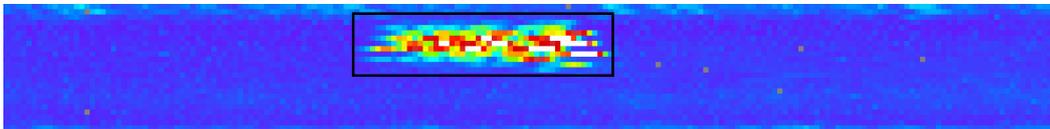
Figure 37: C-scan of part S7D – defects marked by squares. Yellow and red color indicates signal values between 70-100%. White pixels indicate signals over scale.

7.1.3.2 Series 2

This series of measurements was designed to obtain information whether it was possible to use the plate surface as incidence side (i.e. front surface). The defected areas were scanned from two sides. The results in forms of C-scan were compared. As a general observation, it was possible to detect the defect in similar positions, scanning from both incidence surfaces. However, the magnitude of indication were different, see Figure 38.
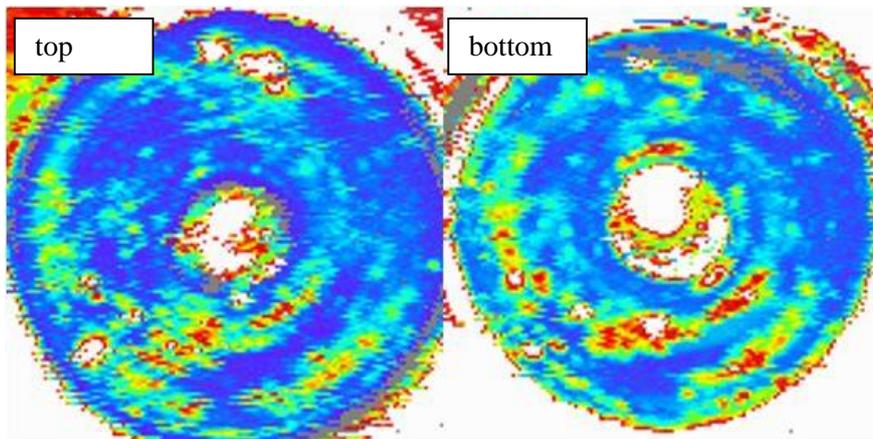
Figure 38: Part S6D scanned from two different incidence surfaces: top – milled surface, bottom - plate side.

7.1.3.3   Series 5

Using top surface as incidence, in close to the surface area a constant indication of approximately 30% of FSH was observed (green pixels in the background). The indication disappears in the area close to the edges of the LMD piece. Indication partially observed while inspecting from the other side. Differences in signals magnitude are observed depending on choice of front surface (i.e. side of incidence), see Figure 39.
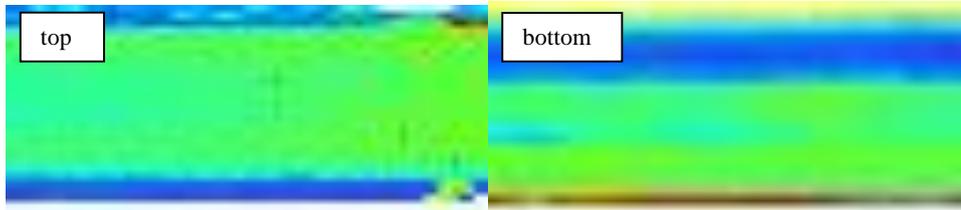
Figure 39: C-scan of the piece S8D, incidence from the milled top surface (top) and raw plate side (bottom).

On the A-scan below, the indication close to the surface is presented. It is positioned exactly at the point of time line where first amplification is applied, see Figure 40.
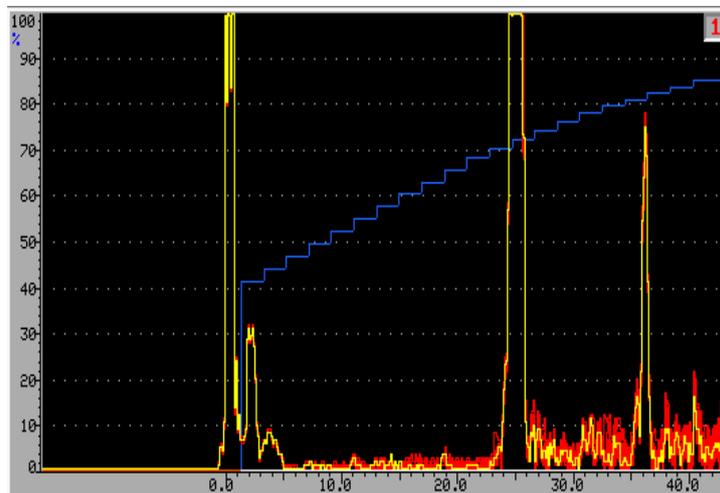
Figure 40: Signal response in form of A-scan. Constant signal of 30% in 2-3 s on the time line. TCG1004F was used for signal amplification – blue step curve.

Measuring the vertical dimension of the area representing the surface of the wall, a difference in values was observed depending on the incidence surfaces. For S8D, scanning from the milled top surface (setup showed in Figure 26 a), the width of the wall on the scan was equal to 13.2 mm. As for the result of scan performed from the raw plate surface (setup showed in Figure 27 b), the width of the wall was measured to be 9.51 mm. This tendency was observed for the other pieces scanned from two sides.

While analyzing the results of measurement, several indications were observed by the edges of all tested pieces, see Figure 41. More detailed results of inspection can be seen in Appendix 2. The indications were investigated more in subsequent measurements to assess their origin.
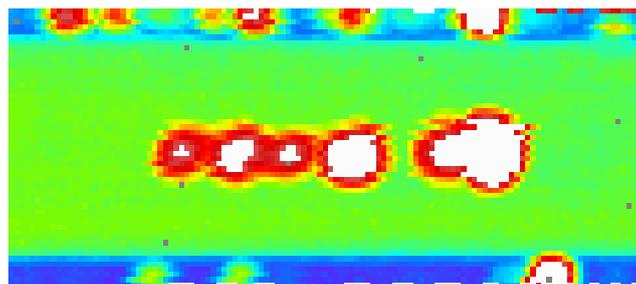
Figure 41: The C-scan presentation of the piece S7D with visible indications by the edges.

38

7.1.3.4 Series 6

The vertical area was measured again in respect to the incidence surface. Considering sample S8D, for the milled top surface the width value remained similar; 13.25 mm. On the contrary, the width value measured on the C-scan performed from the milled plate side increased to 11.98 mm. This indicates that milling bottom surface enabled to acquire more signals induced in the wall. This tendency was observed for other pieces after milling the plate side. Still, the A-scan of the signal from close to the edge area of the piece shows the influence of the signal generated by the surface of the plate on magnitude level of 30% FSH.

On the contrary to measurements from series 5, see Figure 41, no indications close to the edges were observed after milling the bottom surface of the plate.

The scans performed in series 6 are visible below in Figure 42 and Figure 43. The yellow pixels visible in the top right corner in Figure 42 are partial signals of the back wall captured by the gate and should be disregarded. More detailed results of the inspection of piece S7D are presented in Appendix 3.
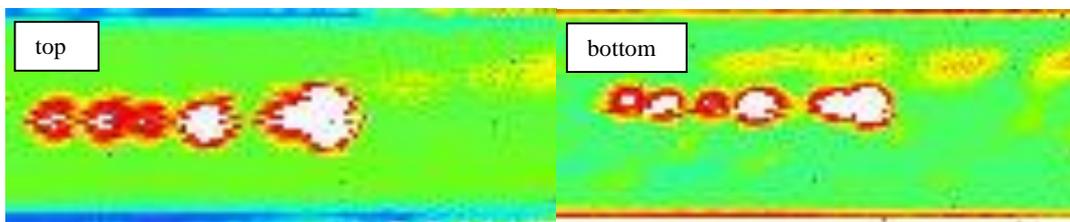
Figure 42: Scan of part S7D in series 6.
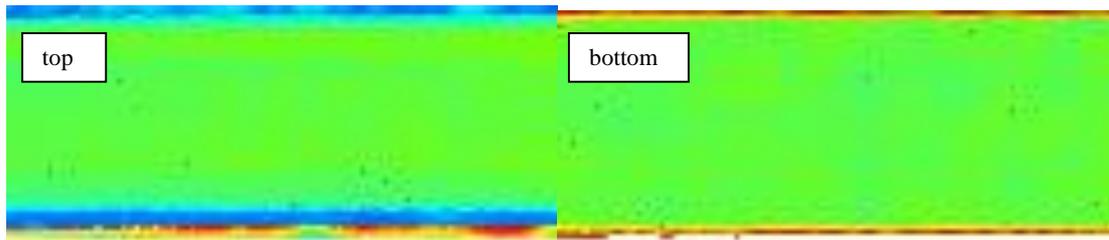
Figure 43: Scan of part S8D in series 6.

7.1.3.5 Series 11

Results of scans with tilted probe show that plate surface in raw condition as well as polished surface (Figure 44, a, b) support reflection of the sound beam in directions other than normal to the plain surface of the piece. The two stripe-like, continuous indications mark distortions caused by deposition of two beads. White color of pixels indicates high magnitude of signal, over set scale. In milled conditions all the energy of the wave beam was reflected away from the probe, see Figure 44 c. Several gray pixels visible on the scans are marking area where no signal was acquired.
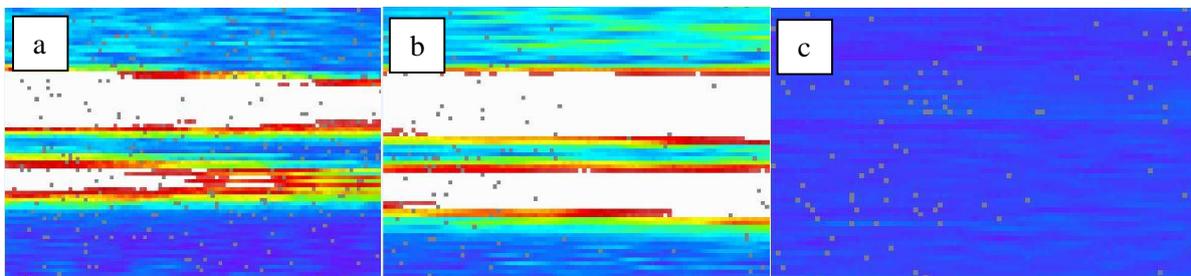
Figure 44: C-scans of the piece S1ND: a) raw plate surface, b) polished plate surface, c) milled plate surface.

Results of series 12 show the influence of surface roughness of the side wall on ultrasonic signal, see Figure 45 a. Based on different colors of the pixels on the C-scan it can be shown that the surface conditions of the side wall cause loss of signal. The assessment is based on different amplitudes of signals reflected from the surface. Additionally, the scan with gate to acquire signals between front and back echo does not indicate presence of flaws was identified in previous scans, see Figure 45 b.
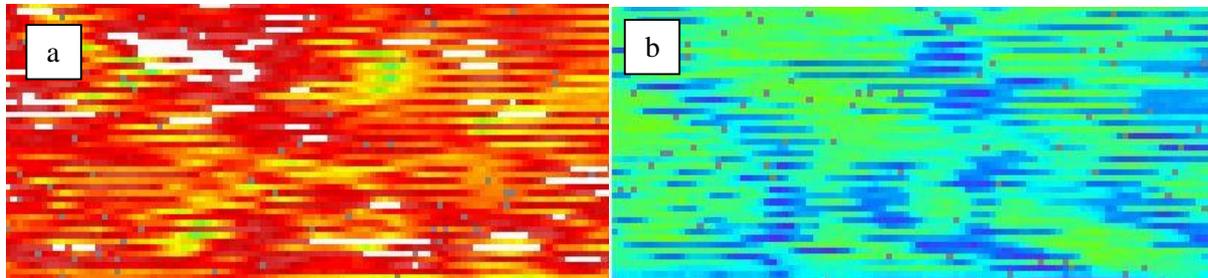
Figure 45: C-scan of the piece S10D with incidence surface being rough side surface of the wall: a) gate on the incidence surface 80% FSH, b) gate between front and back echo TCG1004F.

7.2 Simulations

The line scan was performed using IS1010GA in order to establish reference values for the simulation. The obtained values are presented below in Table 9.

Table 9: Values of the signal obtained from the line scan of SDHs with the diameter 2.4 mm.

SDH 1	SDH 2	SDH 3	SHD 4
Signal value [% FSH]			
83.843	32.385	18.117	8.313
Loss of signal [dB]			
0	-8.262	-13.307	-20.0742

The initial approach was to vary values of piezo element's diameter. The results of these simulations are presented below in Table 10.

Table 10: Results of the simulations – element's diameter as the variable. The values of the loss of signal are provided in decibel scale.

	SDH 1	SDH 2	SDH 3	SHD 4
D [mm]	Loss of signal [dB]			
5	0	-6.7595	-11.6889	-14.9906
5.5	0	-6.7508	-11.2557	-14.6334
6	0	-7.0011	-11.822	-15.4235
6.5	0	-7.0645	-12.2497	-15.8969
7	0	-7.6674	-12.8935	-16.8236
7.5	0	-8.1084	-13.9617	-18.3006
8	0	-8.8570	-15.3675	-20.2358

The attempt to include damping in the model of immersion probe was unsuccessful due to a malfunction of the simulation software. In order to examine the influence of the damping coefficient of the material on signal losses several simulations were made using contact method of ultrasonic testing, see Table 11. The side drilled hole 2 was used as the reference.

Table 11: The results of the simulation of contact probe including damping.

SDH 2	SDH 3	SDH 4
Damping = 0		
-0.0007	-7.2919	-11.9389
Damping = 0.05		
0.0154	-9.9213	-17.843

7.3   X-ray inspection

Considering results of X-ray inspection no significant indications were detected. Even in case of the piece S7D, where ultrasonic measurement indicated small defects forming line, no indications were visible on X-ray image.

7.4   Eddy current testing

The section below describes results of inspections performed using eddy current technique. Both the reference plate and LMD wall were examined. Results of the verification of reference defects are provided in Appendix 4.

7.4.1   Eddy current inspection of reference plate

Since the phase was adjusted to align indication with the vertical axis of screen the results show only values of impedance change in Y axis.

In Figure 46 the results of probe positioning tests are presented. In case of the longer side of the probe was parallel to the notches length, reliable indications were obtained, see Figure 46 a. When the probe was positioned with longer side perpendicular to the notches length, the amplitude of noise was of similar magnitude as the indications of the flaws, see Figure 46 b. The tests were performed for the notches 0.8 mm long from 0.4 to 1.6 mm below the surface.
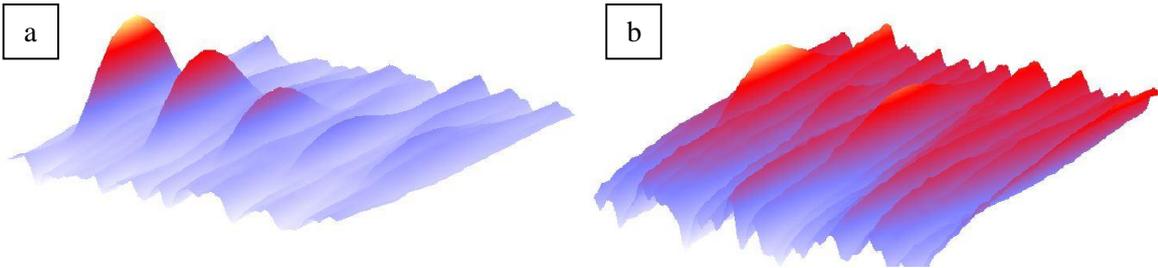
Figure 46: Graphical representation of signals obtained from the scan of area containing 0.8 mm long notches: a) probe longer side parallel to the length of notch, b) probe longer side perpendicular to the length of notch.

Using established probe's positioning and parameters presented in the table 12 below it was possible to obtain indication of the 0.8 mm notches on all depths. The settings were established for subsurface inspection.

Table 12: Established settings enabling detection of all 7 notches in subsurface inspection.

Frequency [kHz]	Phase [deg]	Amplification [-]	Low Pass filter [kHz]
100	56	64/64	10

Figure 47 shows the graphical representation of data acquired while scanning over the area containing 0.8 mm long notches. All the indications of notches were identified. The amplitudes of indications were plotted against the position under the surface to assess the limits of inspection depth. The results can be seen in Figure 48. A linear tendency can be observed in the decrease of signal. All of the notches except no. 10 fulfill the criterion of signal to noise ratio (SNR) equal or higher than 3. Due to the influence of noise the indication of the last notch has considerably changed shape. More detailed results of the inspection including presentation of indications on impedance plane can be seen in Appendix 5.
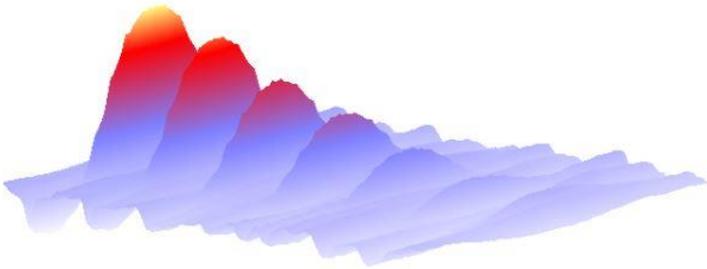

Figure 47: Graphical representation of data obtained from scan of the area containing all seven notches of 0.8 mm length.
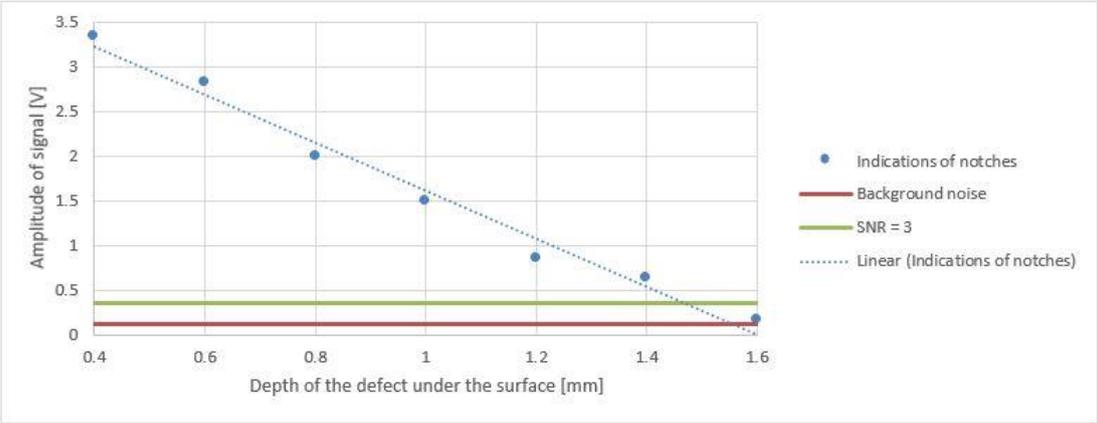

Figure 48: Graph presenting the amplitude decrease with the increase of depth under the surface of inspection of 0.8 mm long notches.

Smaller notches of 0.4 mm in length were inspected using previously established settings. The results of this inspection are presented in Figure 49 and Figure 50.

It was possible to identify only notches from no. 4 to no. 8. Overall, the amplitude values were lower comparing to previous case. Additionally, for all the notches, indications were much more influenced by disturbances; electronic and thermal noise. The amplitudes of the indications were plotted against the positioning under the surface to assess the limits of inspection's depth. The results can be seen in Figure 50. More detailed results of the inspection including presentation of indications on impedance plane can be seen in Appendix 6.
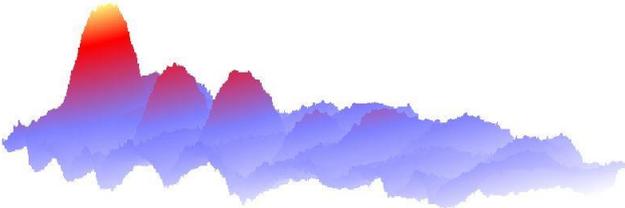
Figure 49: Graphical representation of data obtained from scan of the area containing all seven notches of 0.4 mm length.
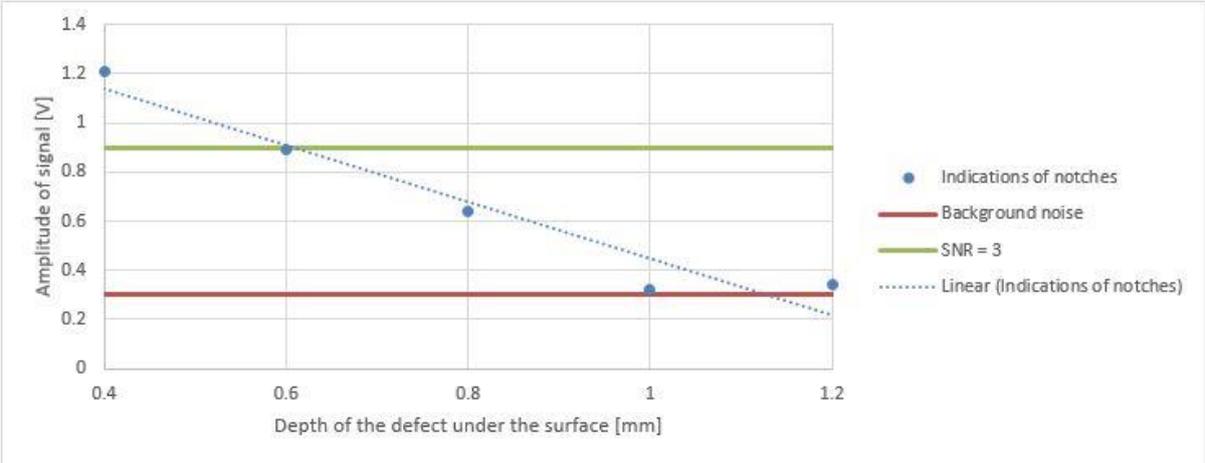
Figure 50: Graph presenting the amplitude decrease with the increase of depth under the surface of inspection for 0.4 mm long notches.

For surface inspection with probe positioned on the surface containing notches, the settings of the inspection system stated in Table 13 enabled to detect all seven notches 0.8 mm long.

Table 13: Established settings enabling detection of all 7 notches in surface inspection.

Frequency [kHz]	Phase [deg]	Amplification [-]	Low Pass filter [kHz]
100	130	52/52	10

Similarly to the previous results, Figure 51 shows the graphical representation of data acquired while scanning over the area containing 0.8 mm long notches. All the indications of notches were identified. The amplitudes of indications were plotted against the depth of corresponding defect to assess the limits of inspection's depth. The results can be seen in Figure 52. A linear tendency can be observed in the decrease of signal. For surface inspection the magnitude of indications is higher than for the previous subsurface experiments. More detailed results of the inspection including presentation of indications on impedance plane can be seen in Appendix 7.
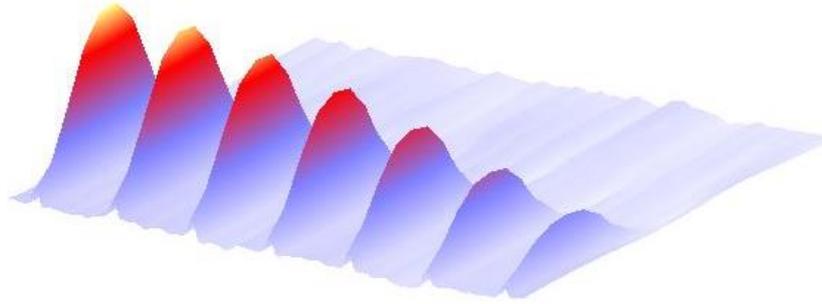
Figure 51: Graphical representation of data obtained from scan of the area containing all seven notches of length 0.8 mm.
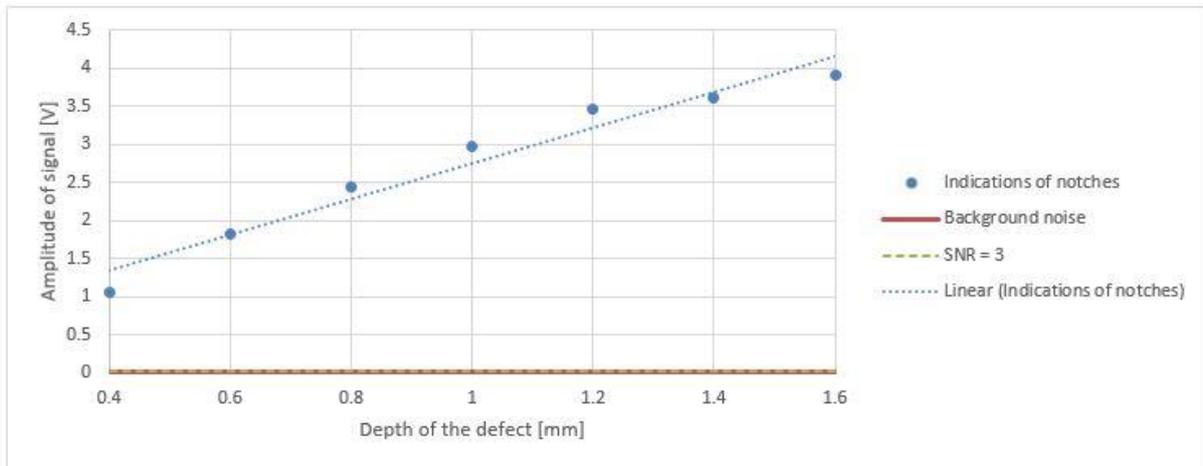
Figure 52: Graph presenting the amplitude decrease with the increase of depth under the surface of inspection for 0.8 mm long notches.

The same settings were used to inspect area containing small 0.4 mm long notches. It was possible to obtain reliable indication for all seven notches. Figure 53 shows graphical representation of the artificial defects. The amplitudes of the indications were plotted against the depth of corresponding defect to assess the limits of inspection's depth. The results can be seen in Figure 54. More detailed results of the inspection including presentation of indications on impedance plane can be seen in Appendix 8
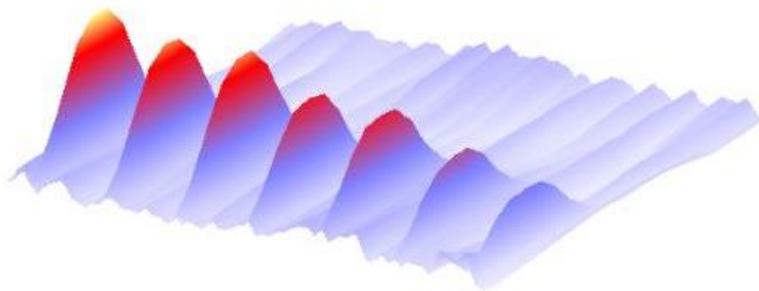
Figure 53: Graphical representation of data obtained from scan of the area containing all seven notches of length 0.4 mm.
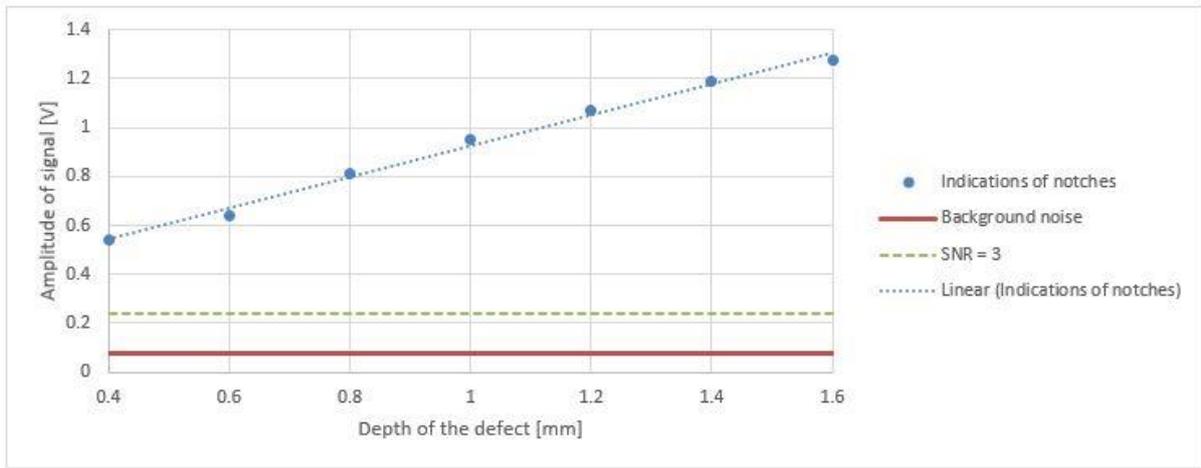
Figure 54: Graph presenting the amplitude decrease with the increase of depth under the surface of inspection for 0.4 mm long notches.

7.4.2 Eddy current inspection of LMD piece

Both settings, for surface and subsurface inspection, were used for measurements preformed on LDM piece.

Results show the influence of surface conditions on the impedance changes. Figure 55 presents examples of impedance changes registered during line scans along the side surface of the piece in milled and raw conditions respectively. For the milled condition, average peak-to-peak value, based on 10 measurements, was measured to be 0.31 V. As for the second condition, impedance change was established to be equal to 1.4 V, see Figure 56 and Figure 57. The color scale in Figure 55 is rescaled automatically to the highest amplitude of impedance change. Due to this, it cannot be used for comparison purposes.
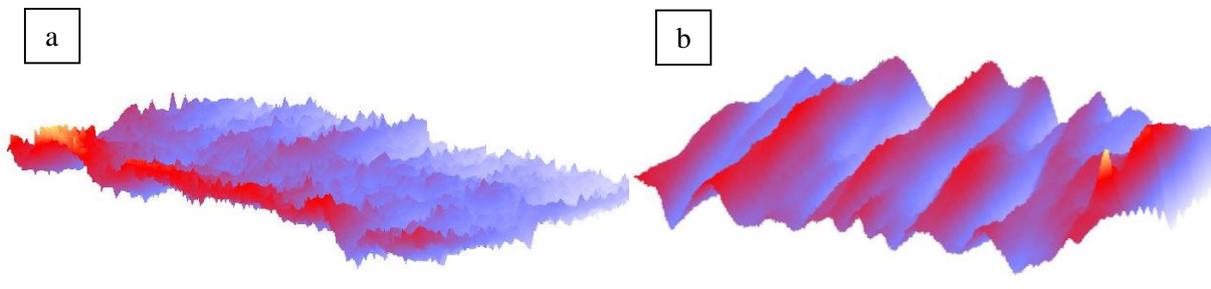
Figure 55: Results of inspection using settings for subsurface detection: a) milled side surface, b) raw side surface.
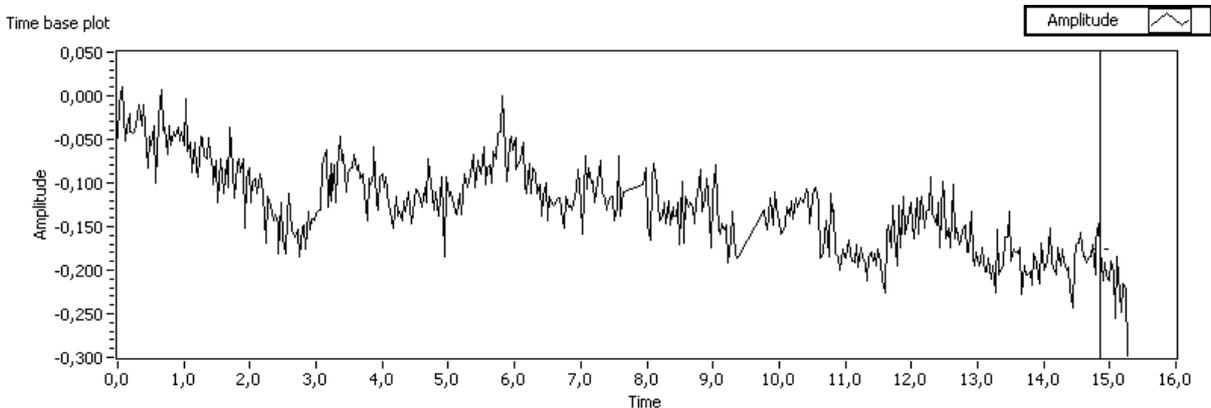
Figure 56: Impedance signal acquired during line scan - milled conditions.

45
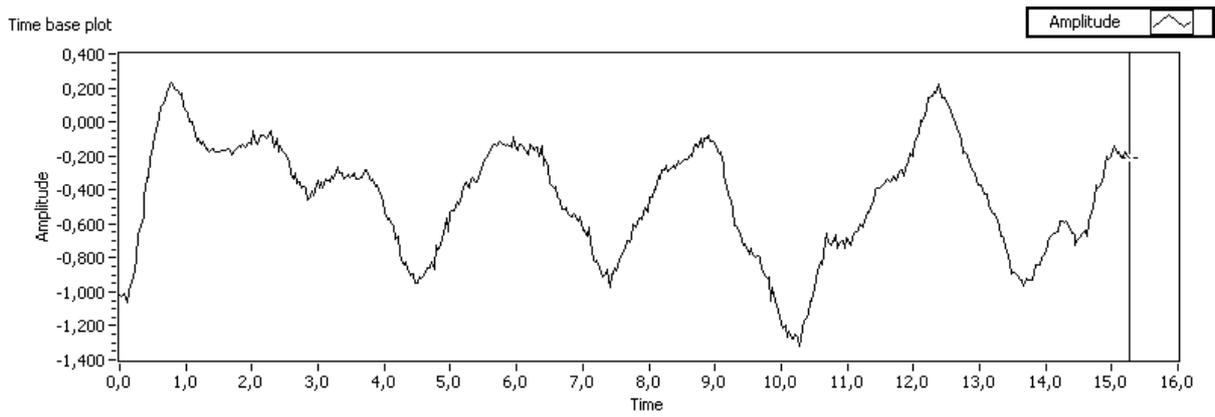
Figure 57: Impedance signal acquired during line scan - raw conditions.

Similar measurements were performed using settings for surface inspection. The results in for of C-scan visualizations can be seen in Figure 58. The color scale used in Figure 58 is rescaled automatically to the highest amplitude of impedance change. Due to this, it cannot be used for comparison purposes. Considering milled surface, average peak-to-peak value, based on 10 measurements, was measured to be 0.16 V. As for the second condition, impedance change was established to be equal to 3.25 V. Examples of impedance changes acquired during line scans can be seen in Figure 59 and Figure 60.
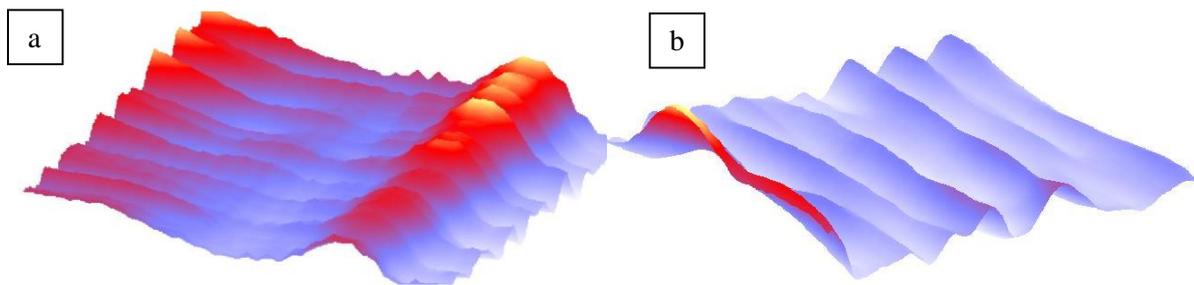
Figure 58: Results of inspection using settings for surface detection: a) milled side surface, b) raw side surface.
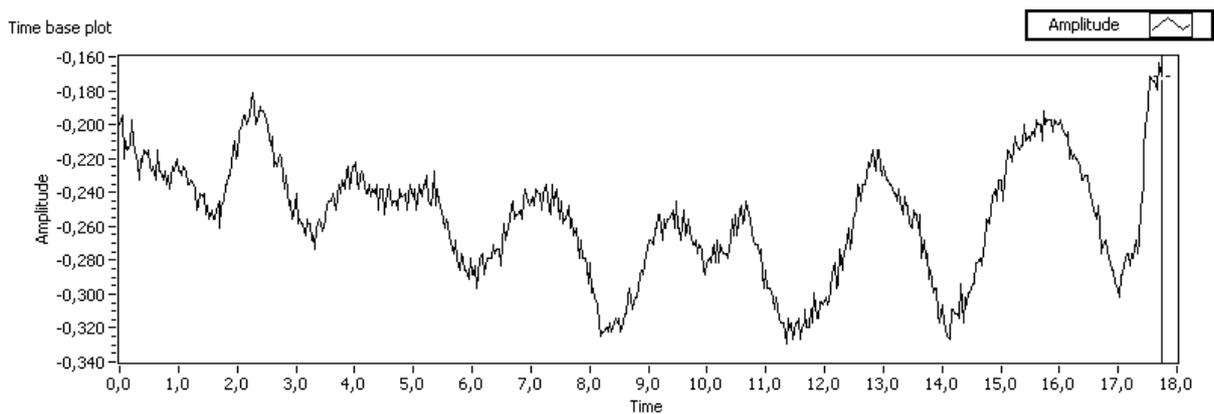
Figure 59: Impedance signal acquired during line scan - milled conditions.

46
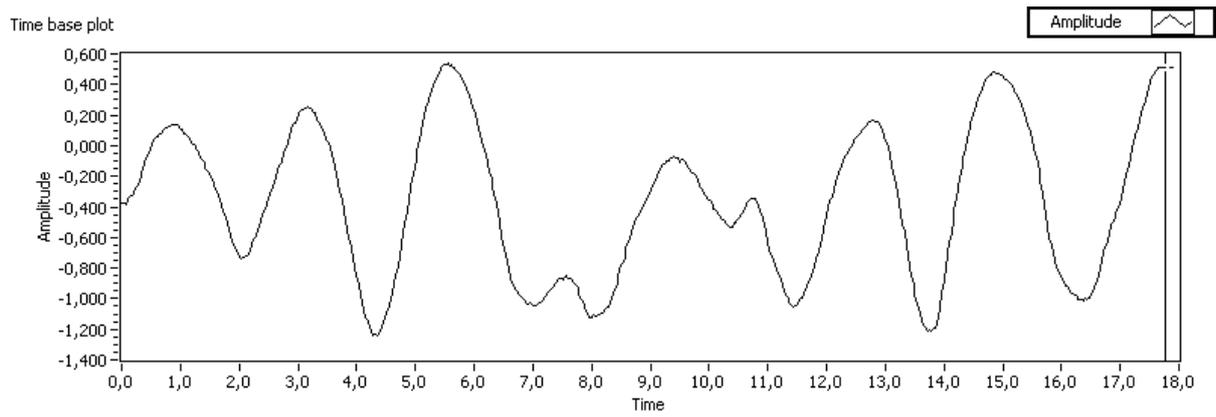
Figure 60: Impedance signal acquired during line scan - raw conditions.

8 Discussion

Based on the results of ultrasonic and eddy current inspection several inferences were drawn.

8.1 Ultrasonic testing

8.1.1 Evaluation of probes

Regarding theoretical values of wavelengths of all 4 probes, it can be inferred that the most suitable probes for detection 0.4 FBH related defects are transducers IS101GA, V317 and I3-2504-R. This is due to the fact that their wavelength is of the same order as the size of reference defect. Yet, the experiments showed that all of the four transducers are capable of detecting 0.4 FBH.

The evaluation of probes as well as creating TCG curves shows that the probe IS1010GA (10 MHz) is the most universal for this application. It is possible to reduce the dead zone down to about 1.2 mm close to the front surface and at the same time the probe provides good detectability of the 0.4 FBHs on all reference depths. Yet, created TCG1004F curve for the step 5 reached about 85% of available amplification. It implies that using established settings no elements thicker than 45 mm can be inspected in one scan. There are a few possible alternatives for inspection of thicker elements. Firstly, the piece could be divided it into a few areas for separate scans. Yet, one has to consider the time factor of this operation. Secondly, based on results of evaluation, the probe I7-0512-RG (5 MHz) can be considered useful in cases where higher depth of penetration than 45 mm is required. However, at this moment no proper reference is available to assess limiting depth of inspection using this probe.

The TCG curves used within this project were established according to the preliminary evaluation of the probes. However, the later phase of the project showed that it is possible to obtain more optimal positioning of the probe as well as different value of the water path using steel ball as point reflector. Due to this, the TCG curves need to be reestablished.

8.1.2 Limitations of the inspection

The analysis of results obtained during measurements shows several limitations caused by the characteristics of ultrasonic immersion testing method in combination with design and conditions of LMD samples.

To start with, while using longitudinal waves and $\alpha = 90°$ as incidence angle all of the probes were characterized with a dead zone of a certain extension. Due to this, depending on the probe certain depths close to the incidence surface cannot be inspected. This phenomenon is dependent on the width of the peak visible on the A-scan that corresponds to the interface surface. Since the interface generates much stronger reelection than the defects distinguishing these two could not be possible. The echo of interface between water and metal block will hide indications of flaws.

Considering inspection surface conditions, none of the raw surfaces can be used as incidence surface for ultrasonic inspection. Starting from the raw top surface, due to the curvature some amount of signal is being lost even if the bottom surface is used as incidence side. Based on the results of measurements in series 5 and 11 the loss of energy was observed due to the conditions of raw bottom surface. Though using both milled top surface and raw plate surface at the bottom of specimens enabled to obtain indication of the flaws, measurements in series 11 show that, in case of the raw plate surface, some amount of signal is reflected with random angles. Considering this, it can be stated that the surface conditions influence both reflection and refractions angles, causing some amount of energy to be reflected away from the transducer. Regarding natural flaws, for some cases, there was a change in the signal intensity and shape of the flaws observed in the C-scan. Yet, it is important to mention that this phenomenon might be caused not only by difference in surface conditions but also by different reflection angles caused by positioning and irregular shape of defects.

What is more, based on results of series 5 and 6, if scan is performed with raw plate surface being the incidence side, in the result the width of the wall visible on the C-scan appears to be about 2 mm decreased compared to the real thickness of the wall. Since the problem is diminished when the plate's surface is milled, the conclusion is that the waviness of the raw plate surface is causing some parts of the wave beam to refract away from the transducer.

One should also consider influence of indications produced by the plate's back surface when probe is positioned close to the edge of the wall, see Figure 61. To be more precise, as the plate is 3 mm thick, it produces strong indications appearing between front surface and back wall surface of LMD structure, when the probe approached the edge of specimen. This phenomenon increased when a TCG curves with linear amplification of signal were used. Due to this, the area close to the side of a wall might become blind spot for the inspection.
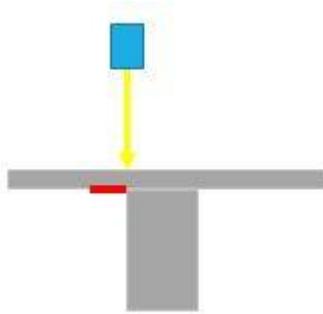
Figure 61: Schematic drawing indicating the surface (marked by red line) generating strong indications close to the edge of a wall.

Based on results of series 12, when side of the wall was chosen as incidence surface the signals magnitude would differ because of the surface conditions. What is more, no indication of LoF was observed in the area where it was detected before. These are related to two issues. Firstly, the surface cannot be used for inspection in raw conditions as there is loss of energy visible by varying signals. Secondly, when incidence beam is normal to the side surface the LoF defects may remain undetected because of the positioning of defects. Yet, in order to gain confidence in this claim more tests should be performed.

In order to examine the issues described above new reference block was designed, however due to manufacturing delays it could not be tested within the time span of this project. Additionally, one has to consider that due to later manufacturing the reference wall became bent and there is variation of the thickness that needs to be taken into account while scanning. Yet another issue is that the indications of SDHs will not entirely correspond to the reference established based on FBHs as they produce stronger reflection. However due to manufacturing constrains it was impossible to produce holes of smaller diameter than 0.4 mm.

What is more, due to the malfunction of the ultrasonic equipment further tests on LMD walls S9D, S10D and S11D could not be continued. Based on quick scan of the entire area of the three walls it can be stated that all of the components contain defects.

8.1.3   Simulations

Regarding the results presented in Table 10, enlarging the diameter of the active element to 7.5 mm enabled to achieve comparable levels of signal loss as measured during the real scan. Due to this, simSUNDT software could be used for simulating ultrasonic inspection using probe IS1010GA. Still, considering the fact that damping of material was not included in simulation the results should be confirmed for the titanium alloy components. It might be the case that the obtained value of diameter is valid only for the specific case of the tested stainless steel block.

The damping was included in the simulation of contact probe of similar properties as IS1010GA. For the SDH 3 the difference in signal loss between the results of simulation with and without damping was -2.7 dB. For the SDH 4 the value was -5.9 dB. Including these differences in the model of immersion probe would give results similar to the values obtained from the real scan.

8.2 Eddy current testing

8.2.1 Subsurface detection

Performing the measurements on available equipment, it was possible to obtain indications of all 7 notches 0.8 mm long. Based on this results and the fact that notch no. 10 did not fulfill the criterion of SNR higher or equal to 3, it can be stated that depth of inspection for ECT in Ti-6Al-4V is about 1.4 mm. This value is applicable for detection flaws with size corresponding to 0.8 mm long notch using specified probe and established settings in subsurface inspection.

It was impossible to obtain optimal parameters for the detection of 0.4 long notches. Since background noise was at the level of indication, using high amplification was destabilizing impedances signal. Due to this settings established for 0.8 mm notches were used. As the results indications down to the depth of 1.2 mm were recognized. However, only the indication of the notch on the depth of 0.4 mm can be considered as reliable.

8.2.2 Surface detection

The amplification used for the detection of surface defects was lower than the one required for former inspection. Using settings established for 0.8 mm notches gave satisfying results for both 0.4 mm and 0.8 mm long defects. Background noise levels were low comparing to signal levels thus all the indications can be considered as reliable.

8.2.3 Inspection of LMD piece

Results of tests performed on the piece S10D show that for both types of inspection the raw surface produces high changes of impedance comparable with the magnitude of impedance change indicating defects. Due to this, raw surface conditions do not support reliable inspection as there is high probability of false indication as well as missing real defects. The average peak-to-peak value for surface inspection is higher than subsurface one, despite lower amplification. This might be caused by influence of the edge of the wall on impedance value.

The average peak-to-peak values measured for the milled surface are of the same magnitude as the noise values measured for surface and subsurface inspection of 0.8 mm long notches on the reference plate.

8.2.4 Limitations of inspection

If the inspection is performed with double coil probe, the positioning of the defect has high influence on its detectability. This fact needs to be considered while adjusting probe's position before performing inspection of components with natural defects. It is essential to align probe's longer side parallel to the expected direction of defects. If natural defects are positioned randomly, a few inspections with different probe's alignments need to be considered.

While performing the tests, it was visible that the inspection is limited due to restricted capabilities of the equipment ELOTEST® B1. If higher amplification of the signal was applied the indication would become unstable. Regarding this, despite stable parameters of test piece as well as probe positioned in the fixed spot, the indication on impedance plane would float in random directions. What is more, vibration of the cable attached do the probe would influence the resistive part of the impedance. All these factors influence detectability defects, especially in case of 0.4 mm long notches.

9 Conclusion and recommendations

This project aimed on verifying whether two NDT techniques, ultrasonic immersion tests and eddy current tests can be applied for quality testing of LMD/w Ti-6Al-4V components. The activities performed within this project mostly focused on developing references and investigation limitations of UT for this specified application in regard to LoF defects.

The general conclusion based on ultrasonic inspection is that it is possible to detect LoF defects that produce the indication of similar magnitude to 0.4 FBH and higher. However, due to the time limitations of the project, the real size of the detected defects could not be verified.

Among testes probes, only the probe IS1010GA (10 MHz) gave satisfying results on defect detection, depth of inspection as well as created limitations in regard to the extension of the dead zone.

As the result of the performed experiments, the areas of limited inspection capabilities were identified. To start with, raw surface conditions prevent fully reliable inspection. Secondly, due to the characteristics of immersion UT the area close to the surface was pointed out as the dead zone. The size of it would depend on the characteristics of a probe. What is more, loss of signal was observed in the area close to the edges of the piece. Yet, the approximate size of the area and magnitude of signal losses could not be estimated due to lack of the reference block with SDHs. When using plate side as incidence surface, influence of signals generated by the surface of the plate was observed when measuring close to the edge of the wall.

Based on ECT measurements, it is possible to detect reference defects of length 0.8 mm for both surface and subsurface inspection. However, both of the inspections required different settings. The detectability of 0.4 mm long notches should be investigated more, preferably using ECT equipment with higher capabilities. Regarding to the results obtained within this project, it was possible to detect all the flaws during surface inspection. Yet, subsurface tests would give reliable results only for the notch no. 4 closest to the surface. Milled surface of LMD components provides similar inspection conditions to the ones of reference plate.

9.1 Ultrasonic testing

Considering ultrasonic inspection for this application several recommendations can be made.

To start with, in order to assure reliable inspection all the surfaces should be machined to obtain flat incidence surfaces as well as uniform dimensions and sharp edges of the pieces. If possible, regarding the final application, the excessive plate outside the circumference of the wall should also be removed to prevent influence of signals generated by the surfaces of plate while scanning close to the edge of component.

In order to address the issue of the dead zone, inspection should be performed using bottom plate side as incidence surface. Yet as mentioned before the surface needs to be machined first. This setup would enable to create a buffer zone of 3 mm (plate thickness) that could be excluded from the measurement. Additionally, to diminish influence of back surface echo, the amplification of TCG curve should be used to suppress the signal. The applicability of this solution should be tested with the new reference containing SDHs close to the surface of component.

Furthermore, if side wall surface is being considered as the incidence one, additional inspection should be performed using incidence angle shifted few degrees from the normal direction. The positioning of the natural defects needs to be considered as in some cases the entire ultrasonic wave can be reflected away from the probe.

Moreover, the results obtained from previous measurements as well as TCG curves need to be verified and validated. It is necessary to perform destructive tests on the components with detected defects in order to compare the real size of the flaws with the indications' magnitude on the C-scan. Yet before

51

destroying the sample it would be beneficial to scan the defected area with the TCG curves created for reference defects 0.4, 0.8 and 1.2 mm to fully assess the size of the defect. Since some of the defects produce signal over the scale, when tested with settings for 0.4 FBH, this would provide verification of all reference curves. Additional information on accuracy of TCG curves could be obtained.

For further measurements, new, improved TCG curve, TCG1008M, should be used. It enables to maintain the dead zone by the surface to the level of 1.2 mm at the same time the constant, faulty signal of 30% close to the surface was removed. As the new settings have not been used yet to test real defects the results need to be compared with previous measurements.

As an extension of this project, the new reference piece with SDHs should be tested. Measurements performed on this piece should give more accurate information about detectability of defects close to the edges, in near surface area as well as in the first layer of deposited material.

What is more, to increase flexibility of the inspection water flaw probes mounted on the manipulator should be considered. The advantage of this approach would be sustaining the automation and repeatability of the inspection and at the same time the necessity to maintain a big tank full of water would be excluded.

Moreover, phased array probe could be considered for future application. The possibility to use wave front of ultrasonic signals produced by arrayed transducers with different time delays could increase efficiency of an inspection, scanning simultaneously material on different depths. Due to this, the resolution of scan could be increased as the produced ultrasonic beams could be focused on different depths. However, the mode of phase array inspection should be adjusted depending on the positioning of the natural defects. Regarding LoF, as it is a planar defect, depending on its positioning and beam's incidence angle it will produce reflection of different intensity. The characteristics of phase array immersion inspection needs to be studied more thoroughly in order to understand its advantages and disadvantages comparing to traditional UT inspection.

Regarding ultrasonic simulation, simSUNDT software could be used to perform comparison studies of signals produced by FBH and LoF defect simulated by circular cracks. Despite the fact that it was not possible to include damping in simulation of immersion testing, theoretical verification of differences in indications of the same size FBHs and LoF would give deeper understanding on correlation between reference defects and natural ones.

9.2   Eddy current testing
Considering eddy current testing a few recommendations can be made.

In order to fully assess detectability of 0.4 mm long notches it is necessary to perform tests using an ECT equipment enabling a stable signal with high amplification.

What is more, one has to consider that for inspection with higher amplification of received signal, it is important to diminish unnecessary noise. Some of the causes to random noise can be prevented. Firstly, adding an additional coil to the double probe, that would measure only the change in the magnetic field caused by the vibration of the cable. This solution could improve the condition of the impedance signal. Additionally, a new fixture could be designed to position the test pieces more accurate. It is necessary to provide stable positioning of the target component at the same time assuring enough distance from other conductive elements influencing the measurement.

Moreover, more excessive examination of the reference plate needs to be performed including other probes. It would be beneficial to perform an inspection using a differential probes that would be less sensitive to the disturbances mentioned before. In addition to that, for comparison purposes, inspections should be performed using remaining two probes.

Finally, obtained settings should be tested against real LoF defects manufactured in LMD components.

10 References

[1]   Chiang, F. P. Speckle Metrology, *ASM handbook Volume 17, Nondestructive Evaluation and Quality Control* (1989). ASM International, 432.

[2]   Peters, M., Kumpfert, J., Ward, C. H., & Leyens, C. (2003). Titanium alloys for aerospace applications. *Advanced Engineering Materials*, 5(6), 419-427.

[3]   Mahamood, R. M., Akinlabi, E. T., Shukla, M., & Pityana, S. (2013). Laser metal deposition of Ti6Al4V: A study on the effect of laser power on microstructure and microhardness.

[4]   Baufeld, B., Brandl, E., & Van der Biest, O. (2011). Wire based additive layer manufacturing: comparison of microstructure and mechanical properties of Ti–6Al–4V components fabricated by laser-beam deposition and shaped metal deposition. *Journal of Materials Processing Technology*, 211(6), 1146-1158.

[5]   [ONLINE] Available at: http://asm.matweb.com/search/SpecificMaterial.asp?bassnum=MTP641. [Last Accessed 5 March 2015].

[6]   Rosell, A. (2012). Finite Element Modelling of Eddy Current Non-Destructive Evaluation in Probability of Detection Studies.

[7]   Brandl, E., Schoberth, A., & Leyens, C. (2012). Morphology, microstructure, and hardness of titanium (Ti-6Al-4V) blocks deposited by wire-feed additive layer manufacturing (ALM). *Materials Science and Engineering*: A, 532, 295-307.

[8]   Dahotre, N. B., & Harimkar, S. P. (2008). Laser fabrication and machining of materials (Vol. 51). *New York: Springer*.

[9]   Steen, W. M., Mazumder, J., & Watkins, K. G. (2003). Laser material processing (p. 123). *London: Springer*.

[10]   Kobryn, P. A., Moore, E. H., & Semiatin, S. L. (2000). The effect of laser power and traverse speed on microstructure, porosity, and build height in laser-deposited Ti-6Al-4V. Scripta Materialia, 43(4), 299-305.

[11]   Kou, S. (2003). Solidification and liquation cracking issues in welding. *Jom*,55(6), 37-42.

[12]   Rihar, G. *Lack of Fusion in welded joints*. [ONLINE] Available at: http://www.ndt.net/article/wcndt00/papers/idn403/idn403.htm. [Last Accessed 22 January 2014].

[13]   Jovanović, M., Rihar, G., & Grum, J. (2006). Analysis of ultrasonic indications in lack of fusion occuring in welds.

[14]   Prakash, R. P. (2009). *Non Destructive Testing Techniques*. New Academic Science.

[15]   Shull, P. J. (2002). *Nondestructive evaluation: theory, techniques, and applications*. CRC press.

[16]   Han, Y. K., & Thompson, R. B. (1997). Ultrasonic backscattering in duplex microstructures: theory and application to titanium alloys. *Metallurgical and Materials Transactions A*, 28(1), 91-104.

[17]   *The British Institute of Non-Destructive Testing*. [ONLINE] Available at: http://www.bindt.org/What-is-NDT/Index-of-acronyms/TCG/. [Last Accessed 18 February 2015]

[18]   [ONLINE] Available at: https://www.olympus-ims.com/data/File/panametrics/UT-technotes.en.pdf. [Last Accessed 05 March 2015]

[19]   Krautkrämer, J., & Krautkrämer, H. (1986). *Ultrasonic testing of materials*. 5. rev.

[20]   Rihar, G., & Uran, M. (2006). Lack of Fusion Characterisation of Indications. *Welding in the World*, 50(1-2), 35-39.

[21]   Shan, H. B., Li, M., Chen, H. D., & LV, T. M. „The Developments of Simulation Software for Ultrasonic Testing ". *In Proceedings of 17th World Conference on Nondestructive Testing (17th WCNDT), Shanghai (China) (Vol. 25, p. 28)*.

[22]   [ONLINE] Available at: https://www.ndt-ed.org. [Last Accessed 05 March 2015]

[23]   *Materials and Manufacturing Technology, Chalmers*. User Guide to simSUNDT 2.0.

Appendix 1

Figures below present elements of technical drawing of the new reference LMD piece with SDHs.

Figure 62 shows front view of the LMD piece. The drawings of the details A and B as well as the cross-section C are presented below. The side surface in milled condition is the one visible on the front view.
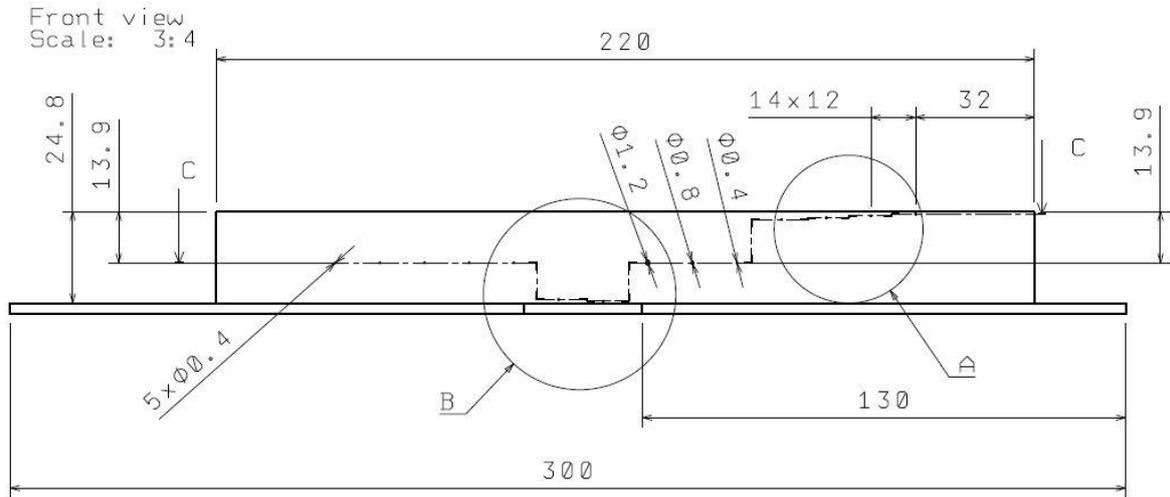
Figure 62: The front view of the reference wall with side drilled holes.

The cross-section below shows horizontal positioning of the holes as well as their depth, see Figure 63. The aim of shallow holes on the left side is to examine detectablility of the defects close to the egdes of the wall. As one of the side surfaces is milled, the influence on surface conditions on the detectability of SDHs can be examined. Remaining SDHs are designed with intention to leave 1 mm of unpenetrated material for ET purposes.
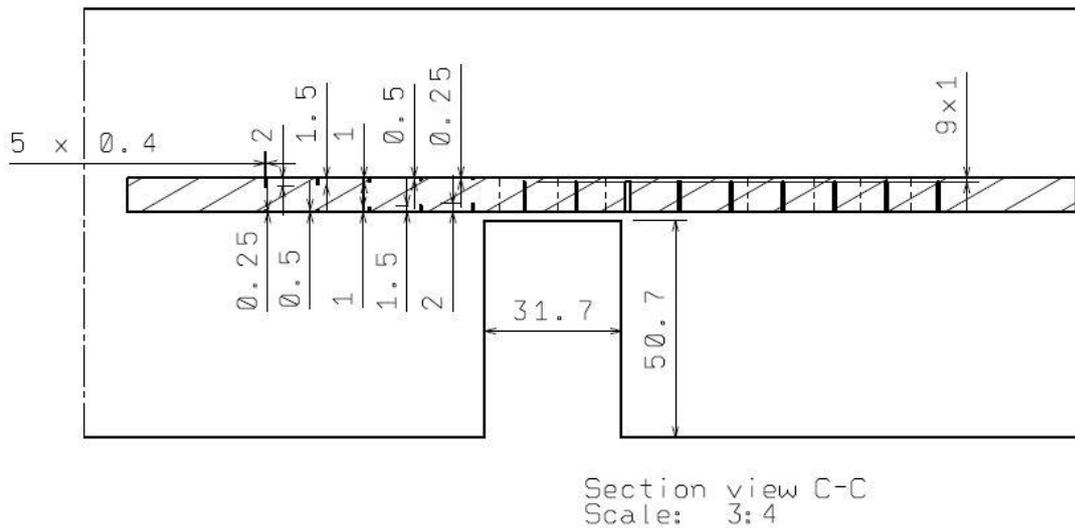
Figure 63:The cross-section C:values of the depth for all holes.

The width of the wall varies, see Figure 64. The variation is caused not only by the inaccuracy of LMD process but also because it was necessary to mill one of the side surfaces in conditions when the wall was bend under influence of residual stresses.
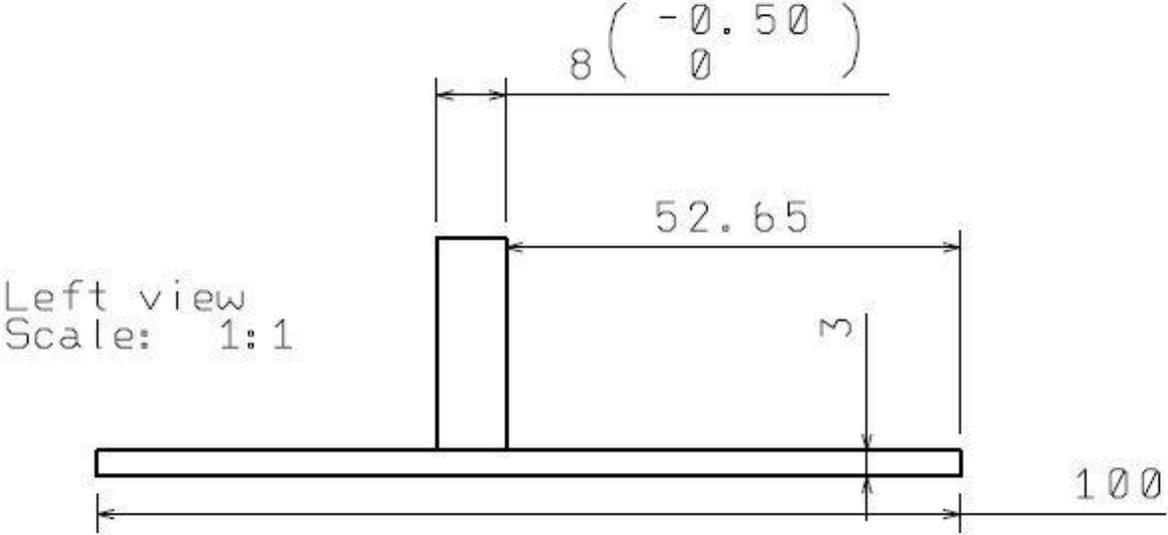
Figure 64: The left view of the new reference – basic dimensions.

The SDHs marked on detail A were designed to suite the purpose of investigating surface sensitivity. They can be applied for the investigation of a dead zone in the area of incidence surface as well as back surface of the component. The detailed information on positioning and size of the defects are shown in the Figure 65.
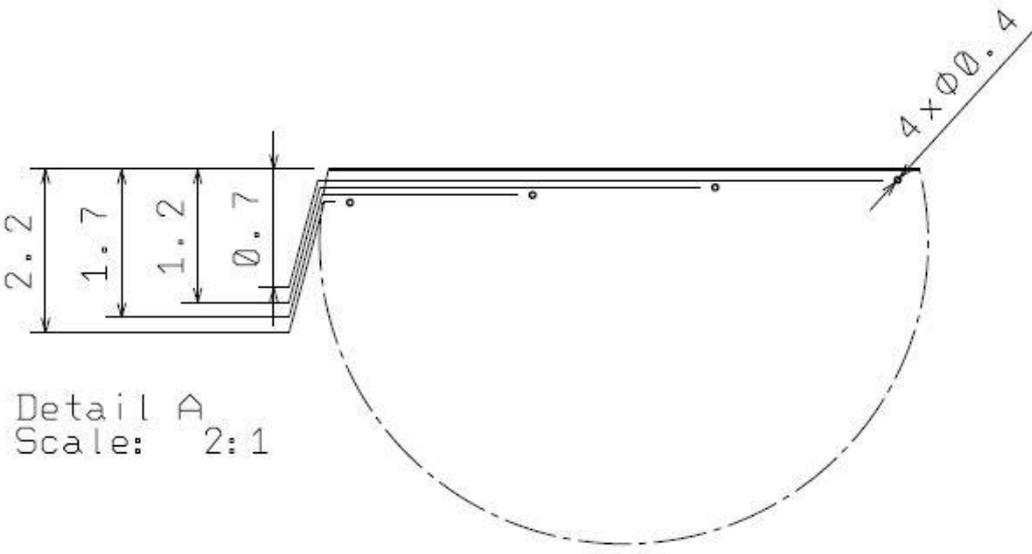
Figure 65: SDHs positioned close to the milled top surface.

The SDHs positioned close to the plate, at the heigth of the first layer of deposited material were designed to give the information on detectablity of the defects in the starting layer of deposition, see Figure 66. The intention was to perfrom scanning procedure using top milled surface and bottom raw surface as incidence one.
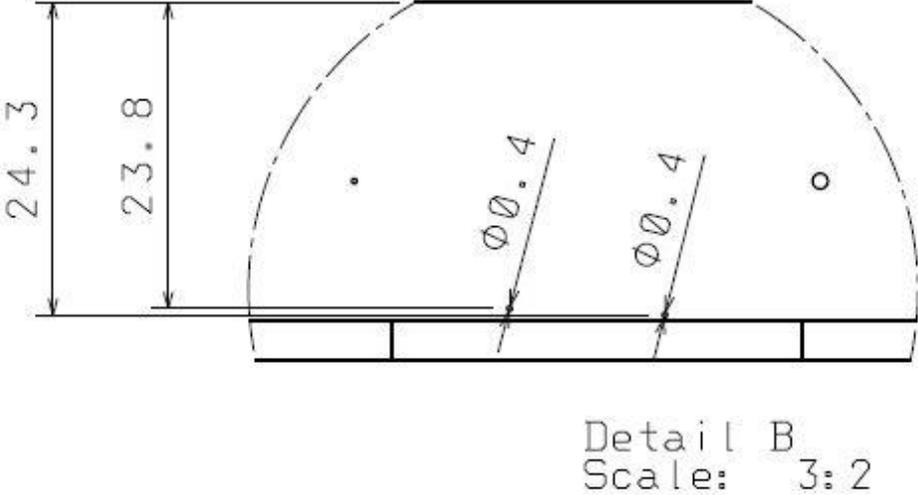
Detail B
Scale: 3:2

Figure 66: SDHs positioned close to the plate, in the first layer of deposited material.

57

Appendix 2

The figures below present more detailed examination of the piece S7D. The A-scan signals were acquired for the entire area where flaws were detected, including zones close to the edges. The measurements are a part of series 5.

The Figure 67 shows the horizontal and vertical B-scan representation of the flaws. It is visible that small LoF like defects form longer chains. The indications appear in two layers at the depth of 17 mm from the top surface. The defects produce indication stronger than the one corresponding to the 0.4 FBH. The scan was made using top, milled surface as the incidence.
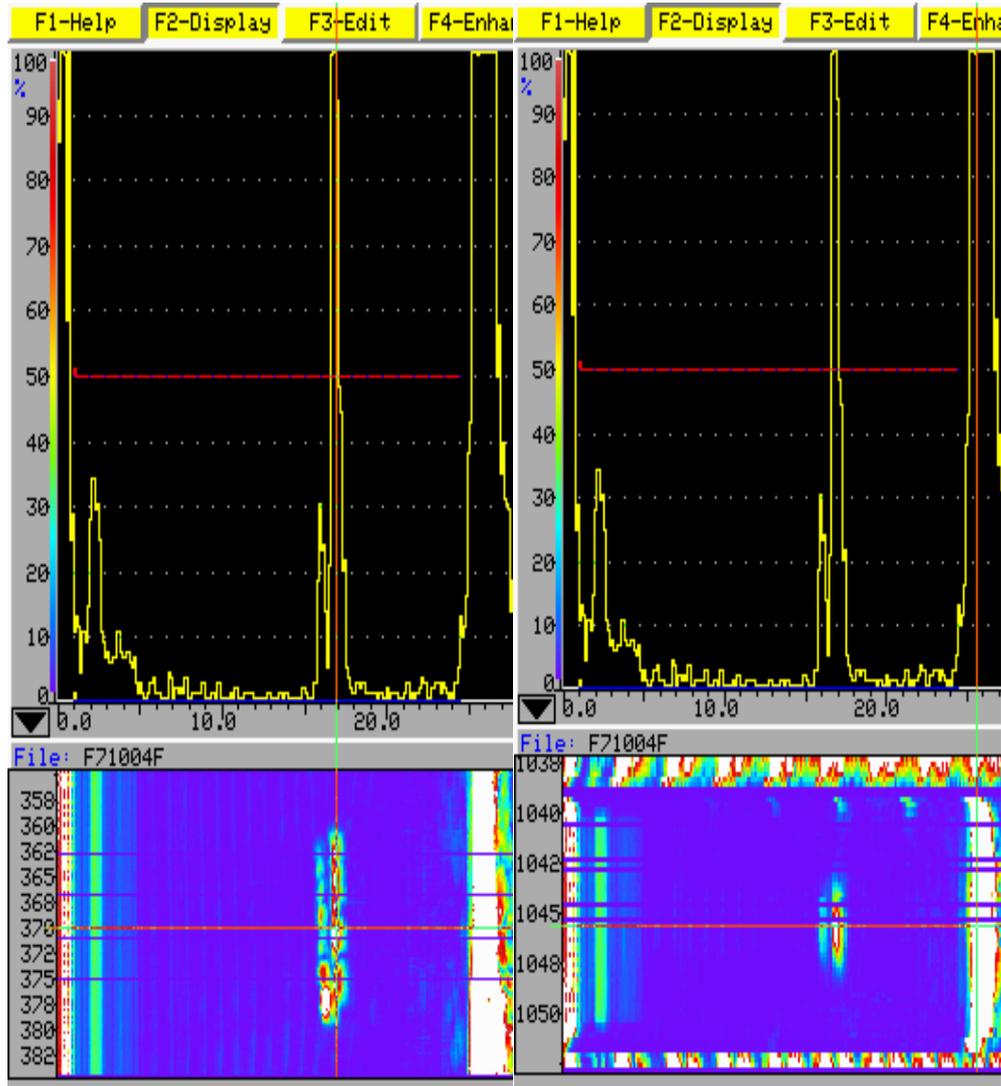
Figure 67:Horizontal (left) and vertical (right) B-scan of he defected area.

Figure 68 below shows the horizontal B-scan of the area close to the edge of the sample. Unidentified indications are visible as well as the stripe like continous indications produces by the back surface of the plate.
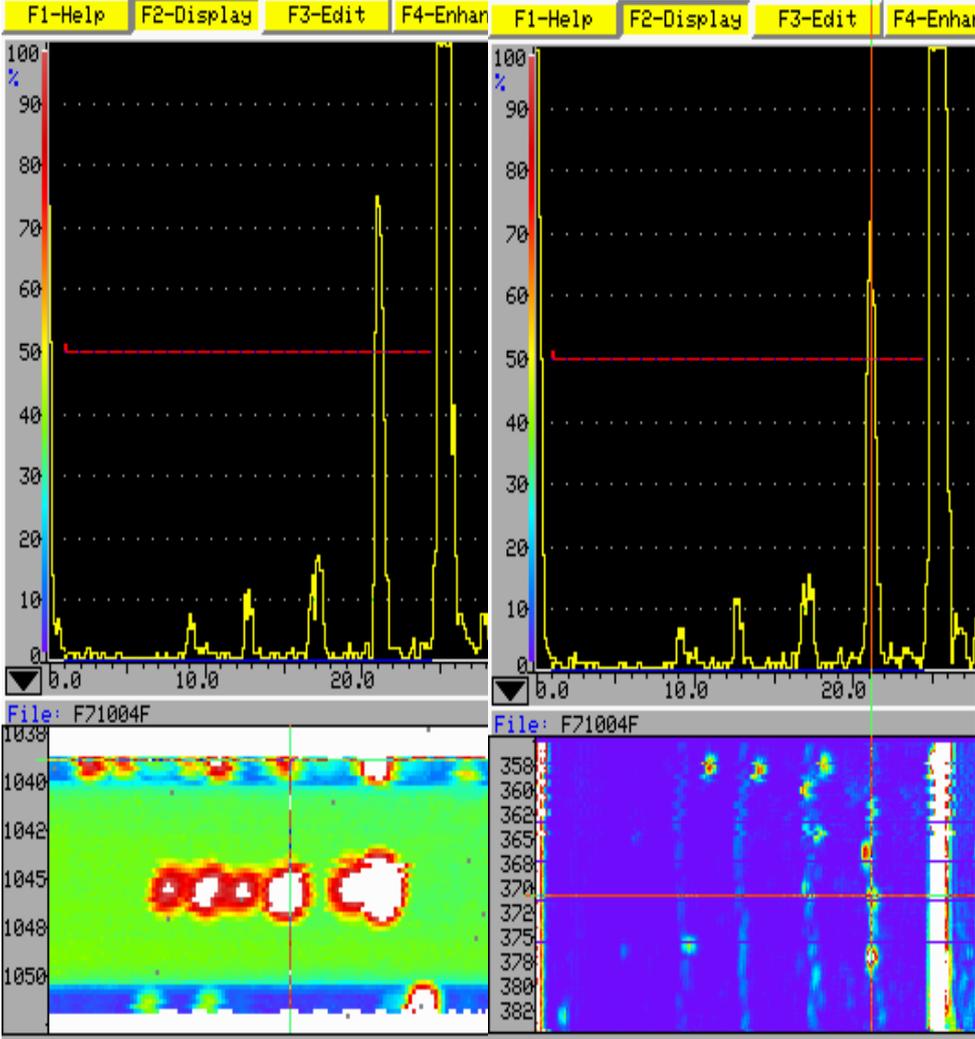
Figure 68:Horizontal B-scan of the area close to the edge of the wall (right).

Appendix 3

Figure 69 below present the scans of piece S7D made in series 6 of measurements. The Figure 69 shows horizontal and vertical B-scan representation of the defect. The scan was performed using top milled side as incidence surface.
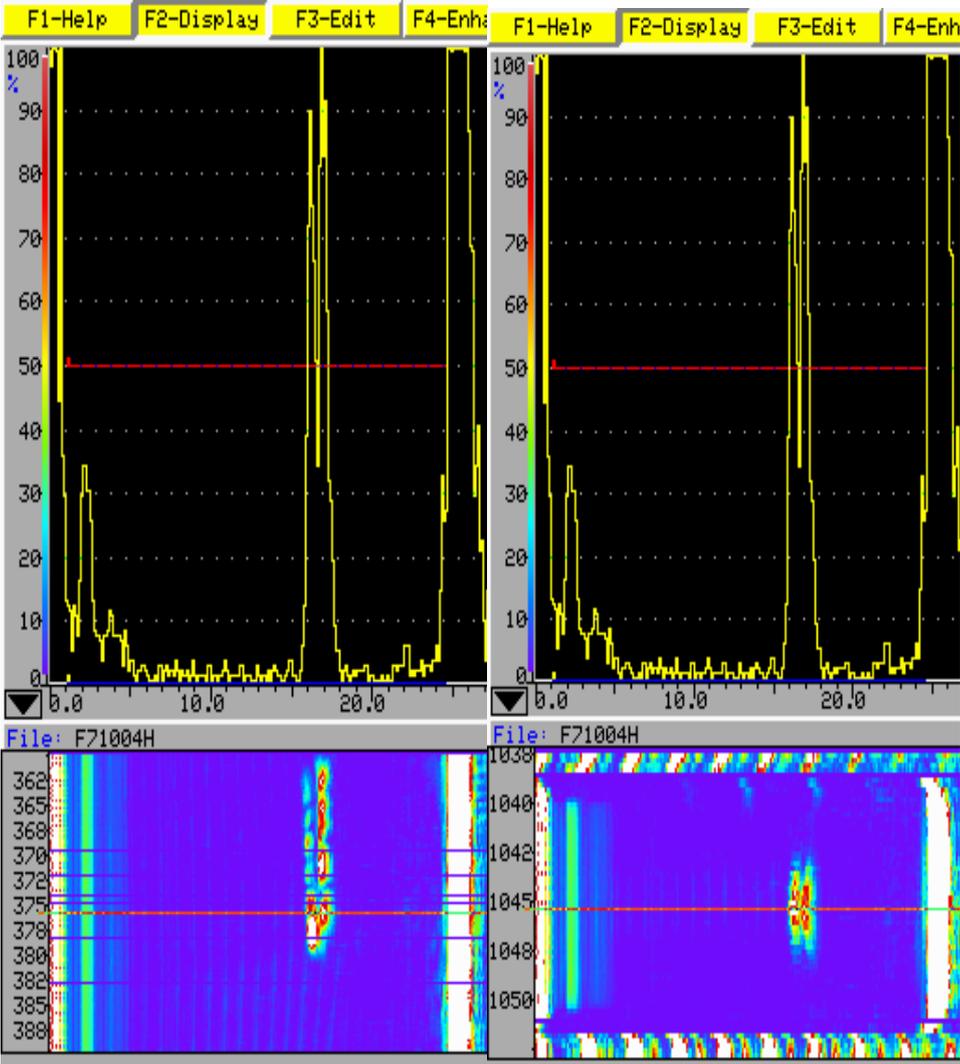
Figure 69: Horizontal (left) and vertical (right) B-scan of the defected area. Scan preformed using milled, top surface as incidence.

For comparison purposes the scan was made using milled plate side as the incidence surface. The result is presented in the Figure 70. The difference between the influences of signals reflected from the plate depending on incidence surface is visible comparing vertical B-scans in Figure 69 and Figure 70. For the later one the area with indication of reflected from the plate is bigger. The A-scan presenting the signal reflected from the plate is shown in the Figure 71.
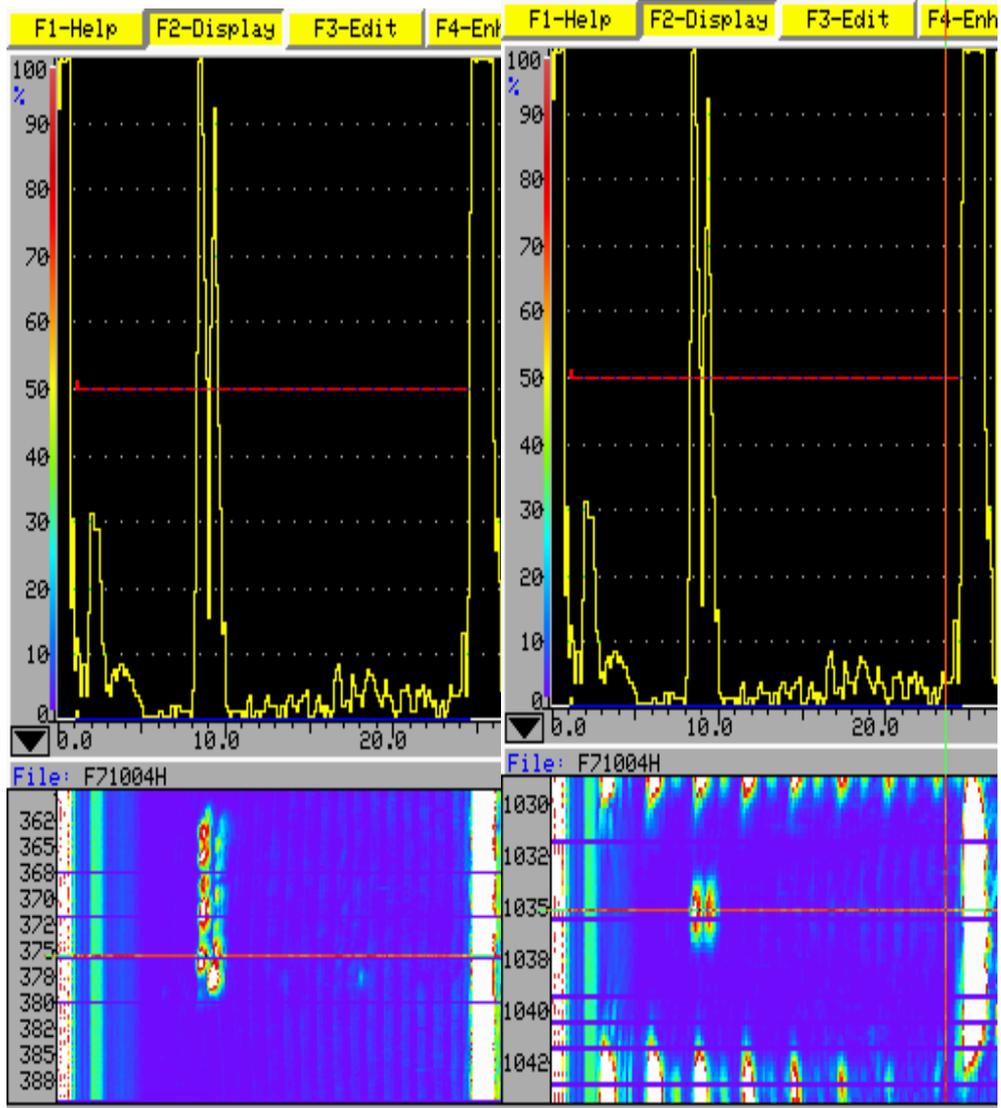
Figure 70: Horizontal (left) and vertical (right) B-scan of the defected area. Scan performed using the milled, plate side as the incidence surface.
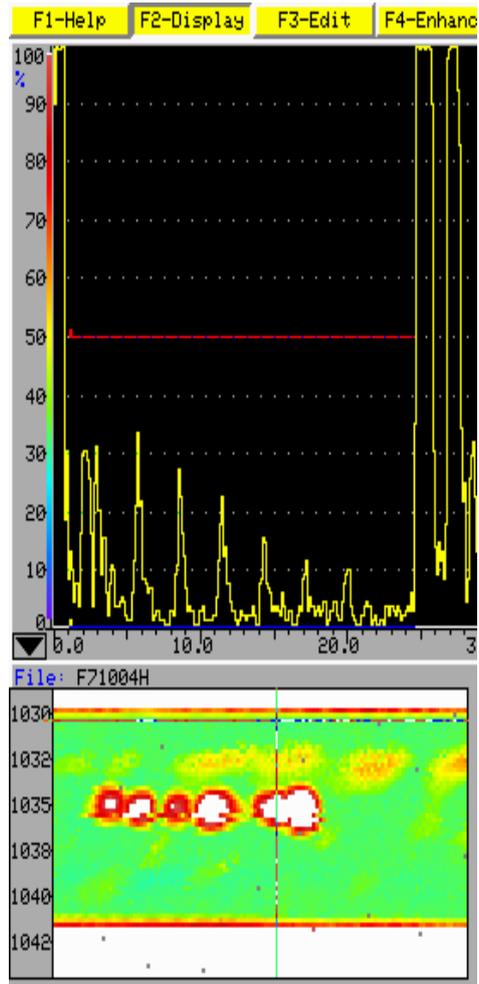
Figure 71: The A-scan of the signal acquired close to the edge of the wall. Influence of signal generated by the plate. Scan performed using milled surface of the plate.

Appendix 4

Results of length and width measurements are presented as an average of three measurements.

The measurements of depth were possible only for limited number of notches. This was due to the fact that the possibility of gaining image of the bottom of a notch is dependent on amount of light introduced in the cavity. For some small and deep notches the amount of light was insufficient.

The inaccuracy of depth measurements was assessed to be $\pm 0.04\ mm$.

Using second type of microscope with more focused light, it was possible to establish that all of the notches are positioned on expected depths. However, exact depth measurement was not possible since the microscope was not equipped with calibrated depth indicator.

Table below presents measured dimensions of the notches after manufacturing using electro discharge machining (EDM).

Table 14: Results of measurements of notches' real dimensions.

Dim.\No.	1	2	3	4	5	6	7	8	9	10
30										
width [mm]	0.146	0.126	0.114	-----	-----	-----	-----	-----	-----	-----
length [mm]	-----	-----	-----	-----	-----	-----	-----	-----	-----	-----
depth [mm]	1.17	0.760	0.420	-----	-----	-----	-----	-----	-----	-----
0.8										
width [mm]	-----	-----	-----	0.115	0.112	0.102	0.101	0.095	0.096	0.083
length [mm]	-----	-----	-----	0.861	0.859	0.882	0.855	0.856	0.847	0.841
depth [mm]	-----	-----	-----	-----	-----	-----	-----	0.750	0.570	0.390
0.4										
width [mm]	-----	-----	-----	0.118	0.106	0.106	0.102	0.104	0.091	0.129
length [mm]	-----	-----	-----	0.460	0.461	0.459	0.448	0.447	0.454	0.446
depth [mm]	-----	-----	-----	-----	-----	-----	-----	-----	0.6	0.45

Figures below show examples of the results obtained using optical microscope. The examples of measured values of length and width are presented in Figure 72 and Figure 73.

A few images of captured bottom surface of the notches are visible in Figure 74, Figure 75 and Figure 76.
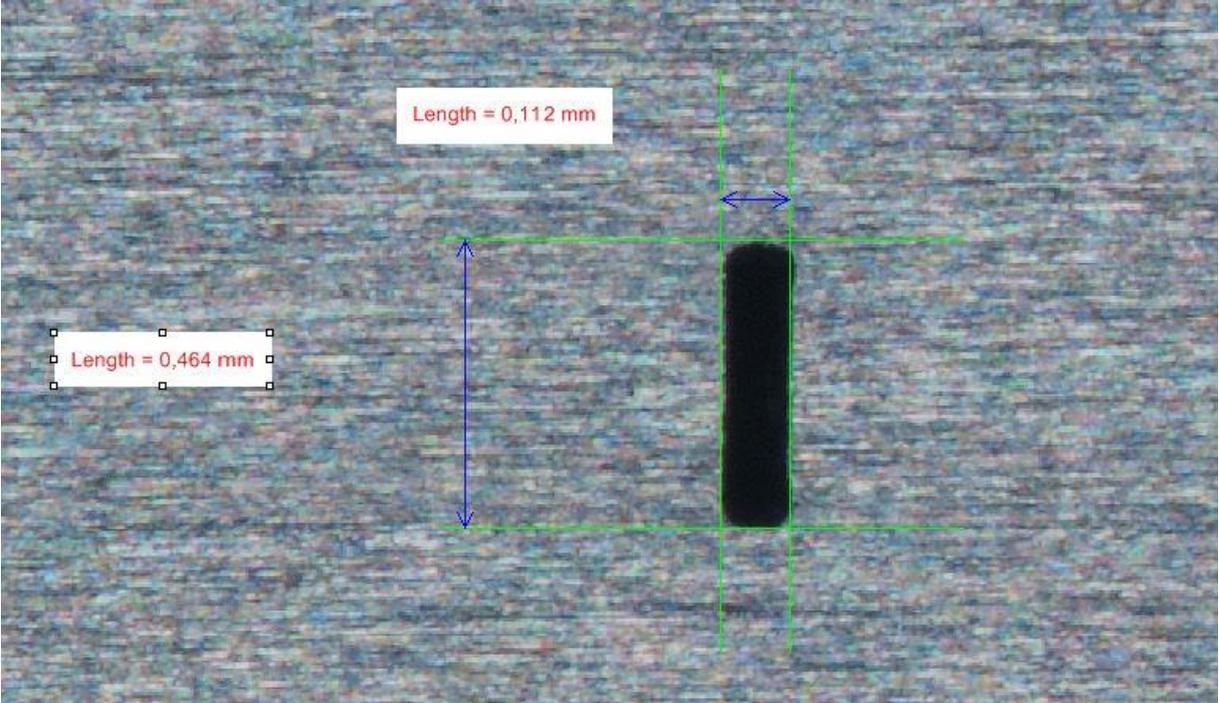
Figure 72: Example of length and width measurement performed on 0.4 mm notch.
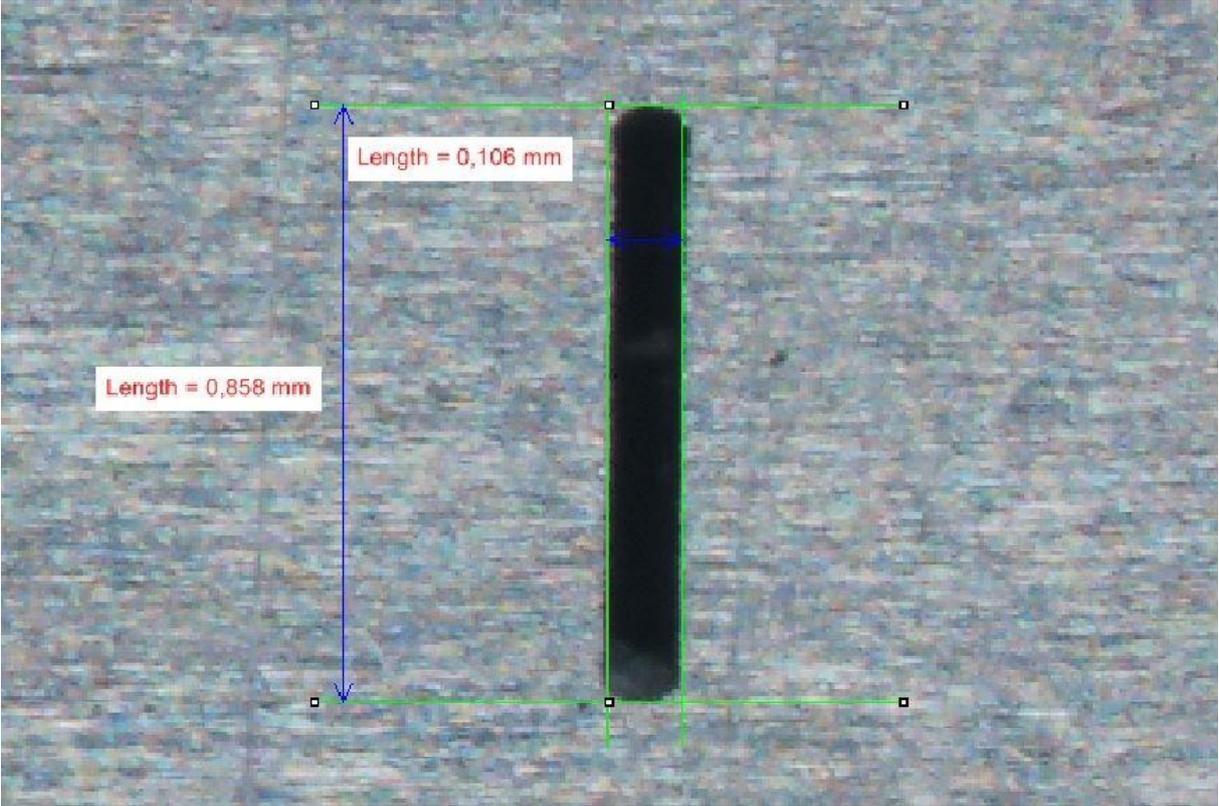
Figure 73: Example of length and width measurement performed on 0.8 mm notch.

Figure 74: Captured bottom of the notch 0.4 mm at the depth of 0.4 mm.
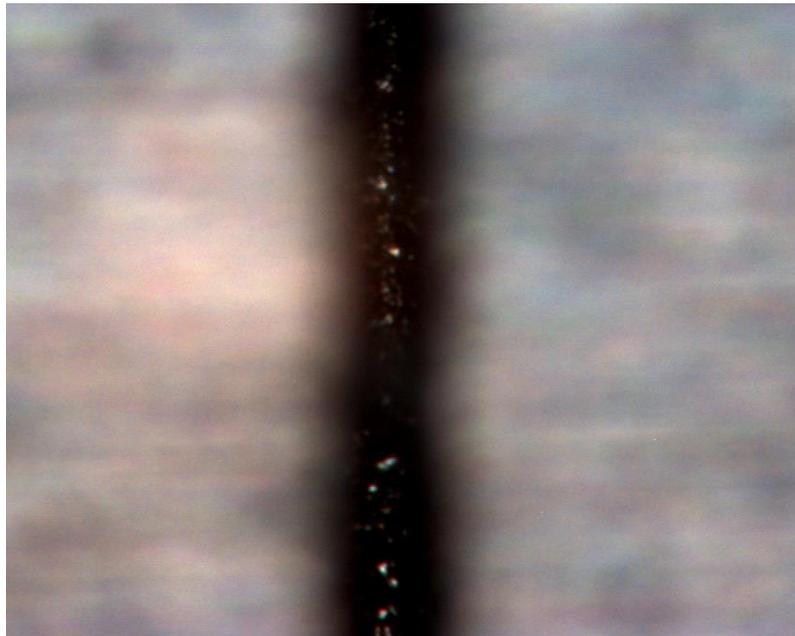
Figure 75: Captured bottom of the notch 0.8 at the depth of 0.4 mm.
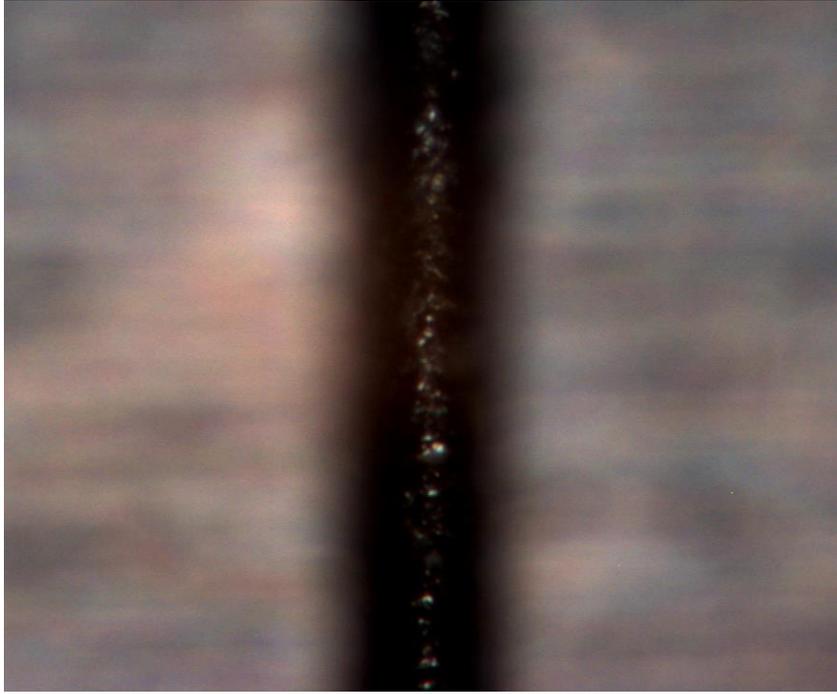
Figure 76: Captured image of the bottom of the 30 mm notch at the depth of 0.4 mm.

Appendix 5

In the section below, detailed results of inspection of 0.8 mm long notches are presented. Eddy current inspection is performed using plane, defect free surface.

Figure 77 presents signal acquired while scanning over the area with 0.8 mm long notches. The eddy current response, documented with this curve, is the highest obtained.
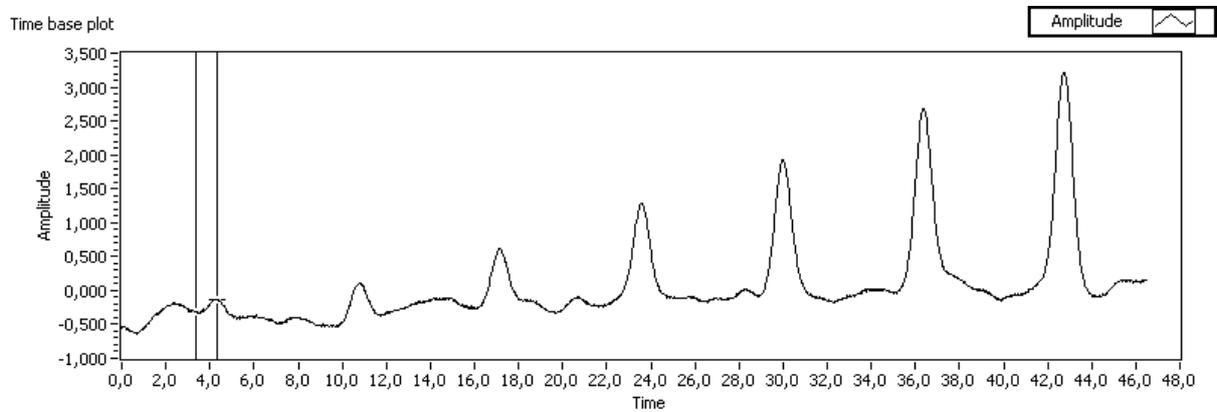

Figure 77: Plot of inductive reactance acquired while scanning area with 0.8 mm notches. Response with highest amplitudes is presented in the figure.

Figures below show the shape of indications produced by the notches plotted on impedance plane.
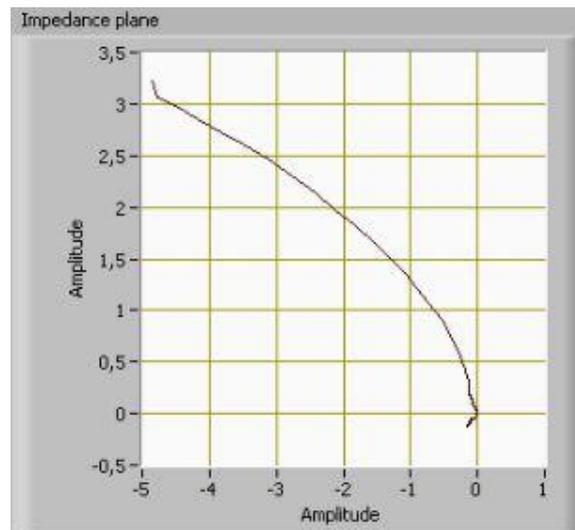

*Figure 78: Indication of notch 4 presented on the impedance plane.*
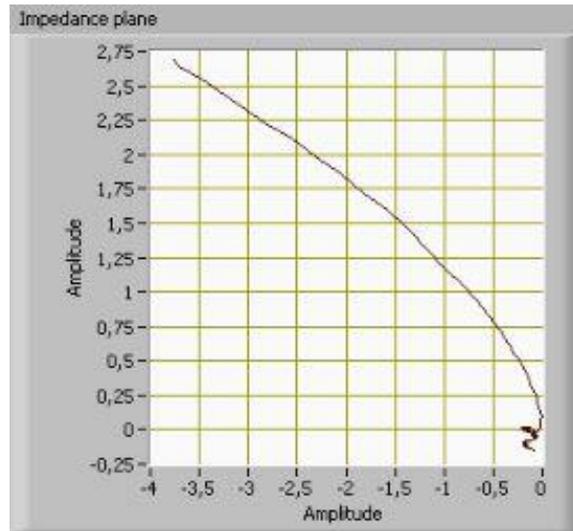
Figure 79: Indication of notch 5 presented on the impedance plane.
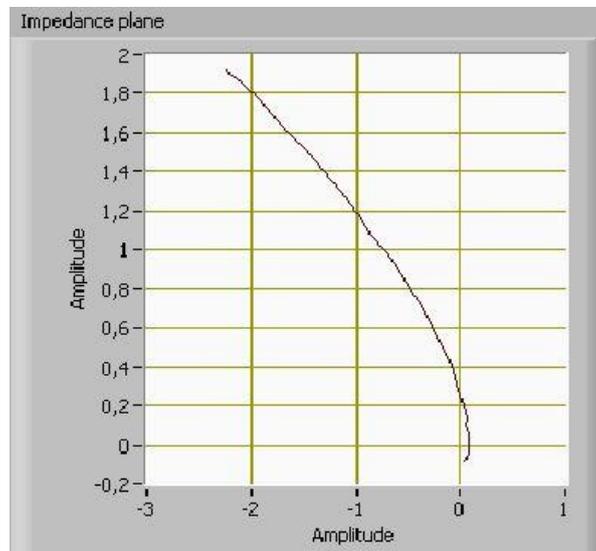
Figure 80:Indication of notch 6 presented on the impedance plane.
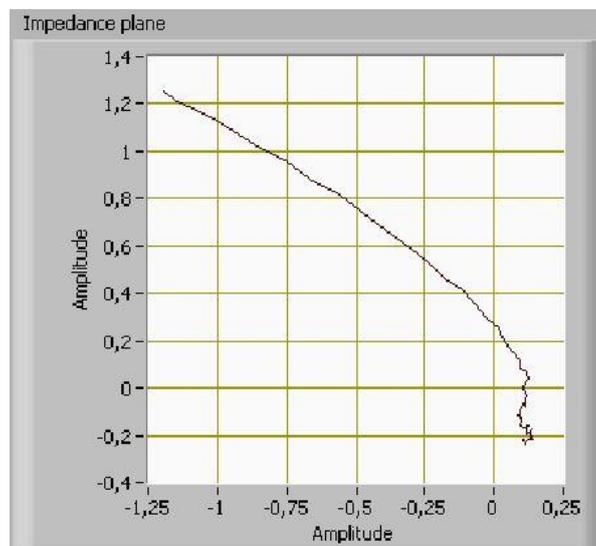
Figure 81: Indication of notch 7 presented on the impedance plane.
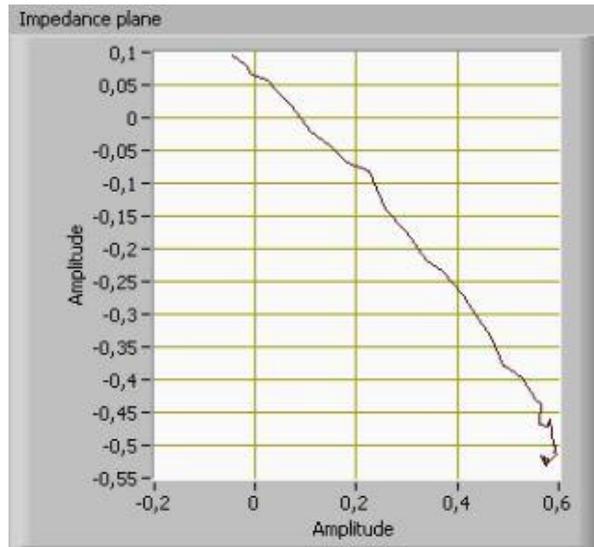
Figure 82: Indication of notch 8 presented on the impedance plane.
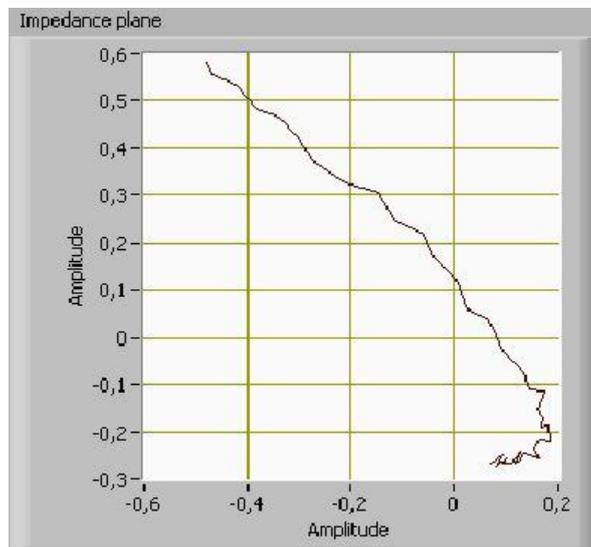
*Figure 83: Indication of notch 9 presented on the impedance plane.*
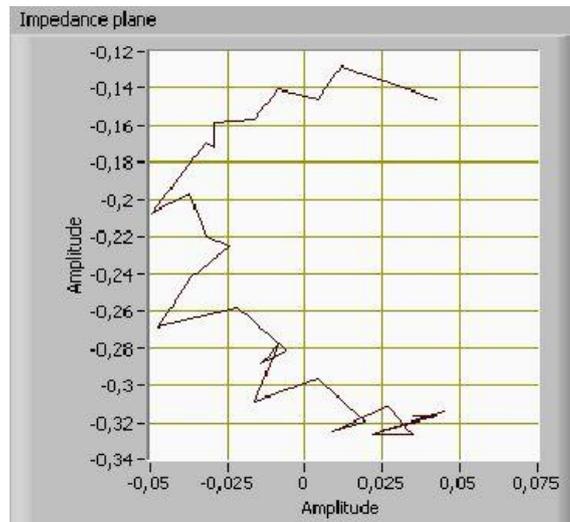
*Figure 84: Indication of notch 10 presented on the impedance plane.*

69

Appendix 6

In the section below, detailed results of eddy-current inspection of 0.4 mm long notches are presented. The inspection is performed using plane, defect free surface.

Figure 85 presents impedance signal acquired while scanning over the area with 0.4 mm long notches. The eddy current response documented with this curve is the highest obtained.
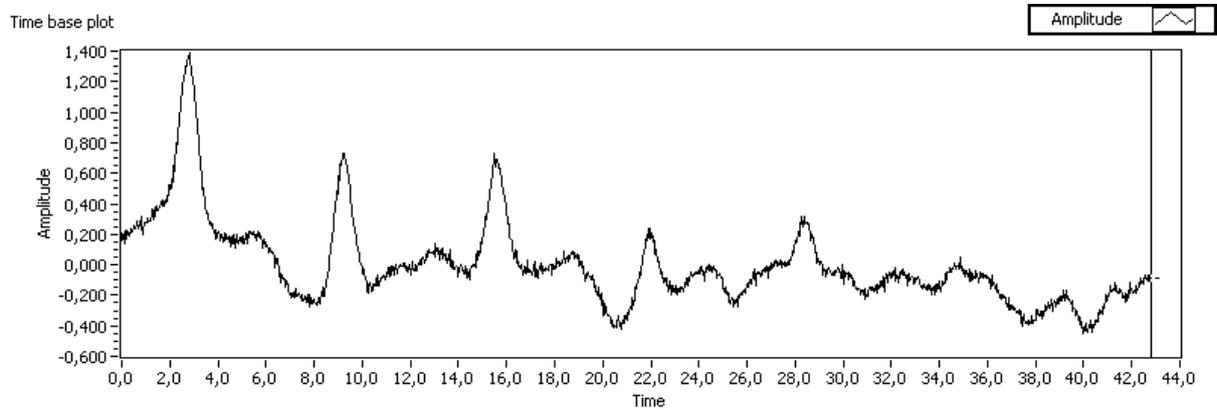
Figure 85: Plot of reactive inductance acquired while scanning area with 0.4 mm notches. Response with highest amplitudes is presented in the figure.

Figures below show the shape of indications produced by the notches plotted on impedance plane.
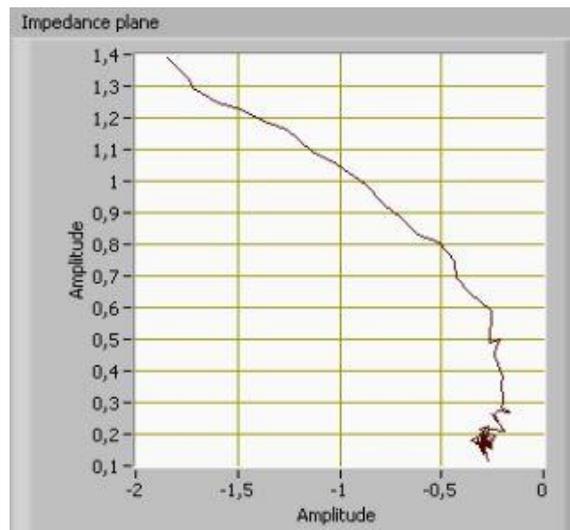
Figure 86: Indication of notch 4 presented on the impedance plane.
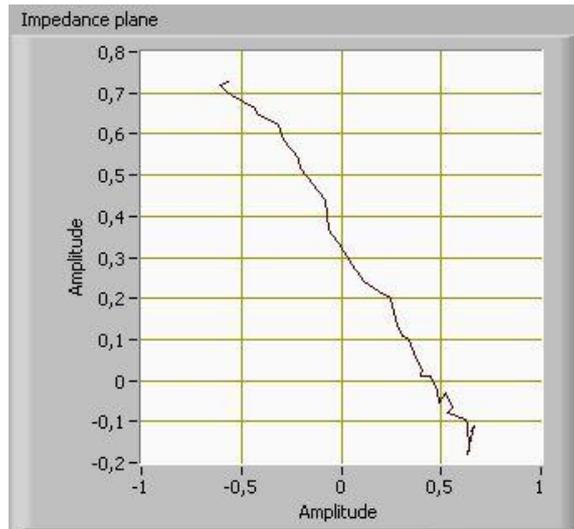
Figure 87: Indication of notch 5 presented on the impedance plane.
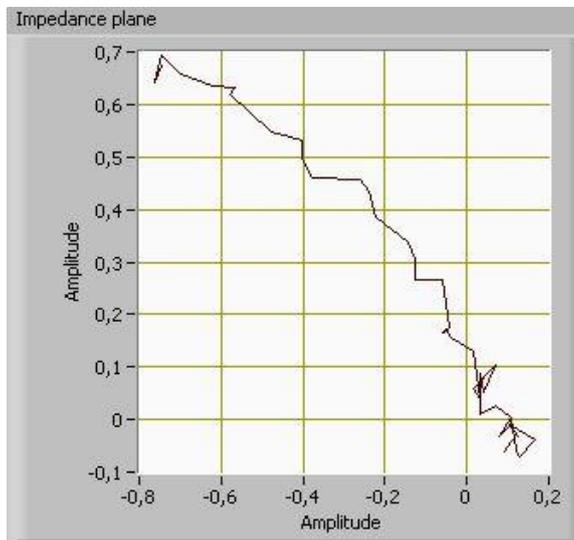
Figure 88: Indication of notch 6 presented on the impedance plane.
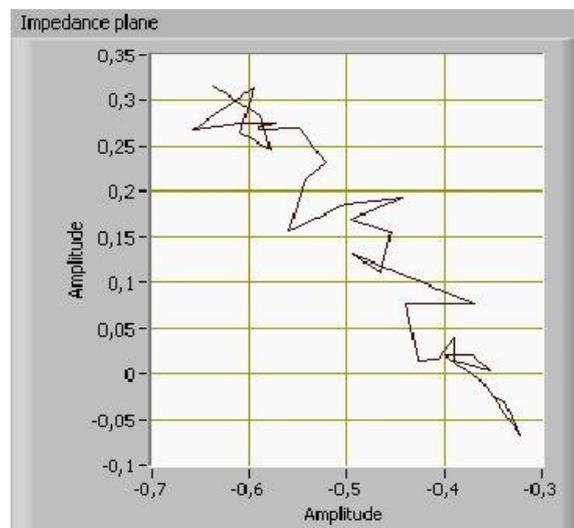
*Figure 89: Indication of notch 7 presented on the impedance plane.*

71

Figure 90: Indication of notch 8 presented on the impedance plane.

Appendix 7

In the section below, detailed results of eddy current inspection of 0.8 mm long notches are presented. The inspection is performed using surface containing notches.

Figure 91 presents impedance signal acquired while scanning over the area with 0.8 mm long notches.
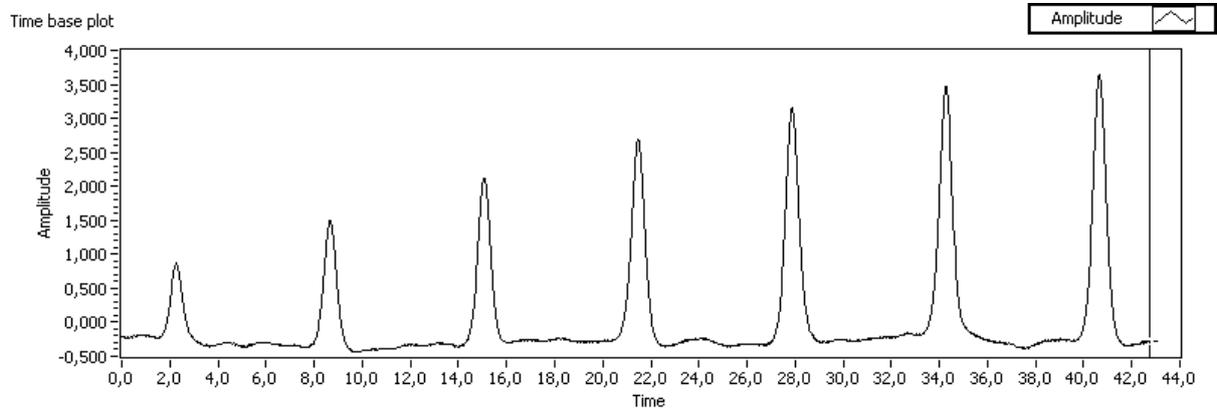

Figure 91: Plot of inductive reactance acquired while scanning area with 0.8 mm notches. Response with highest amplitudes is presented in the figure.

Figures below show the shape of indications produced by the notches plotted on impedance plane.
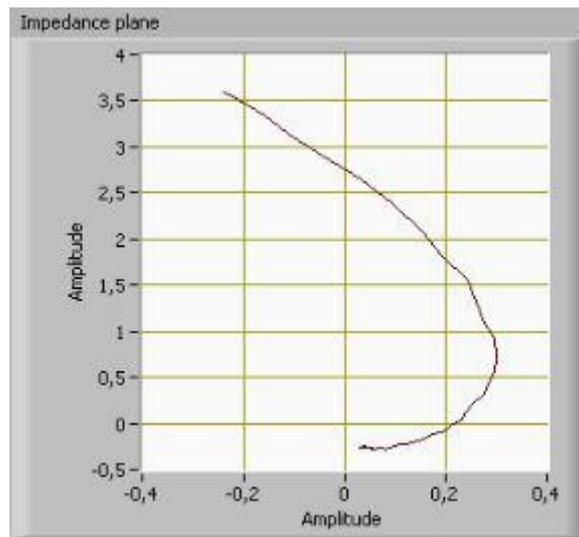
Figure 92: Indication of notch 4 presented on the impedance plane.
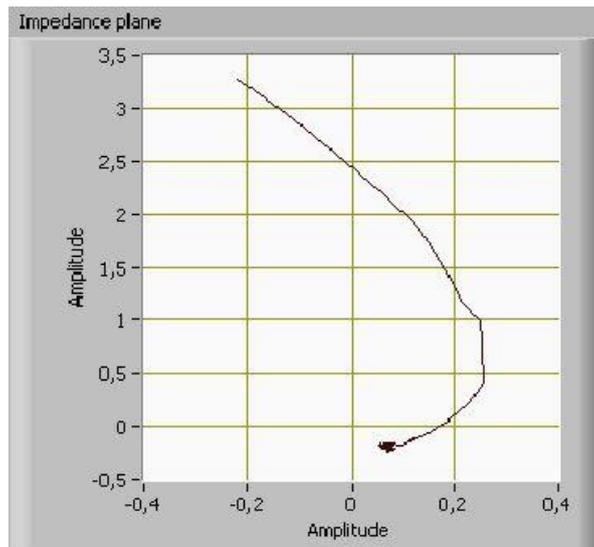
Figure 93: Indication of notch 5 presented on the impedance plane.
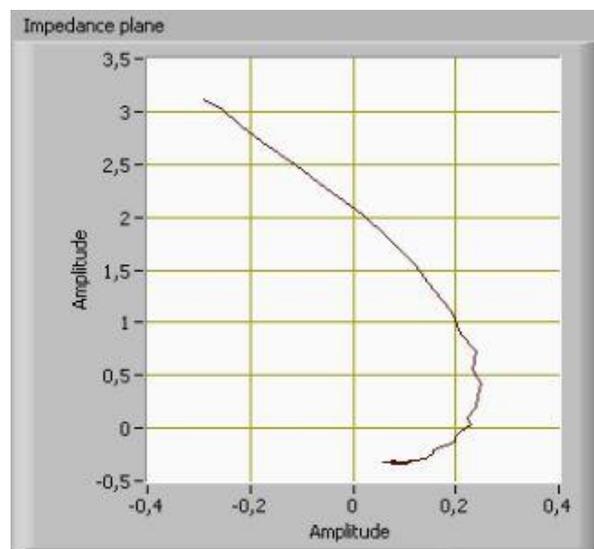
Figure 94: Indication of notch 6 presented on the impedance plane.
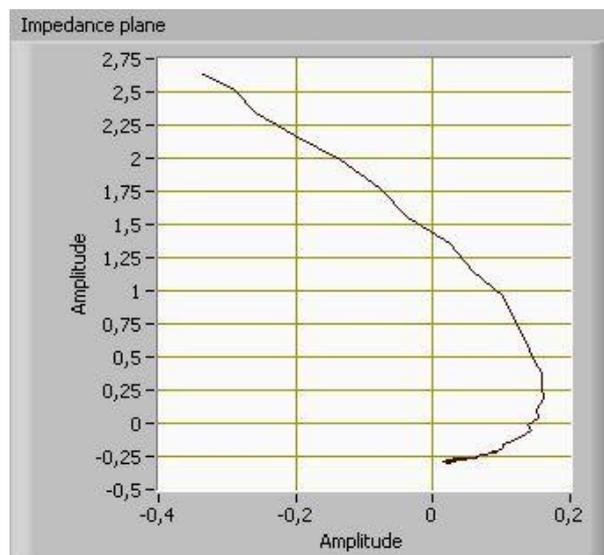
*Figure 95: Indication of notch 7 presented on the impedance plane.*

74
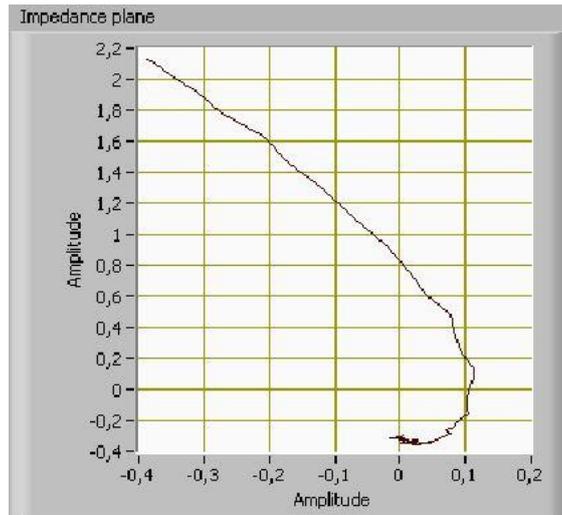
Figure 96: Indication of notch 8 presented on the impedance plane.
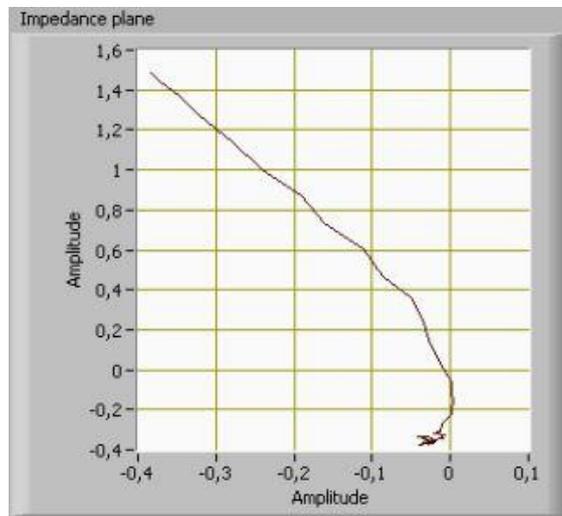
Figure 97: Indication of notch 9 presented on the impedance plane.
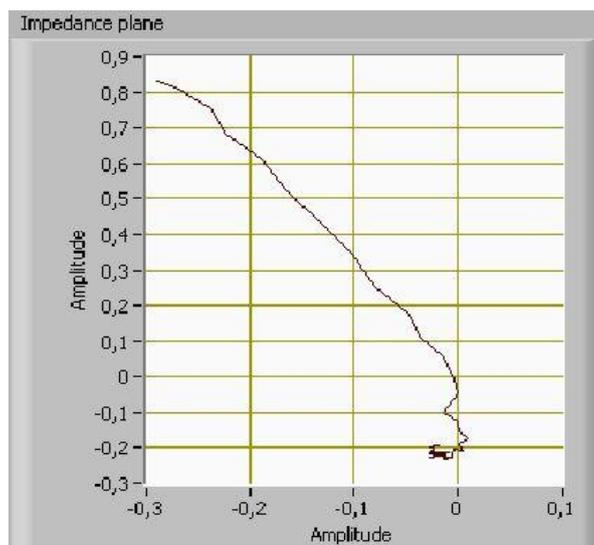
Figure 98: Indication of notch 10 presented on the impedance plane.

75

Appendix 8

In the section below, detailed results of eddy current inspection of 0.4 mm long notches are presented. The inspection is performed using surface containing notches.

Figure 99 presents impedance signal acquired while scanning over the area with 0.4 mm long notches.
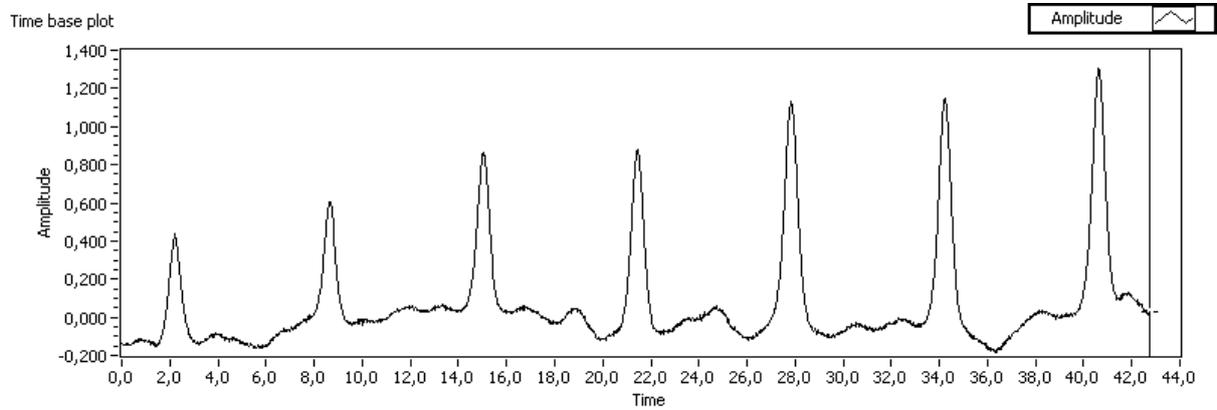
Figure 99: Plot of inductive reactance acquired while scanning area with 0.8 mm notches. Response with highest amplitudes is presented in the figure.
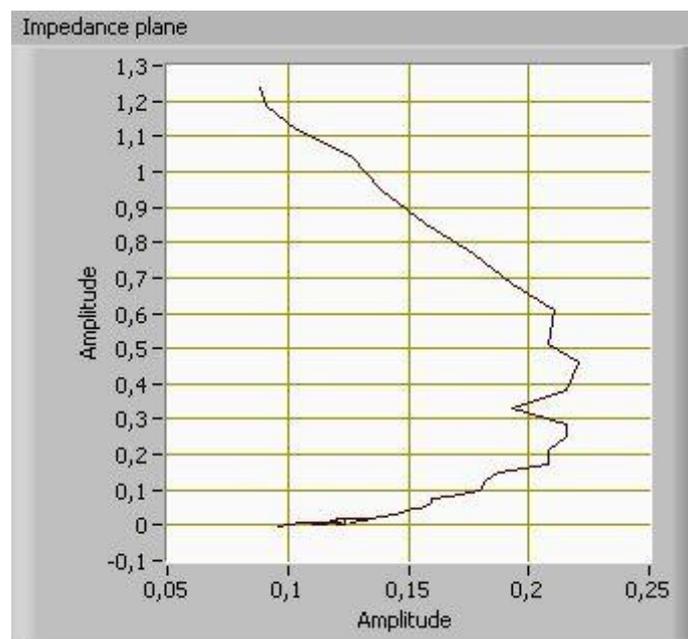
Figure 100: Indication of notch 4 presented on the impedance plane.
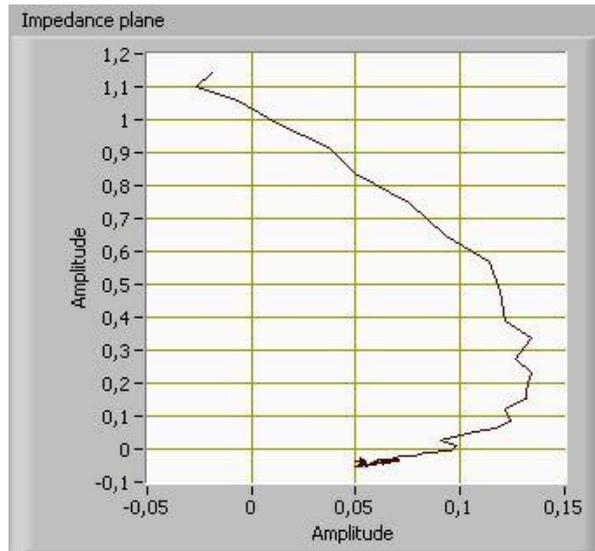
Figure 101: Indication of notch 5 presented on the impedance plane.
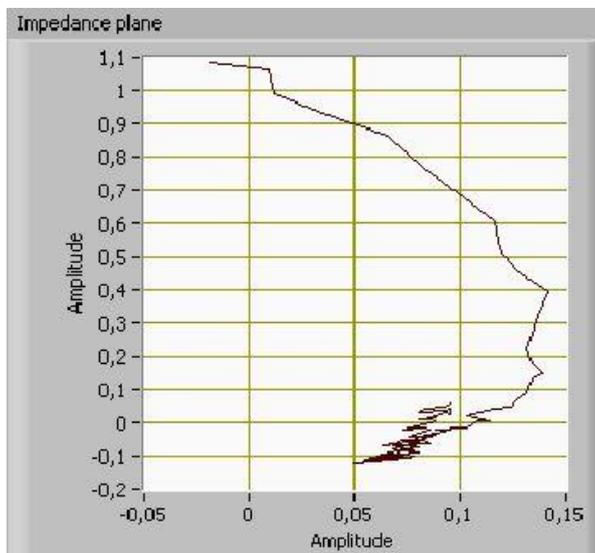
*Figure 102: Indication of notch 6 presented on the impedance plane.*
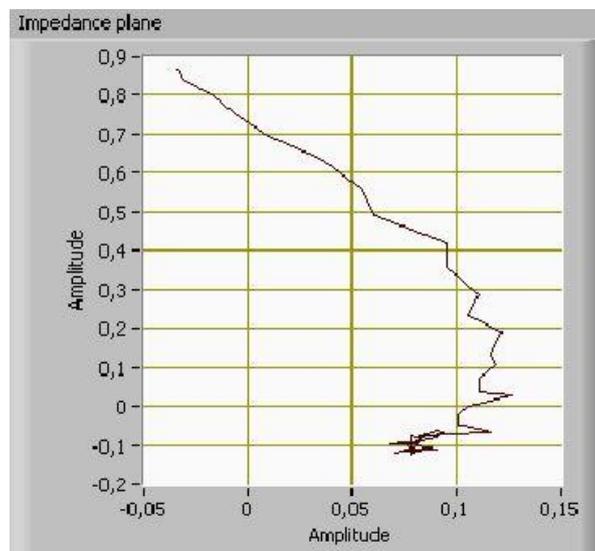
*Figure 103: : Indication of notch 7 presented on the impedance plane.*
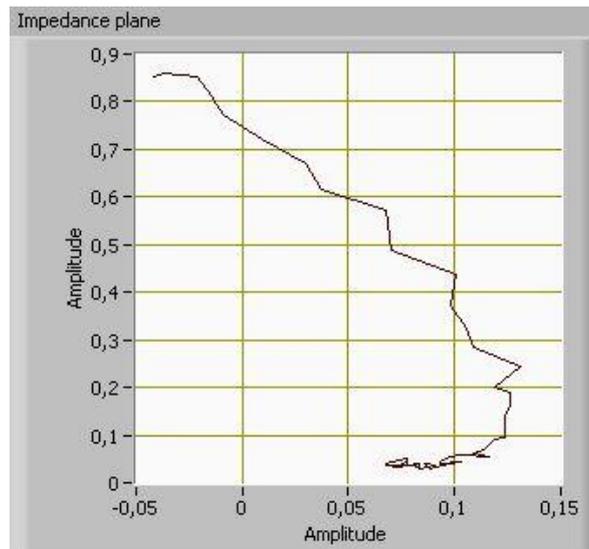
*Figure 104: Indication of notch 8 presented on the impedance plane.*
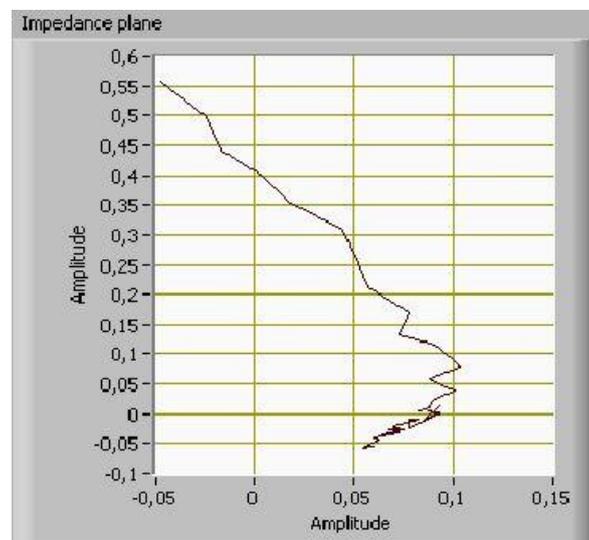
*Figure 105: Indication of notch 9 presented on the impedance plane.*
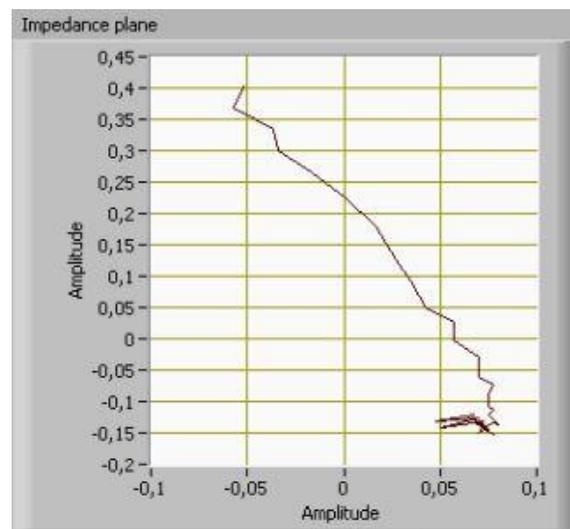
Figure 106: Indication of notch 10 presented on the impedance plane.

78